UNIVERSITY OF HELSINKI REPORT SERIES IN PHYSICS

N:o D272 (2021)

FINE STRUCTURE AND RADIAL EVOLUTION OF SHEATH REGIONS DRIVEN BY INTERPLANETARY CORONAL MASS EJECTIONS

MATTI ALA-LAHTI

Department of Physics
Faculty of Science

University of Helsinki
Helsinki, Finland

ACADEMIC DISSERTATION

To be presented, with the permission of the Faculty of Science of the University of Helsinki, for public criticism in auditorium B123 (Exactum), Pietari Kalmin katu 5, on January 22nd, 2021, at 14 o'clock.

Helsinki 2021

Author's Address: Department of Physics
P.O. Box 64
FI-00014 University of Helsinki
matti.ala-lahti@helsinki.fi

Supervisor: Prof. Emilia K. J. Kilpua
Department of Physics
University of Helsinki

Pre-examiners: Prof. Eija Tanskanen
Sodankylä Geophysical Observatory
University of Oulu

Prof. Emer. Bruce Tsurutani
Jet Propulsion Laboratory
California Institute of Technology

Opponent: Prof. Mats André
Swedish Institute of Space Physics
Uppsala University

ISBN (printed version) 978-951-51-6895-5
ISSN 0356-0961
Helsinki 2021
Helsinki University Printing House Unigrafia Oy

ISBN (PDF version) 978-951-51-6896-2
http://ethesis.helsinki.fi/
Helsinki 2021
Electronic Publications @ University of Helsinki

”It is the small steps which bring you satisfaction at the end of the day.”
Rafael Nadal

Matti Mikael Ala-Lahti
University of Helsinki, 2021

Abstract

A continuous flow of charged particles emanating from the Sun is ubiquitous in the solar system. This solar wind carries the magnetic field of the star and constitutes a fluid that has an electromagnetic interplay with flow obstacles, such as planetary magnetic fields. The regular conditions in the solar wind flow are drastically disturbed by transients that originate from huge eruptions of plasma and magnetic flux in the Sun. In interplanetary space, these eruptions are known as interplanetary coronal mass ejections (ICMEs). An ICME propagating faster than the ambient solar wind ploughs the solar wind deflecting it aside. Consequently, a solar wind plasma region having distinctive characteristics is formed in front of the driving ICME. These sheath regions driven by ICMEs consist of shocked turbulent plasma that in our imagination is comparable to the flow in the immediate downstream of a waterfall or to the flow around an obstacle in rapids. The magnetic configuration of an ICME sheath is exposed to continuous modification and thus has a complicated fine structure, which varies with distance from the Sun.

In this thesis, the fine structure and radial evolution of ICME sheaths are investigated particularly in terms of their magnetic field by performing in-situ studies that utilise spacecraft measurements taken at 1 AU and closer to the Sun. The research conducted in this thesis shows that although ICME sheaths are highly turbulent plasma environments, a structure appearing on larger scales is embedded in sheath magnetic fields. Furthermore, magnetic fluctuations on smaller scales do result from different physical processes, more precisely, from plasma being regulated by plasma instabilities such as mirror and Alfveń ion cyclotron instabilities. These smaller-scale fluctuations can be interpreted to manifest the gradual energy dissipation process that ensures an irreversible shock crossing of the solar wind plasma. They may, however, be so localised and their origins so temporary that the consequent magnetic fluctuations display strong spatial inhomogeneity and no coherency is observed in sheath magnetic fields at those scales. This spatial inhomogeneity gradually decreases towards larger scales.

This thesis contributes to the understanding of ICME-driven sheath regions not only by reporting the observations that result in the conclusions stated above but also by discussing the relevant physical processes occurring in the sheath that significantly contribute to the sheath magnetic fields. The shock preceding the sheath modifies

the solar wind plasma and interplanetary magnetic field and is concluded to have a major role in the occurrence of the smaller-scale fluctuations that result from plasma instabilities. Together with field line draping, in which magnetic field drapes around the driving ICME ejecta, the shock also regulates the global magnetic field configuration of ICME sheaths. Moreover, these processes continuously modify and regulate the sheath fields when an ICME travels through interplanetary space. This results in steady accumulation of magnetic fields in the sheath.

This thesis also discusses what avenues of research may be particularly scientifically beneficial. To include ICME sheaths in models that forecast space weather, the consequences of the spatial inhomogeneity should be comprehensively resolved. Thus, there is a need for additional multi-spacecraft studies on the non-radial extent of different magnetic fluctuations embedded in the magnetic fields of ICME sheaths. In addition, the latest missions providing high-resolution data offer great opportunities to investigate sheath magnetic fields with an improved accuracy. These missions can be utilised in multi-spacecraft studies on the radial evolution of ICME sheaths. Moreover, this thesis makes a contribution that is generally beneficial to the community by developing algorithms that are suitable for further applications, in which magnetic field waves are investigated in different space plasma environments, and also by applying novel techniques and thus adapting them in the context of space plasmas.

Contents

Preface

My journey towards attaining a doctoral degree becomes concrete in this thesis. I think during the past four-odd years I have learnt a lot about myself: If I had to define myself the definition would likely include the term *theory-based approach* paired with an expression that puts my interest in various things into words. My doctoral studies have, in addition, given me so many great experiences such as visiting places where top-class research is done, meeting people who had carried a senselessly expensive scientific instrument on the public transport of London, and attending to a lecture given by a person that pricks astronauts for a living. For me this all has been very intriguing.

I am much obliged to Emilia Kilpua, my supervisor, for this all. I am truly grateful to her for always being open to my ideas and for the freedom she gave me to execute them. This has enabled getting versatile, important experiences. All these years she has also coped with my stress, and I want to express my gratitude to her for the time she used to guide and support me. I extend my gratitude to Tuija Pulkkinen whose encouraging comments have helped me to built my confidence during these years. I truly appreciate her many recommendations and her scientific and career-wise advice.

I am grateful to my pre-examiners, Eija Tanskanen and Bruce Tsurutani, for their time spent evaluating this thesis. I want to thank them for their elucidating comments that clarified my writing and, most importantly, scientific thinking. I also thank sincerely Mats André, my opponent, for his acceptance to conduct the final examination of this thesis. I appreciate his expertise being present in my doctoral thesis defence.

I would like to also thank my co-authors, Simon Good, Andrew Dimmock, Adnane Osmane, Jan Souček, Noé Lugaz and Julia Ruohotie, who have contributed to my research and shared their professional knowledge resulting in major improvements of the research conducted in this thesis. I have to admit I have sometimes when discussing with you made comments I knew were wrong but which would be comprehensively answered by you. Thank you for your answers. I wish to thank Simon for his professional relationship and friendship with me. Still no turbulence. I have truly enjoyed our time at the office. I want to express special thanks to Andrew for hosting me in Uppsala. If I had to name one week during which

my thinking improved the most during my PhD studies, it would be the visit in Uppsala. I extend my gratitude to Adnane for his endless patience when guiding me in turbulence and C-H theory, topics that sometimes felt like a labyrinth without an exit.

Massive thanks go to my peers in the space physics corridor, who have offered company, laugh and support. People, including my fellows Maxime Grandin, Daniel Price, Diana Morosan, Eleanna Asvestari and Harriet George, in WhatsApp groups of many names have most of all offered me a channel in which all feelings related to research have been understood. Special thanks go to my bro Maxime for all of the proofreading and long walks. I also want to thank Erika Palmerio for her wide-ranging help from poster printing to navigating through a conference. My colleagues have made my day so many times. Indeed, thanks to every person that has made our work community the place it is. I wish that I have managed to offer back at least some of that friendliness.

I thank my friends who have had a crucial part in balancing my life. I want to express my gratitude to Joona and Hilda Rantanen. They have been essential for my well-being, and I appreciate our close friendship and the time we have spent together. In this, racket sports have had a major role. I have truly enjoyed all the games and mirroring my behaviour in a court to what I am as a person. Joona, going into a court with you has been my lifeline. I want to also thank my family-in-law whose warm and overwhelming hospitality really cannot be described by words. Sharing a morning with them at their kitchen table is one of best things I know.

My sincere thanks and appreciation go to my family; to my brother, who has always been there understanding my mentality like no one does and also cheering for me, and particularly to my parents, who have offered me everything having always emphasised kind-heartedness and the importance of education. They have always been there for me and my life is full of great, valuable experiences because of them. Kiitos kaikesta äiti ja isä.

Finally, Irina, my wife, you have my deepest gratitude. Thank you for everything, for all love, for all adventures, for every bad and every good day. Thank you for being humanitarian you. Your support is the foundation of my well-being, success and happiness.

Matti Ala-Lahti
Helsinki, December 2020

List of Acronyms

ACE	Advanced Composition Explorer
AIC	Alfvén ion cyclotron
AU	Astronomical unit
CIR	Co-rotating interaction region
CME	Coronal mass ejection
DSCOVR	Deep Space Climate Observatory
FH	Firehose
GSE	Geocentric Solar Ecliptic
HCS	Heliospheric current sheet
HEEQ	Heliocentric Earth Equatorial
HMF	Heliospheric magnetic field
ICME	Interplanetary coronal mass ejection
IC	Ion cyclotron
IMF	Interplanetary magnetic field
LH	Left-hand
MESSENGER	MErcury Surface, Space ENvironment, GEochemistry, and Ranging
MHD	Magnetohydrodynamics
MM	Mirror mode
PMS	Planar magnetic structure
PSD	Power spectral density
RH	Right-hand
RMS	Root-mean-square
RTN	Radial-Tangential-Normal
SEP	Solar energetic particle
SI	Stream interface
SIR	Stream interaction region
STEREO-A (B)	Solar TErrestrial RElations Observatory - Ahead (Behind)
ULF	Ultra-low frequency

List of Publications

This thesis collects four research articles into an integrated complex that are preceded by an introductory review. The articles are peer-reviewed and published by international journals and they have not been included in other theses. They are referred throughout the thesis according to their Roman numerals.

I Ala-Lahti, M., Kilpua, E. K. J., Dimmock, A. P., Osmane, A., Pulkkinen, T. I., and Souček, J.: Statistical analysis of mirror mode waves in sheath regions driven by interplanetary coronal mass ejection, *Annales Geophysicae*, 36, 793–808, doi.org/10.5194/angeo-36-793-2018, 2018.

II Ala-Lahti, M., Kilpua, E. K. J., Souček, J., Pulkkinen, T. I., and Dimmock, A. P.: Alfvén ion cyclotron waves in sheath regions driven by interplanetary coronal mass ejections, *Journal of Geophysical Research: Space Physics*, 124, 3893–3909, doi.org/10.1029/2019JA026579, 2019.

III Ala-Lahti, M., Ruohotie, J., Good, S. W., Kilpua E. K. J., and Lugaz, N.: Spatial coherence of interplanetary coronal mass ejection sheaths at 1 AU, *Journal of Geophysical Research: Space Physics*, 125, e2020JA028002, doi.org/10.1029/2020JA028002, 2020.

IV Good, S. W., **Ala-Lahti, M.**, Palmerio, E., Kilpua E. K. J., and Osmane, A.: Radial evolution of magnetic field fluctuations in an interplanetary coronal mass ejection sheath, *The Astrophysical Journal*, 893, 110, doi.org/10.3847/1538-4357/ab7fa2, 2020.

1 Introduction

Space physics refers to a field of science consisting in exploring outer space where direct observations, i.e. in-situ measurements, are possible. This definition effectively defines the Sun and its sphere of influence, the heliosphere that encloses in the planets of the solar system, as the subject of its research. Space physics examines the solar wind, a continuous stream of charged particles from the Sun, which carries the Sun's magnetic field interacting with planetary magnetic fields it encounters. The state of matter of this stream is plasma, and this field of natural sciences is also often called space plasma physics. Plasma constitutes the absolute majority of baryonic matter in the universe and therefore has a role in various astrophysical phenomena and physical occurrences of interest to humankind. In a plasma, matter neutral in total includes a substantial number of charged particles so that collective electromagnetic interactions become crucial for its behaviour. Space plasma physics is thus focused on investigating phenomena in a fluid generated by the electromagnetic interaction of matter, which is theoretically characterised by Maxwell's equations and the Lorentz's force.

Efforts to understand space plasma physics have considered plasma with descriptions of different levels of accuracy. This enables the effective development and utilisation of science. In practice, to explain large-scale plasma phenomena, individual particles in the domain of electromagnetic interaction are collected to particle populations given by distribution functions or simplified as macroscopic fluids. Acquiring an extensive understanding on the electromagnetic interaction, however, eventually also requires research on the fundamental physics of individual particles at microscopic, kinetic scales that furthermore enables improvements of statistical and macroscopic theories. Comprehensive fundamental research utilising different theoretical approaches results in a profound knowledge of physics and thus in the capability to predict the behaviour of matter accurately. This knowledge is best achieved with science having a high intrinsic value.

Space plasma physics has lead us to our current knowledge of the near-Earth space environment, where solar activity drives time-varying disturbances which cause large configurational changes in the Earth's magnetic field and in high-energy particle environment. This – variable solar wind conditions affecting the geomagnetic field and magnetospheric plasmas – is referred to as space weather. Further space

weather effects at the Earth for instance are auroras, damage on satellites due to collisions with high-energy particles, disturbances of satellite navigation services because of changes in the chemical composition and bulk properties, such as density, of the upper atmosphere, and induced currents in power systems which cause saturation of transformers, voltage fluctuations or even black-outs of the whole system. Space weather disturbances having the aforementioned consequences can last from several hours to days and exemplify an instrumental value space physics has.

Coronal mass ejections (CMEs) are drastic eruptions of clouds of plasma and magnetic field from the Sun whose interplanetary manifestations, ICMEs, are major drivers of space weather at the Earth. ICME ejecta refers to an isolated ejecta whose magnetic configuration is often suitable for a rearrangement of magnetic connections with the Earth's magnetic field. This rearrangement, known as magnetic reconnection, enables the aforementioned transfer of matter and energy from the solar wind to near-Earth space. Furthermore, an ICME complex often consists of, in addition to the ejecta, a shock and a sheath region. This entity – shock, sheath and ICME ejecta – is referred to in this thesis with the term *ICME*. A shock and a sheath form in front an ICME ejecta when the propagation speed of the ejecta relative to the ambient solar wind exceeds the magnetosonic speed, the local maximum speed of information in the plasma.

The solar wind plasma properties are strongly modified in a shock crossing when the plasma enters a sheath. The plasma stream in the sheath is compressed and turbulent, the latter being manifested by local and abrupt changes in magnetic field magnitude and direction and in plasma variables such as density and temperature. Sheath regions of ICMEs are unique plasma environments in the solar system, and both the shock and the sheath are geoeffective solar wind transients, i.e. they have the ability to drive space weather effects. Magnetic fields favouring the occurrence of magnetic reconnection with the Earth's magnetic field are indeed frequently embedded in ICME sheaths. The research in the space physics community, however, has mostly focused on the understanding of ICME ejecta. The sheath region can also affect the geoeffectiveness of the ejecta via magnetic reconnection at the boundary of these two plasma regions, which causes the erosion of the isolated ejecta.

The research reported in this thesis is constructed to investigate magnetic configuration of ICME-driven sheath regions on various scales. The research considers the interactions of magnetic field fluctuations with individual particles and local particle populations as well as global modification of the field due to large-scale physical

mechanisms in an ICME, which can cause variation in geoeffectiveness within a single sheath. These issues are attached to the radial, that is outwards from the Sun, evolution of the sheath. Thus, the impact of this thesis varies from fundamental plasma physics – due to an exploration of kinetic and macroscopic physics of a unique solar wind transient – to possible future improvements in space weather predictions, which may provide a more accurate understanding of the dynamics of near-Earth space during ICME passages. This will enhance the utilisation of space for the benefit of humankind due to increased practical safety of technological devices. The scientific issues this thesis particularly contributes to are

- Occurrence of magnetic wave structures generated by plasma instabilities driven by the excess perpendicular temperature of plasma in ICME sheaths (Papers I and II).
- Longitudinal coherence and extent of magnetic structures in ICME sheaths (Paper III).
- Evolution of the fine structure of magnetic field in a radially outwards propagating ICME sheath (Paper IV).
- Global physical mechanisms contributing to the modification of magnetic field in ICME sheaths (Papers I – IV).

This thesis is composed of an introductory part, which is followed by four original research articles referred to as Papers I–IV. The introductory part is organised as follows. Chapter 2 introduces the solar wind, structures embedded into it and relevant physics concerning ICME sheaths such as turbulence and plasma instabilities. Also, near-Earth space and space weather are briefly covered to give a relatively comprehensive picture on space physics and its impact. Chapter 3 focuses on shocks and sheath regions driven by ICMEs. An overview of sheath characteristics is first given, which is then followed by a review of shock physics. Finally, the chapter extensively discusses sheath magnetic fields, how they consist of ubiquitous fluctuations and what processes define and align the global sheath field. Chapter 4 first discusses the relevant instabilities regarding this thesis on a more detailed level compared to Chapter 2 but it particularly focuses on discussing the research conducted in Papers I–IV by reviewing their main results and conclusions. Chapter 5 gives concluding remarks on the impact this thesis has and starts with a summary of the key results. This is followed by a brief discussion that takes a stand on the research conducted in the future. Finally, Chapter 6 summarises Papers I–IV and the author's contribution in the preparation of each of them.

2 Background

For thorough discussion of sheath regions driven by interplanetary coronal mass ejections (ICMEs) and the research conducted in this thesis, relevant plasma environments are introduced in this chapter. This contains describing the concepts of the solar wind and near-Earth plasma environment which is linked to corresponding environments of other planets in the solar system. In addition, fundamental plasma physics phenomena in these environments such as turbulence and plasma instabilities as well as space weather are discussed.

2.1 Solar wind

The solar wind is a continuous radial flow of charged particles from the Sun, which transfers energy to interplanetary space (e.g. Coles & Maagoe, 1972; Echim et al., 2011). It is primarily composed of protons (∼95% by mass), ionised helium (∼4%) and electrons which maintain the quasi-neutral state of the plasma (e.g. Bame et al., 1968). Minor populations of heavier ions such as ionised oxygen and carbon are also present (e.g. Gloeckler et al., 1992; von Steiger et al., 2000). The solar wind flow by its extent defines the sphere of influence of the Sun in terms of space plasma physics. This sphere is outlined by a boundary surface termed heliopause, where the solar wind achieves pressure balance with the plasma of the interstellar medium. The heliopause is located beyond the orbit of Pluto approximately at a distance of 120 astronomical units (AU – the distance between the Earth and Sun; $\sim 1.50 \cdot 10^8$ km) from the Sun (e.g. Stone et al., 2013, 2019).

The solar wind manifests the expansion of the solar atmosphere into interplanetary space. The expansion happens as a result of a large pressure gradient directed outwards from the Sun, which allows the solar wind to escape the Sun's gravitational field. This pressure gradient is caused by the extremely hot solar corona, which has a temperature of two million Kelvin (Bame et al., 1974). The existence of the solar wind was theoretically predicted by Parker (1958), who considered the expansion of an ideal gas as a time-independent radial flow of protons and electrons with negligible magnetic forces. Parker assumed an isothermal flow, in which protons and electrons have the same number density (n) and temperature (T) in the corona, and derived the so-called Parker solar wind equation

$$\frac{1}{u_r}\frac{du_r}{dr}({u_r}^2 - \frac{2k_\mathrm{B}T}{m_\mathrm{p}r}) = \frac{4k_\mathrm{B}T}{m_\mathrm{p}r} - \frac{GM_S}{r^2}, \tag{2.1}$$

where u_r is the radial flow speed, r the radial distance from the solar surface, k_B Boltzmann's constant, m_p the proton mass, G the gravitational constant and M_S is the solar mass.

Mathematically Parker's solar wind equation has six solutions, which are illustrated in Fig. 2.1a. Solution A is known as the Parker solar wind and depicts a flow that initially travels at subsonic speeds but is accelerated becoming supersonic at the distance of the so-called the critical radius (r_c), which is typically thought to be located at a distance of 4 – 8 solar radii ($R_S = 6.96 \cdot 10^5\,\mathrm{km}$) from the solar surface (Kasper & Klein, 2019). The critical radius defines an information horizon beyond which sunwards propagating sound waves are convected away from the corona. The speed profile is further extended to larger distances and exemplified for different coronal temperatures (Bame et al., 1974) in Fig. 2.1b. The existence of a supersonic stream of charged particles was eventually confirmed by spacecraft measurements (e.g. Gringauz et al., 1960; Snyder et al., 1963).

Parker's solution simplifies the solar wind by not considering issues such as differing proton and electron temperatures, the presence of heavier ions, and thermal conduction and cooling of plasma (e.g. Gurnett et al., 1979; Good, 2016; Wilson et al., 2018). It also does not take into account the solar rotation (e.g. Thompson et al., 2003). In addition, because the solar wind plasma is collisionless, protons and electrons have different cooling rates (Hartle & Sturrock, 1968; Koskinen, 2011). In the inner heliopshere the proportionality of temperature to the radial distance from the Sun varies from $\sim r^{-0.2}$ to $r^{-0.5}$ for electrons and is $\sim r^{-0.8}$ for protons (Eyni & Steinitz, 1978; Miyake & Mukai, 1987; Marsch et al., 1989). Also, in the outer heliosphere, the solar wind cools off slower than expected for the adiabatic cooling, for which the temperature declines as $r^{-4/3}$ (Richardson & Smith, 2003). However, despite its restrictions, Parker's solar wind model estimates surprisingly accurately the speed profile. Namely, when considering observed coronal temperature values (see Fig. 2.1b), the model predicts so-called fast solar wind, whose speed typically varies between 600 and 800 km/s at 1 AU (Neugebauer and Snyder, 1966; Gosling et al., 1976; Ebert et al., 2009; see also Tsurutani et al., 2011a).

At times, the solar wind flows with a smaller speed; the wind with speeds below 500 km/s is called slow solar wind (e.g. Neugebauer & Snyder, 1966; McComas et

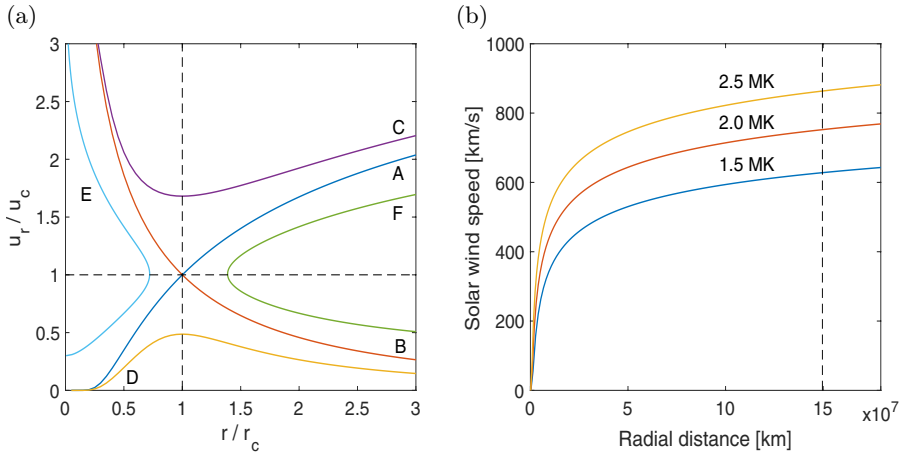

Figure 2.1: Parker solar wind solution. (a) Six possible solutions of Parker's solar wind equation. Solution A illustrates the real solar wind. Radial solar wind speed (u_r) and distance from the Sun (r) are given with respect to the sound speed ($u_c = \sqrt{2k_{\rm B}T/m_{\rm p}}$) and so-called critical radius ($r_c = (GM_s m_{\rm p})/(4k_{\rm B}T)$) beyond which Solution A is supersonic. u_r and r_c are given by setting the right-hand side of Eq. 2.1 equal to zero. (b) Solar wind speed of Solution A as a function of distance from the Sun for specific coronal temperatures based on the temperature variation in the corona reported by Bame et al. (1974). Black dashed line indicates the location of the Earth's orbit.

al., 1998; Ebert et al., 2009). The fast and slow solar winds emerge from different regions at the Sun, whose locations vary during a solar cycle and are related to the configuration of the coronal magnetic field (McComas et al., 2008). This is illustrated in Fig. 2.2. The difference in source regions is most distinguishable during a solar minimum, when the Sun's magnetic field is the most dipolar. The slow solar wind emanates near the equator, whereas the fast solar wind originates from open field line regions, coronal holes, located at higher heliographic latitudes in both hemispheres. During solar maximum, when the magnetic field configuration is more complex due to a strong toroidal field component, the source regions are mixed and less distinct. The origin of the slow solar wind is still under debate but it is generally thought to emanate from the boundary between open and closed field regions (Wang et al., 1998; McComas et al., 2008). New insight into the open question of the origin of the slow solar wind is expected to be provided by the current Parker Solar Probe mission (Fox et al., 2016). For example, the spacecraft recently observed the slow solar wind emerging from a coronal hole near the equator (Bale et al., 2019).

The slow solar wind is denser than the fast solar wind, both the plasma density and

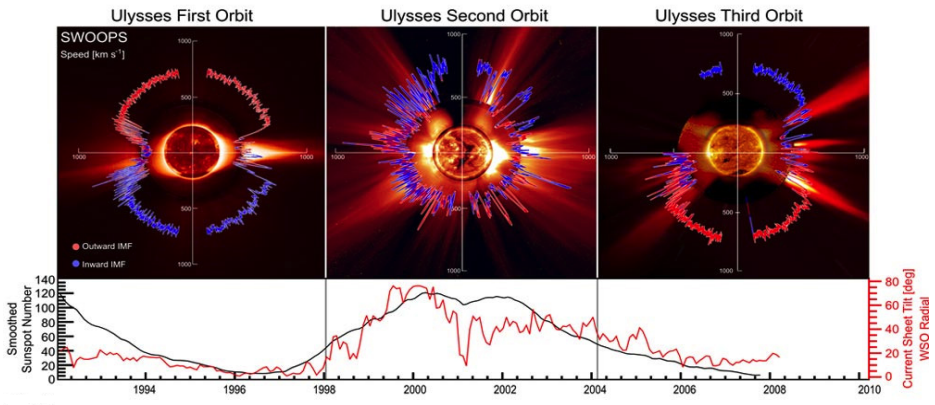

Figure 2.2: Solar wind speed as a function of heliographic latitude measured by the Ulysses spacecraft and contemporary sunspot number. The low and high latitude source regions of slow and fast wind, respectively, are distinct in the first panel that illustrates a solar minimum whereas the second panel shows that the regions are mixed during a solar maximum. The red and blue colour in the upper panels indicate outwards and inwards interplanetary magnetic field (IMF), and the red curve in the bottom panel the tilt of the current sheet. These both structures are discussed in coming sections. Reproduced from a figure in McComas et al. (2008).

magnetic field magnitude being higher in the slow ($\sim$6 cm^{-3} and $\sim$5 nT for protons at 1 AU) than in the fast wind ($\sim$2 cm^{-3} and $\sim$4 nT). The slow wind, however, has smaller thermal pressure ($\sim$6 versus $\sim$8 nPa) because it is colder ($0.8 \cdot 10^5$ versus $2 \cdot 10^5$ K) than the fast wind. The slow wind also cools down slower than the fast wind (cooling rates $\sim r^{-0.7}$ and $\sim r^{-1}$; Ebert et al., 2009).

2.1.1 Large-scale structures

Interplanetary magnetic field

The solar wind drags out coronal magnetic field with itself into interplanetary space. The interplay between plasma flow and magnetic field originates from the flow and field being frozen-in to each other due to the high conductivity of the corona, which results in convective effects controlling the temporal variations of the field (e.g. Schrijver & Siscoe, 2009; Kilpua & Koskinen, 2017). The interplay is regulated by the thermal (p) and magnetic (p_B) pressures relative to each other. In the lower

corona the magnetic pressure exceeds the thermal pressure of plasma (plasma beta $\beta = p/p_B = nk_BT/\frac{B^2}{2\mu_0} < 1$, where B and μ_0 are the magnitude of the magnetic field and the vacuum permeability) and the dynamics of the fluid are dominated by magnetic forces. The thermal pressure, however, increases towards the upper corona and finally takes over ($\beta > 1$) the control of fluid movements (Gary, 2001). The boundary at which the change in dominance approximately happens is called the source surface and modellers believe it is located at a distance of 2 – 2.5 R_S (e.g. Hoeksema et al., 1982). The source surface defines a boundary region below which the magnetic field is considered to form closed loops; on which the flow and field become close to radial; and above which the magnetic field is carried by the outflow out from the corona and has an open field configuration. This advection of the field forms the interplanetary magnetic field (IMF).

In interplanetary space, the IMF maintains its connectivity to the Sun and as a consequence of the solar rotation, the magnetic field acquires an azimuthal component. This field configuration was first modelled by Parker (1958) and it has a geometrical pattern known as Parker's spiral where magnetic field lines are defined by streamlines

$$\frac{1}{r}\frac{dr}{d\phi} = \frac{B_r}{B_\phi} = -\frac{u_r}{\Omega r \sin\theta}, \tag{2.2}$$

where ϕ and θ are the azimuth and polar angles of the spherical coordinate system centred at the Sun and Ω is the angular velocity of the Sun's rotation. These streamlines are sketched in Fig. 2.3a at different heliographic latitudes during a solar minimum when the Sun's dynamo generates a quasi-dipolar field. Red and blue curves in the figure illustrate magnetic field lines outwards and inwards the Sun, respectively. The Sun (orange sphere) is surrounded by a grey sphere, which gives the source surface. Beyond the source surface, the IMF has the pattern of Parker's spiral. Close to the Sun within the source surface, magnetic field lines still form closed loops that connect opposite magnetic polarities and form the so-called coronal streamer belt near the solar equator. The field, however, becomes less quasi-dipolar towards the poles and, in the vicinity of the streamer belt, at the intersection of closed and open field lines the dragged-out field forms a possible source region of slow solar wind.

Parker's solution (Parker, 1958) predicts a Parker's spiral angle – the deviation of the IMF direction from radial – of $\sim 45°$ for a solar wind speed of 400 km/s at 1 AU. This prediction coincides fairly well with observations as is seen in Fig. 2.3b, which gives probability distributions of observed Parker's spiral angle for different solar wind speeds at the Earth's orbit and their theoretical counterparts.

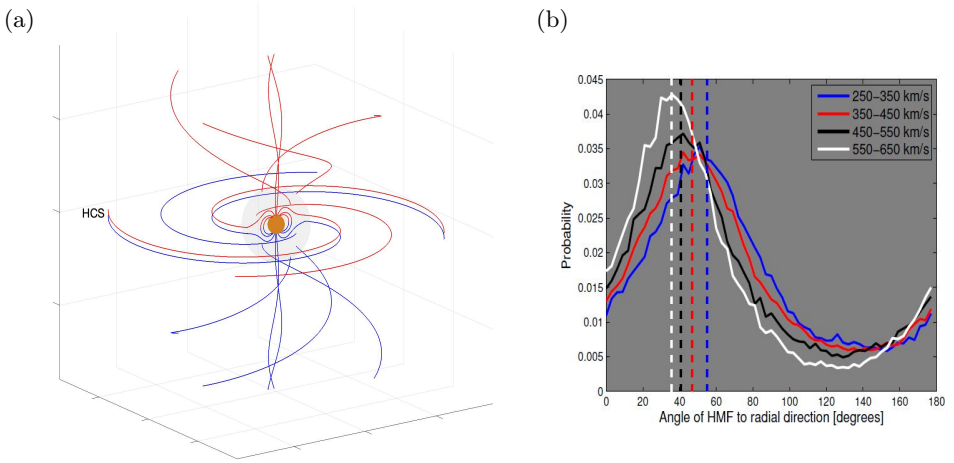

Figure 2.3: The interplanetary magnetic field. (a) A sketch of the time-independent interplanetary magnetic field (IMF). Magnetic field lines are shown by red (outwards the Sun) and blue (inwards) curves. Orange sphere and grey sphere illustrate the Sun and the source surface on which IMF is purely radial. Coronal streamer belt is illustrated inside the source surface, and heliospheric current sheet (HCS) is also exemplified in the figure. (b) Probability distributions of the Parker's spiral angle of the IMF at the Earth's orbit for different solar wind speeds. Dashed vertical lines indicate the angles according to Parker (1958). Heliospheric magnetic field (HMF) refers to the IMF. Panel (b) reproduced from a figure in Owens and Forsyth (2013).

The solution of supersonic solar wind becomes more complex than the introduced solution in Fig. 2.1a when the physics of frozen-in magnetic field is taken into account. Instead of one, there are three critical radii for the magnetic solar wind, which express the flow speed reaching the speed of slow, Alfvén and fast modes (Alfvén, 1942), which are the wave modes predicted by magnetohydrodynamics (MHD; e.g, Kilpua & Koskinen, 2017). The maximum speed of the slow mode is the sound speed. The Alfvénic critical point is defined as the distance from the Sun at which the flow speed equals the Alfvén speed ($v_A = B/\sqrt{\mu_0 n m_\mathrm{p}}$). The Alfvénic critical point of the solar wind is located at $\sim$25 R_S (Kasper & Klein, 2019) beyond which the flow is superalfvénic. Last at $\sim$26 R_S the solar wind exceeds the boundary of the magnetosonic speed ($v_{ms} = \sqrt{v_A^2 + u_c^2}$), which is the maximum speed of a magnetohydronamic wave. Flow speed with respect to wave speeds can be indicated by Mach numbers M_A and M_MS, which give the ratios of the flow speed to the Alfvén and magnetosonic speeds.

Heliospheric current sheet

As is seen in Fig. 2.3a, solar hemispheres are divided into the one dominated by inwards magnetic field and the one by outwards field during a solar minimum. In the vicinity of the solar equatorial plane, there is an abrupt change in the magnetic field direction as open field lines of opposite polarity are close to each other. According to Ampére's law a current sheet occurs between these oppositely directed field lines. This heliopsheric current sheet (HCS), discovered by Smith et al. (1978), is embedded in the so-called heliospheric plasmasheet characterised by an enhanced plasma beta due to an increased plasma density and diminished magnetic field strength (Winterhalter et al., 1994a; Smith, 2001). The HCS extends, similarly as the solar wind and IMF, from the tip of the streamer belt to the whole heliosphere.

The solar rotation and magnetic axes are, in reality, inclined relative to each other (e.g. Hanslmeier, 2007) with a varying tilt (e.g. Jones et al., 2003). This results in the HCS being an undulating structure, which is frequently crossed by an observer locating in the solar equatorial plane. Moreover, despite a polarity reversal during a 22-year solar magnetic cycle, the HCS is systematically coned southwards at times of solar minimum (Mursula & Hiltula, 2003). During a 11-year cycle in the Sun's activity, the structure of the HCS varies from the one described above to a more complex one that has multiple current sheets some of which can nearly reach the solar poles (Hoeksema et al., 1983).

Stream interaction regions

The tilt between the rotation and magnetic axes also causes the sources of the solar wind, coronal holes and the frontiers of open and closed field regions, to alternate at some circle of a constant heliographic latitude as the Sun rotates. As a consequence, successive periods of the slow and fast solar wind originate from the Sun along the radial flow lines. The fast wind catches up with the preceding slow wind, which results in a region of compressed magnetic field and plasma at a stream interface (SI). These regions of different solar winds interacting with each other are referred to as stream interaction regions (SIRs). The fast wind is, furthermore, followed by slow wind which cannot reach the fast wind. This causes a region with a rarefaction in field and density behind the fast wind. As the sources co-rotate with the Sun and are long-lasting, SIRs also display a similar Archimedean spiral as the IMF and

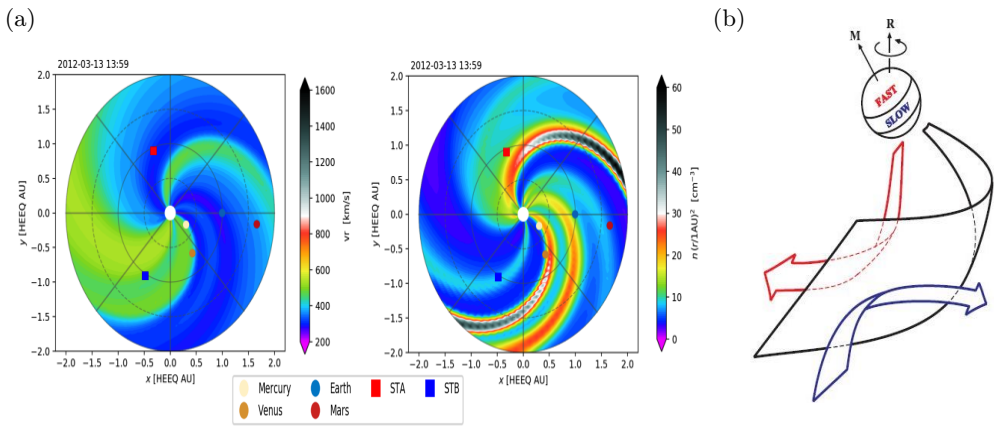

Figure 2.4: Stream interaction region. (a) Radial velocity and density of the solar wind in the inner heliosphere modelled by EUFHORIA (Pomoell & Poedts, 2018) in the Heliocentric Earth Equatorial (HEEQ) coordinates. Regions of higher and lower density associated to the alternation of different solar wind speeds indicate the presence of SIRs. Legends indicate the locations of different planets and the STEREO-A and -B spacecraft. (b) Solar wind flow deflection at a SI (surface bounded by black curves). The fast solar wind (red) is directed towards solar east and polewards and the slow wind (blue) towards west and equatowards with respect to the heliographic equator. Image credit of panel (a): Eleanna Asvestari. Panel (b) reproduced from a figure in Owens and Forsyth (2013; original construction by Pizzo, 1991).

show repeating occurrence at a given heliospheric longitude, which is why they are also known as co-rotating interaction regions (CIRs; Smith & Wolfe, 1976; Pizzo, 1991).

The IMF being frozen-in to the solar wind flow means that the connectivity between two plasma elements is conserved (Alfvén, 1943). As a consequence, the magnetically separated slow and fast wind plasma cannot pass through the SI and mix with each other. This results in disturbance waves which steepen into a forward shock propagating outwards from the Sun and reverse shock propagating towards the Sun, respectively (see Sec. 3.2 on shocks; Smith & Wolfe, 1976; Jian et al., 2006). The shocks deflect the flows along the interface and introduce non-radial components to the bulk solar wind flow (Owens & Forsyth, 2013), which diminish the aforementioned interaction between the slow and fast streams the interaction thus occurring mainly in the inner heliosphere close to the Sun (e.g. Burlaga, 1983; Schwenn, 1990; Balogh et al., 1999). The fast wind reaching the SI is decelerated

and directed along the interface towards solar east and polewards whereas the slow wind is accelerated and deflected towards solar west and the heliographic equator (Gosling et al., 1993). SIRs and deflection of solar wind flows against the SI are illustrated in Fig. 2.4.

2.1.2 Turbulence

The discussion in this thesis has so far considered the solar wind as a laminar flow. The flow is, however, sensitive to the development of local gradients, i.e. shear which generates eddies into the flow. Thus, the solar wind is a turbulent flow, i.e. it evolves non-linearly exhibiting rapid variations in fluid variables such as magnetic field, velocity and density (Schrijver & Siscoe, 2009). This thesis focuses on the magnetic field in which turbulence is often considered to occur due to shear induced by magnetic fluctuations counter-propagating relative to each other or to velocity shear in plasma flow with a frozen-in magnetic field (Bruno & Carbone, 2013). However, the non-linear evolution of Alfvénic waves is also argued to explain the turbulent characteristics (Tsurutani et al., 2018). In turbulence, energy injected into a flow on a certain spatial scale eventually spreads out into a wide range of smaller scales due to the non-linear dynamics of the flow. Turbulent fluctuations look irregular and quantities varying at a single point of a fluid are not predictable. The general aspect of the flow is however reproducible and, in terms of eddies, remains the same expressing some level of self-similarity, which is why turbulence is typically examined with a statistical description. An extensive review of turbulence is provided for example by Bruno and Carbone (2013).

Turbulence is often investigated by constructing a power spectral density (PSD) distribution of a studied variable. PSD implies the power of fluctuations at a certain frequency (f) and is given by the time average of the squared Fourier transformation of the variable. Figure 2.5 shows a PSD of magnetic field fluctuations of the solar wind observed at the Earth's orbit and it illustrates a turbulent process depicting its different relevant scales.

At very long temporal scales there is the so-called f^{-1} range, which is traditionally related to Alfvén waves propagating outwards from the Sun (e.g. Velli et al., 1989) and interpreted as the energy-containing range which drives the turbulence process. This energy is injected into the flow at the Sun and by large-scale transients, such as SIRs in which fast wind collides with the slow wind (Schrijver & Siscoe, 2009). Fluctuations on wavelengths above (lower frequencies) the correlation length λ_c

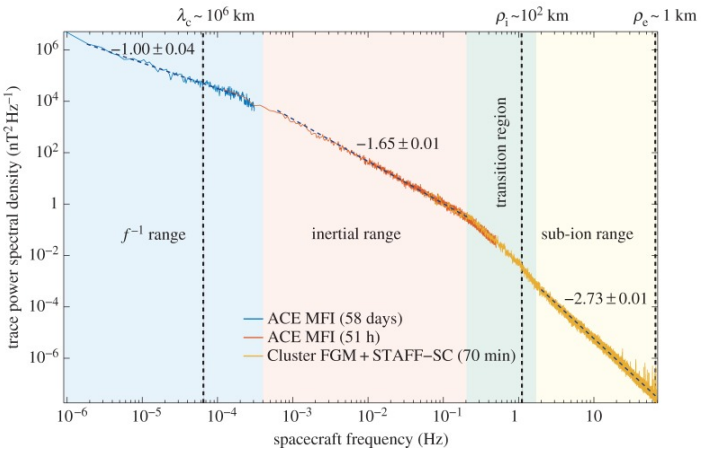

Figure 2.5: Total (trace) power spectral density of magnetic field fluctuations of the solar wind at 1 AU as a function of spacecraft frequency. Different colours of the data-based curve indicate the spacecraft measurements (ACE or Cluster) used to construct a specific part of the distribution. Shaded colours mark classical ranges of a turbulent fluid. Dashed lines at the top of the data-based curve give least-square fittings, whose slopes are given. λ_c indicates the correlation length and ρ_i and ρ_e the ion (proton) and electron gyroradii. Reproduced from a figure in Kiyani et al. (2015).

shown in Fig. 2.5 can still theoretically be traced to their origin. This does not apply to fluctuations below λ_c, which are rather a product of the in-situ dynamics. The correlation length namely gives the largest scale of energy containing eddies that in a turbulent process start to break up into smaller ones transporting energy into smaller scales (Kiyani et al., 2015).

Energy cascade refers to this energy being gradually transported into higher frequencies, which happens by turbulent eddies continuously breaking into smaller and smaller ones. The range of frequencies at which this cascade takes place is the inertial range indicated by salmon colour in Fig. 2.5. The inertial range has in hydrodynamics a spectral slope of $-5/3$ and is most often referred to as Kolmogorov turbulent cascade (Kolmogorov, 1962). This slope also appears in the magnetohydrodynamic solar wind. Within the inertial range, the dynamics of the fluid have lost information on an energy source and develop statistically in a scale-invariant manner. The low-frequency boundary of the inertial range is shifted towards lower frequencies suggesting that energy does transfer between scales and that the cascade develops as a function of distance from the Sun (e.g. Horbury et al., 2005).

Eventually energy is transported close to the scales that correspond to the proton gyroradius. This transition region is further followed by the sub-ion range at higher frequencies. These two regions are indicated by green and yellow in Fig. 2.5, respectively. Finally, the energy transportation also reaches the scales of the electron gyroradius. On the scales of particles' gyroradii, wave-particle interactions take over and energy is dissipated into particle heating, the Landau damping being an essential mechanism (Chen et al., 2019; see also Norqvist et al., 1996). This continuous turbulent heating of plasma particles is considered to explain the deviations from the adiabatic cooling discussed earlier (e.g. Vasquez et al., 2007a; Matthaeus & Velli, 2011; Montagud-Camps et al., 2018).

As mentioned earlier, the slow and fast solar winds cool down at different rates. Moreover, spectral break from the f^{-1} range to the inertial range is actually only observed for the fast wind (Bruno et al., 2009) suggesting, as stated by Yordanova et al. (2009), that the slow solar wind leaving the corona is already multi-scale, composed of waves and convected structures, which interact locally and therefore the turbulent dynamics of the slow wind differ from the one of the fast wind.

In addition, in both slow and fast winds there occur anisotropies, such as the perpendicular fluctuations being larger in amplitude compared to the parallel ones with respect to the background magnetic field (e.g. Belcher & Davis, 1971; Sari & Valley, 1976; MacBride et al., 2010). This so-called variance anisotropy tends to diminish at higher frequencies (e.g. Oughton et al., 2015). Moreover, there is an anisotropy in the turbulent energy in wavevector (k) space (e.g. Horbury et al., 2005). This anisotropy is known as the spectral anisotropy and reasoned by considering MHD turbulence with an occurrence of counter-propagating Alfvénic fluctuations (Iroshnikov, 1964; Kraichnan, 1965), the phase speed of which is $v_A \cos\theta_{kB}$ where θ_{kB} is the angle between k and the background magnetic field. Oppositely propagating waves interact with each other on a timescale that is proportional to $1/\cos\theta_{kB}$. When this timescale is smaller than the timescale of energy being transferred by non-linear effects, the energy transport within the inertial range is slowed down by wave propagation effects and a spectral slope of $-3/2$ is observed. This is known as Kraichnan-like turbulence (Kraichnan, 1965). The non-linear effects, however, dominate in plasma occupied by fluctuations that have the aforementioned timescale sufficiently large due to their propagation direction not being simply parallel or anti-parallel to the background magnetic field (see Oughton et al., 2004; Oughton & Matthaeus, 2005). This leads to the slope of a Kolmogorov-like

energy cascade. In the solar wind, most of the fluctuation energy is indeed in these fluctuations having a sufficiently large θ_{kB} and non-linear effects do control the energy transport (e.g. Roberts et al., 2017). Consequently, the solar wind typically has a slope of $-5/3$ within the inertial range as is shown in Fig. 2.5. Interestingly, according to observations reported by Tsurutani et al. (2018), these non-linear effects actually refer to the non-linear evolution of Alfvénic waves that experience phase-steepening and dissipate heating plasma particles. The authors moreover question the role of counter-propagating Alfvén waves. For a more detailed discussion see for instance Horbury et al. (2005) and Tsurutani et al. (2018), and references therein.

Furthermore, energy cascade might not be fully developed or turbulence contains intermittency, which both cause a spectral slope deviating from the ones of traditional theories of turbulence. In non-fully developed turbulence, aforementioned self-similarity does not exist yet whereas intermittency, spatial inhomogeneity in a turbulent energy cascade, results in fastened energy transport. Intermittency thus leads to steeper slopes and is a characteristic of solar wind turbulence (Marsch and Tu, 1997; see also Yordanova et al., 2008).

2.1.3 Solar wind regulation - plasma instabilities

In turbulence, as described in the previous section, magnetic energy transferred through the inertial range finally heats plasma particles on kinetic scales. Transfer of energy from particles, for example to a wave, does also happen in plasma. Indeed, energy accumulated in a non-equilibrium state can be transferred from particles to waves via wave-particle interaction mechanisms called plasma instabilities. This energy is known as free energy, a possible source of which are deviations from the isotropic Maxwellian distribution of particles (Hellinger et al., 2006). Temperature anisotropy, which refers to the temperature of particles being different for components parallel ($T_\parallel$) and perpendicular ($T_\perp$) to the background magnetic field, causes these deviations and occurs in the solar wind plasma (e.g. Hundhausen et al., 1967; Matteini et al., 2007). The discussion in this thesis is concentrated on the instabilities that are driven by a proton temperature anisotropy of $T_\perp > T_\parallel$ (see also Sec. 4.1 and Papers I and II for more detailed discussion). Protons are traditionally described in that case with a bi-Maxwellian distribution function

$$f(v_\parallel, v_\perp) = \sqrt{\frac{m_\mathrm{p}}{2\pi k_\mathrm{B} T_\parallel}} \frac{m_\mathrm{p}}{2\pi k_\mathrm{B} T_\perp} e^{-\left[\frac{m_\mathrm{p}}{2k_\mathrm{B}}\left(v_\perp^2 T_\perp^{-1} + v_\parallel^2 T_\parallel^{-1}\right)\right]}, \tag{2.3}$$

where $v_\parallel$ and $v_\perp$ are velocities parallel and perpendicular to the background

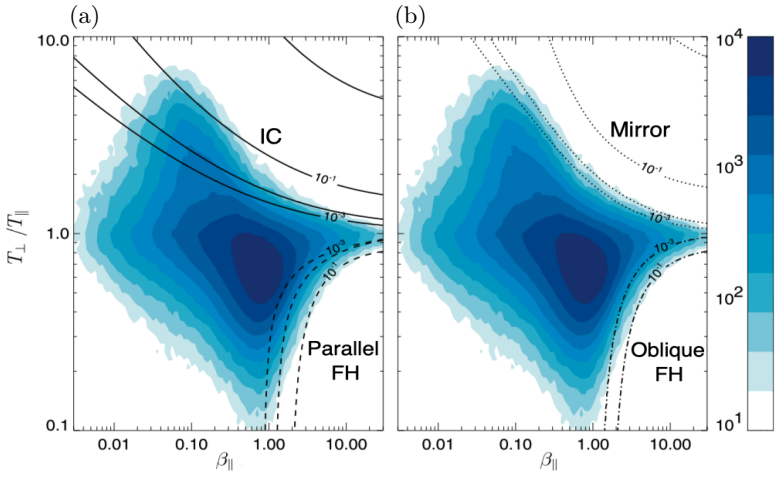

Figure 2.6: The relative frequency of the solar wind plasma with speed $\leq 600\,\mathrm{km/s}$ at 1 AU in proton ($\beta_\parallel$, $T_\perp/T_\parallel$)-space. The black curves indicate the contours of maximum growth rate (10^{-3} and 10^{-1}) for (a) the ion cyclotron (IC; solid) and parallel firehose (FH; dashed) instabilities, and (b) mirror (dotted) and oblique firehose (dash-dotted) instabilities. Adapted from a figure in Hellinger et al. (2006).

magnetic field.

Excess $T_\perp$ is known to drive the mirror (Hasegawa, 1969) and ion cyclotron (IC; Davidson & Ogden, 1975) instabilities, and the anisotropy required to trigger these instabilities is observed to depend on the parallel plasma beta ($\beta_\parallel = nk_\mathrm{B}T_\parallel/\frac{B^2}{2\mu_0}$). A commonly used (Yoon, 2017) relationship implying a marginal condition of instability is that of Hellinger et al. (2006)

$$\frac{T_\perp}{T_\parallel} = 1 + \frac{S}{(\beta_\parallel + \beta_0)^\alpha}, \tag{2.4}$$

where S, α and β_0 are empirical fitting parameters for different instabilities. Instability thresholds defined by the relation are plotted for different growth rates in Fig. 2.6 in proton ($\beta_\parallel$, $T_\perp/T_\parallel$)-space. The figure shows the thresholds not only for the IC and mirror instabilities but also for the parallel and oblique firehose instabilities, which are driven by excess $T_\parallel$. Plasma above or below these curves is considered to be unstable with respect to a given instability. Figure 2.6 furthermore illustrates the role instabilities have in astrophysical plasmas: a majority of the solar wind plasma is in a stable state because the instabilities regulate the shape

of particle distribution functions saturating the temporal unstable state of plasma. In other words, excess $T_\perp$ is dissipated by the IC or mirror instability by energy being transferred from protons to waves and thus plasma is kept in the state of marginal stability (see for instance Tsurutani et al., 1982). Consequently, the generated waves occurring in stabilised plasma manifest the activity of an instability.

Since both are driven by the same temperature anisotropy condition, the IC and mirror instabilities compete with each other (e.g. Remya et al., 2013). The IC instability tends to have a larger growth rate compared to the mirror instability under many space plasma conditions (Gary, 1992; Shoji et al., 2009) but theoretical suggestions and observations of the IC (mirror) instability dominating in low (high) beta plasma have been made (Lacombe & Belmont, 1995; Anderson & Fuselier, 1993; Gary et al., 1993). Growth rates are, furthermore, dependent on the composition and state of plasma. For example, helium ions present in plasma reduce the growth rate of the IC instability but do not effectively influence the mirror instability (Price et al., 1986). A substantial reduction in the growth rate of the IC instability also occurs in plasma having a temperature anisotropy of electrons ($T_{\perp e} > T_{\parallel e}$) whereas this increases the growth rate of the mirror instability (Lakhina & Buti, 1976). Recent research has moreover concluded that the electron temperature anisotropy and plasma beta are the dominant components determining which instability dominates in plasma (Remya et al., 2013, 2017a). Interestingly, the free energy available in plasma due to proton temperature anisotropy can eventually be mostly consumed only by the mirror instability because non-linear processes between protons and IC waves limit the growth of IC waves (Shoji et al., 2009). The mirror instability is therefore believed to be dominant for both the slow and fast solar winds (Hellinger et al., 2006).

2.2 Near-Earth space

The solar wind propagating in interplanetary space encounters the Earth and especially its magnetic field which is generated by electrically conductive fluid motion in the inner part of the planet. Here different plasma environments occupying the near-Earth space and the coupling between the solar wind and Earth's magnetic field, which drives space weather phenomena are introduced.

2.2.1 Earth's magnetosphere

The magnetic field of the Earth forms an obstacle for the IMF and solar wind flow because of the separate magnetic connectivities the two have (see the discussion of SIRs). This obstacle is referred to as the magnetosphere, which due to an interplay with the solar wind is not symmetrical: the Earth being the centre, the magnetosphere is compressed at the dayside – the side facing towards the Sun – and extended at the nightside – the side facing away from the Sun.

The outer boundary of the magnetosphere is defined by the surface where there is a pressure balance between the Earth's magnetic field and the solar wind. This boundary is the magnetopause and it deflects incoming protons and electrons of the solar wind in opposite directions and is thus a current layer carrying the so-called Chapman-Ferraro current (Chapman & Ferraro, 1931). At the dayside, the magnetopause is typically located approximately at a distance of 10 Earth radii ($R_E = 6371\,\mathrm{km}$) from the centre of the Earth (Cahill & Amazeen, 1963).

The characteristics of the solar wind flow propagating from the Sun with supermagnetosonic speed have to be modified for the solar wind to be able to flow around the magnetosphere. The bow shock (Gold, 1955; Sonett & Abrams, 1963; Ness et al., 1964) converts kinetic energy of the flow to heat and magnetic energy, and thus decelerates the solar wind to subsonic speeds. The decelerated subsonic flow is then able to deflect around the magnetosphere in the region called the magnetosheath. The location of the bow shock is dependent on how much the speed of the incoming solar wind exceeds the magnetosonic speed (Farris & Russell, 1994). Thus the width of the magnetosheath varies. Typically, the nose of the bow shock is located approximately at a distance of $14\,R_E$ from the centre of the Earth (e.g. Fairfield, 1971).

At both hemispheres of the Earth, there are polar cusp regions where magnetic field lines of the Earth diverge, bending to both dayside and nightside and exposing the Earth for a direct influence of the solar wind (e.g. Russell, 2000). The nightside magnetosphere – the magnetotail – extends to distances of $220\,R_E$ (e.g. Slavin et al., 1983) and consists of the northern and southern tail lobes, which have open magnetic field configurations mapped to polar caps at the Earth (Tsurutani et al., 1984a, 1984b). The lobes have opposite magnetic field orientations, and due to the change of polarity there is a current sheet – the tail current – which is embedded in the plasmasheet, the nightside part of the magnetosphere current system.

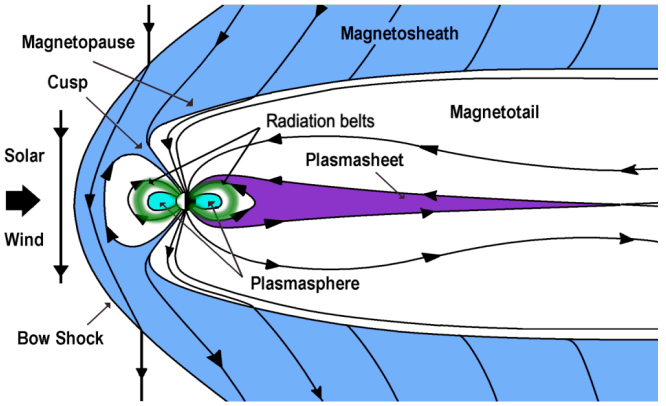

Figure 2.7: Sketch of the Earth's magnetosphere. Black solid lines illustrate field lines of the IMF and the Earth's magnetic field, arrows indicating the field direction. The solar wind flow is assumed to be purely radial. The magnetosheath, plasmasheet, plasmasphere and radiation belts are indicated by colours of blue, purple, cyan and green. Adapted from a figure in Grandin (2017).

In the inner magnetosphere, high-energy particles trapped in the Earth's magnetic field and their longitudinal gradient and curvature drifts (Koskinen, 2011) around the planet constitute the (inner and outer) radiation belts and ring current, respectively (van Allen and Frank, 1959; see also for instance Ripoll et al., 2020). In addition, there is a population of cold plasma which co-rotates with the Earth. This plasma forms the plasmasphere (Brekke, 2012). Figure 2.7 sketches the Earth's magnetosphere and aforementioned different structures and plasma environments.

2.2.2 Space weather

Space weather refers to configurational changes, or disturbances, that occur in the Earth's magnetic field and in magnetospheric plasmas due to solar activity and that may have several effects on different technological systems (see Ch. 1). These disturbances of the magnetosphere can last from several hours to a few days and their intensity is often defined in terms of geomagnetic indices, which are derived from ground-based magnetic observations which measure the configurational changes occurring in the Earth's magnetic field, i.e. geomagnetic activity (Bartels et al., 1939; Sugiura and Kamei, 1991; Gonzalez et al., 1994; see also Tanskanen et al., 2017a).

A major component for the generation of space weather disturbances is magnetic reconnection, which rearranges the topology of magnetic field lines and breaks down the aforementioned magnetic connectivity of plasma particles. The change in connectivity happens when two plasma domains of anti-parallel magnetic fields encounter each other. As the Earth's intrinsic magnetic field, also known as the geomagnetic field, is directed from the south pole of the planet to the north pole, i.e. the field is northward, southward IMF embedded in the solar wind flow is required to trigger magnetic reconnection at the sub-solar nose of the magnetopause. Reconnection opens the Earth's magnetic field by connecting the intrinsic field with the IMF (Dungey,1961; see also André et al., 2016). This results in particle fluxes from the solar wind into the inner magnetosphere. Furthermore, the opened field lines are carried by the the solar wind flow to the tail lobes, where magnetic field is accumulated and the plasmasheet between the lobes thins (see also Tanskanen et al., 2005a). Eventually magnetic reconnection triggers and rearranges the magnetic field into completely Earth-connected and Sun-connected domains in the magnetotail. These domains and particle fluxes ejected in the reconnection process are convected towards and away from the Earth, respectively. This cycle of dayside reconnection resulting in magnetic flux being convected to the nightside where reconnection ejects a particle flux that transports magnetic field back to Earth and dayside magnetopause is known as the Dungey cycle (Dungey, 1961). The magnetic field directions of the description above are illustrated in Fig. 2.7.

Reconnection on the dayside magnetopause results in solar wind particles having a direct access to the inner magnetosphere along the open magnetic field lines that have one footpoint at the Earth and one at the Sun whereas reconnection at the nightside ejects a particle flux towards the Earth, which enhances the ring current around the planet. These variations in the plasmas of the inner magnetosphere may also result in magnetic activity near the surface of the Earth at high latitudes (e.g. Birkeland, 1908; Axford & Hines, 1961; Boteler et al., 1998).

Drivers of space weather

Geoeffective solar wind transients are large-scale structures embedded in the solar wind that drive space weather disturbances. These drivers have periods of southward IMF, which enable efficient energy transfer from the solar wind to the magnetosphere and often also high dynamic pressure which compresses the whole magnetosphere (e.g. Fenrich & Luhmann, 1998; Tanskanen et al., 2005b).

Stream interaction regions (SIRs, Sec. 2.1) are recurrent drivers of space weather, which have a ∼27 day periodicity due to the solar rotation. SIRs are typically associated with fluctuating IMF direction (Lindsay et al., 1995) and they mainly drive weak or moderate space weather disturbances (e.g. Tsurutani et al., 2006) that strongly enhance energetic particle fluxes in the outer radiation belt (Miyoshi & Kataoka, 2005). SIRs are most common during the declining phase of a solar cycle towards its minimum of activity (e.g. Chi et al., 2018; Grandin et al., 2019).

Interplanetary coronal mass ejections (ICMEs) are interplanetary counterparts of CMEs, gigantic eruptions of plasma and magnetic field from the Sun (e.g. Kilpua et al., 2017). The details of CME eruption mechanisms are not completely understood but an interplay of magnetic field and plasma including magnetic reconnection and an action of instability that instantly converts a vast amount of magnetic energy into kinetic energy is considered to be present (Webb & Howard, 2012). An ICME, whose ejecta has a speed relative to the ambient solar wind that exceeds the local magnetosonic speed, consists of a leading shock, sheath region, and magnetic ejecta itself out of which especially the shock and sheath are discussed in detail in the next chapter. All parts of an ICME are strong drivers of space weather at the Earth (e.g. Tsurutani et al., 1988; Huttunen et al., 2002; Huttunen & Koskinen, 2004) and periods of southward IMF are regularly embedded in both sheath and ejecta (e.g. Lindsay et al., 1995; Kilpua et al., 2017). ICMEs are in fact the most significant drivers of intense space weather effects and they generate strong global magnetic perturbations in the magnetosphere (e.g. Gosling et al., 1991). ICMEs are non-recurrent drivers, whose occurrence tracks the solar cycle and which are most frequent during a solar maximum (Richardson & Cane, 2012).

3 Shocks and sheath regions driven by ICMEs

ICME ejecta are magnetically confined transients in interplanetary space whose speed relative to the ambient solar wind regularly exceeds the local magnetosonic speed (e.g. Burlaga et al., 1982; Gopalswamy et al., 2001; Kilpua et al., 2017). Thus, in a similar way as when encountering the Earth's magnetosphere, the solar wind is decelerated (in the frame of the ICME ejecta) by a shock when encountering the obstacle the ejecta forms. ICME-driven sheath regions are plasma environments of a submagnetosonic and compressed solar wind flow between the shock and driving magnetic ejecta within which the flow is deflected around the ejecta. This chapter gives an overview of ICME sheaths and it contains discussion on relevant processes influencing the sheath plasma such as the expansion of ICME ejecta and shock physics.

3.1 Characteristics of ICME sheaths

An ICME sheath, preceding shock and driving ejecta are sketched in Fig. 3.1a, and spacecraft measurements of an ICME event are shown in Fig. 3.1b. The figure illustrates large fluctuations of magnetic field and plasma parameters within the sheath, and the transition across the shock, which results in the compression of plasma and magnetic field. The solar wind speed increases drastically from the solar wind to the sheath ($\sim$400 km/s) but so does the magnetosonic speed due to the compressed magnetic field and increased temperature (see Sec. 2.1). It is important to note that the measurements are given in the spacecraft frame of reference and the flow in the sheath is submagnetosonic in the ejecta frame of reference. In addition, the interface between the sheath and ejecta shows a drop in density exemplifying the characteristic of magnetic confinement of the ejecta.

ICME sheaths have characteristics of both propagation and expansion sheaths. Propagation sheaths are sheath regions discussed so far in this thesis in which the solar wind deflects sideways at the nose of the obstacle, flows around the obstacle and finally leaves it behind. Expansion sheaths do not propagate with respect to the surrounding solar wind but expands, which causes plasma not flowing around but piling up all around the driver (Siscoe & Odstrcil, 2008). ICME sheaths expand due to the lateral expansion of the ICME ejecta (e.g. Riley & Crooker, 2004; Schwenn et al., 2005) which maintains its angular width constant in interplanetary space (e.g.

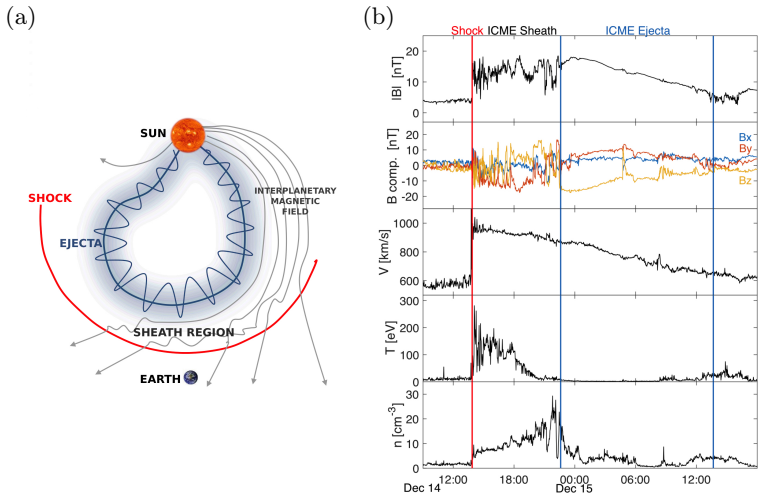

Figure 3.1: Interplanetary coronal mass ejection. (a) Sketch of an ICME. The ICME is driven by a magnetically confined ejecta, which drives a preceding shock and sheath region. (b) An ICME observed by the Wind spacecraft on December 15, 2006. The panel shows the measurements of magnetic field magnitude ($|B|$), magnetic field components, speed (V), proton temperature (T), and proton density (n). Panel (a) reproduced from a figure in Kilpua et al. (2017).

Burlaga et al., 1981; Bothmer & Schwenn, 1998; Russell & Mulligan, 2002; Moore et al., 2007). The expansion happens because of the internal pressure of the ejecta being larger than that of the ambient solar wind. The lateral expansion of an ICME ejecta, furthermore, happens faster than its radial expansion (Klein & Burlaga, 1982; Russell & Mulligan, 2002; Liu et al., 2006a; Nieves-Chinchilla et al., 2018). The radial expansion presumably occurs also due to the aforementioned pressure gradient or alternatively due to different speeds of leading and trailing edges of the ejecta. Pure expansion sheaths can occur when an ICME ejecta has similar speed to that of the solar wind and it expands radially driving compressive waves which can steepen into a shock. ICME sheaths being pure expansion sheaths have occurred at high heliographic latitudes simultaneously with the fast solar wind (Gosling et al., 1998).

The majority of ICME sheaths, however, are combinations of propagation and expansion sheaths and non-radial flows, which result from deflections around the ejecta, are commonly observed (Owens & Cargill, 2004). Because of the expansion, this deflection around the ejecta actually happens slower than the speed of the leading edge of an ICME ejecta as an individual factor implies. Consequently,

plasma tends to accumulate along the face of the body of the propagating ejecta. The deflection speed has its maximum towards the sheath flanks but does not exceed the lateral expansion speed near the nose of the ICME (Siscoe & Odstrcil, 2008). Due to the accretion, ICME sheaths can contain layers of plasma and magnetic field at the back of the sheath, which retain the record of interactions happened at different distances from the Sun (Kaymaz & Siscoe, 2006; Siscoe & Odstrcil, 2008). This allows an interpretation that, for example, large fluctuations within an ICME sheath originate from SIRs or the HCS being swept by the ICME. Possible dynamical processes, such as magnetic reconnection at the interface of the sheath and the ejecta leading edge (e.g. Wei et al., 2006), can however significantly modify the sheath plasma. The accumulation nevertheless results in an ICME sheath increasing its radial width as an ICME propagates in interplanetary space. This increase is directly proportional to the relative speed difference of the driver and the ambient solar wind, inversely proportional to the compressibility of plasma, and reduced by a three-dimensional expansion which spreads plasma out within a sheath (Siscoe & Odstrcil, 2008). In addition, there is also a dependency on the shape of the driver (e.g. Russell & Mulligan, 2002).

The lateral expansion of an ICME is illustrated in Fig. 3.2, which shows MHD simulations of the evolution of an ICME ejecta that is modelled as a flux rope. A flux rope is a magnetic structure that is typically cylindrically symmetric and in which helical magnetic field is twisted around the axial field at the central axis of the structure (Marubashi, 1986; Burlaga, 1988). Contours in the figure indicate radial velocity (colour) and density ((a) black; (b) red) of the solar wind plasma, and the magnetic field magnitude of the ejecta ((a) blue; (b) black). The figure exemplifies the evolution of an ICME sheath in large scale and the topic is further discussed in Sec. 4.2 (Paper IV).

Figure 3.2a shows the evolution of the ICME ejecta and sheath from the solar corona to a distance of $\sim$0.5 AU from the Sun and captures the gradual development of the ICME. Namely, the magnetosonic speed is very high near the solar corona due to low plasma beta and it decreases as a function of heliospheric distance simultaneously with the temperature and magnetic field magnitude of the solar wind (e.g. Tsurutani et al., 2003; Ebert et al., 2009). Thus, only very fast ejecta can drive a shock already in the corona. For example, in the study by Ontiveros and Vourlidas (2009) shocks driven by a CME were observed in the corona when the speed of the CME exceeded 1500 km/s. As the average speed of CMEs is $\sim$500 km/s (e.g. Yashiro et al., 2004), a significant proportion of shocks and sheaths are, however, formed

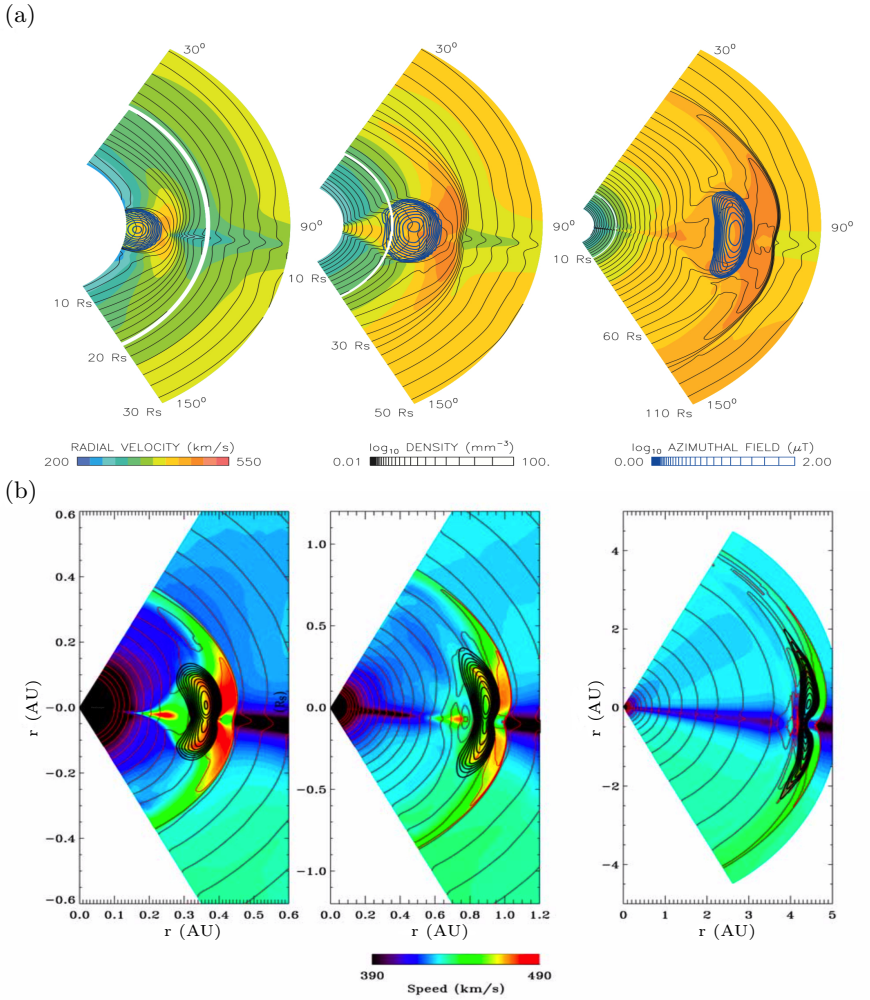

Figure 3.2: MHD simulations of the evolution of a flux-rope like ICME ejecta. (a) Evolution of the ejecta from the solar corona to ∼0.5 AU (1 AU ∼215 R_S) with an extent of ±60° in heliographic latitude and, from left to right, 30, 50 and 110 R_S in radial distance from the Sun corresponding to times of 292, 304 and 320 hours after the start of the simulation. The contours indicate the radial velocity (colour) and density (black) of heliospheric plasma, and azimuthal (out-of-plane) magnetic field of the ejecta (blue). The white solid line in the left and central snapshots indicate the boundary of coronal and heliospheric models used in the simulation. (b) Evolution of ejecta in the heliosphere snapshots having, from left to right, radial extents of 0.6, 1.2, and 5 AU from the Sun giving the times of 312, 360, and 696 hours after the start of the simulation. All snapshots have a latitudinal extent of ±60°. The contours indicate the radial velocity (colour) and density (red) of heliospheric plasma, and magnetic field of the ejecta (black). Reproduced from figures in Riley et al. (2003).

beyond the corona where the CME is referred to as an ICME. Figure 3.2a does not unambiguously imply whether the shock and sheath exist in the first snapshot of the simulation but illustrates the deepening of the density, which appears as an abrupt change in the final snapshot. Furthermore, the initially circular cross section of the ejecta becomes elliptical and finally exhibits a convex outward shape. A region of accumulated compressed plasma, which has high velocity compared to the ambient solar wind speed, is also observed in front of the ejecta and its radial width increases with the distance from the Sun.

In Fig. 3.2b, the colour scale clearly indicates a sheath and shock preceding the ejecta marked by black magnetic field contours. Plasma accumulates in front of the ejecta, which in the beginning has a convex outward shape. The piled-up region increases its width from $\sim$0.04 to $\sim$0.1 AU between the first two snapshots. The radial and longitudinal widths of the ICME sheath in the middle snapshot of Fig. 3.2b represent the average values of 0.13 AU (Kilpua et al., 2017) and $\sim$1 AU (Liu et al., 2006a), respectively, observed at 1 AU. The centre and last snapshots display an ejecta and shock interface that both have a concave outward shape. This is a typically observed shape of an ICME during a solar minimum, when the source regions of the slow and fast solar winds are most distinct (e.g. Liu et al., 2006a). Slow and dense wind originating near the solar equator resists the expansion of an ICME due to larger dynamical pressure compared to less dense and faster wind at higher heliographic latitudes. This causes the formation of a dimple, which is apparent in Fig. 3.2b. In turn, ICMEs during a solar maximum maintain a convex outward bent shape because of their radially even expansion, which happens due to the less structured origins of the fast and slow solar winds over different latitudes (Odstrčil et al., 1996; Liu et al., 2006a).

3.2 Shocks

In interplanetary space the magnetosonic speed is lower than in the corona and ICMEs are more prone to drive shocks. At the orbit of the Earth approximately 56% of ICMEs have preceding shocks (Lepping et al., 2015). ICME shocks are fast forward shocks, i.e. fast magnetosonic waves that have steepened into a shock that propagates in the same direction as its driver (away from the Sun; Tsurutani et al., 2011b).

In general, interplanetary shocks are plasma discontinuities that abruptly increase the thermal and magnetic energies of the solar wind at the expense of the flow energy. Thus, there is a mass flow and consequently also a magnetic field permeation across a shock interface. The more supermagnetosonically an ICME ejecta propagates relative to the preceding solar wind, the more flow energy has to be converted to thermal and magnetic energies by a shock to enable submagnetosonic diversion around the obstacle an ejecta forms. This determines the strength of a shock, which is given by the upstream magnetosonic Mach number (M_{MS}), i.e. the ratio of the solar wind flow speed to the magnetosonic speed in the shock frame of reference. Shocked plasma is referred to as the downstream whereas the flow encountering a shock is upstream.

The conservation of mass implies that the density of decelerated plasma is increased in a shock passage. A fast forward shock in interplanetary space also compresses the IMF (see Fig. 3.1), and precisely its component transverse to the shock normal. The conservation of mass, momentum and energy of a magnetohydrodynamic fluid namely predicts that the magnetic field maintains its component parallel to the shock normal constant in a shock crossing but the perpendicular component is compressed. Thus, the perpendicular component maintains its sign but the field is bent away from the shock normal towards the plane of the shock surface. The bending satisfies the coplanarity theorem according to which the upstream magnetic field direction and shock normal define a plane that determines possible directions of downstream magnetic field (Kivelson & Russell, 1995). Consequently, an upstream magnetic field solely perpendicular to the shock normal is compressed by the shock but there is no field rotation at all through the shock whereas in the case of parallel upstream field, the magnetic field is unmodified by the shock and maintains its magnitude and direction in the downstream. A parallel upstream field is however in the downstream prone to strong turbulence (Kennel et al., 1984a, 1984b). Shock geometry affecting shock physics is typically indicated by the shock angle (θ_{Bn}), which gives the angle between upstream magnetic field and the shock normal and is 0° (90°) for a solely parallel (perpendicular) shock. Shocks having intermediate θ_{Bn} are called quasi-parallel or -perpendicular shocks based on having either $\theta_{Bn} < 45^\circ$ or $\theta_{Bn} > 45^\circ$.

The aforementioned relations indicating the conservation of mass, momentum and energy (so-called Rankine-Hugoniot conditions) predict the changes in plasma across a shock within the limits of MHD. These relations, however, do not describe the shock physics of the collisionless solar wind plasma, whose understanding requires

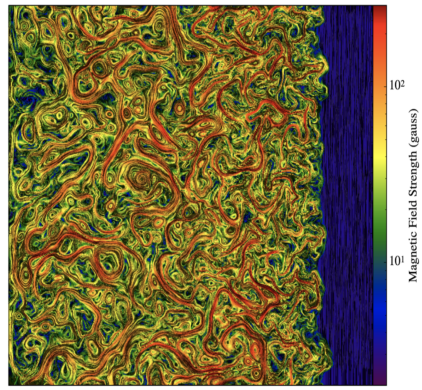

Figure 3.3: Turbulent downstream of a shock. Magnetic field magnitude (strength) of a MHD simulation of plasma that crosses a shock in the high Mach number limit. The magnitude is given in gauss (1 gauss = 10^{-4} T) and indicated by the colour scale. Reproduced from a figure in Ji et al. (2016).

consideration of plasma particles on kinetic scales.

Shock heating and acceleration

Energy is dissipated in a shock crossing, which means that irreversible processes in action finally result in an increase in entropy. Collisionless shocks have a gradually progressing energy dissipation process in which the flow is first decelerated and flow energy is converted into thermal energy (e.g. Kennel et al., 1985). This thermal energy is further scattered in waves and turbulence, which eventually ensures the dissipation (e.g. Kajdič et al., 2012; Pitňa et al., 2017). Turbulent downstream of a shock is illustrated in Fig. 3.3, which is based on an MHD simulation. In a shock crossing, plasma is intuitively decelerated by the electric field that originates from a charge separation at the shock. This electric field is formed because protons encountering a shock penetrate deeper into the shock than electrons due to their much larger inertia. The consequent electric field accelerates electrons and decelerates protons. Those protons that have enough parallel energy with respect to the shock normal are decelerated and heated by Joule heating passing down into the downstream.

Electrical resistivity, however, does not always provide enough heating and additional mechanisms have to occur. A mechanism providing additional heating of

protons is shock drift acceleration, which is exemplified in Fig. 3.4. Shock drift acceleration (e.g. Pesses et al., 1984) is based on the heating resulting from the conservation of the first adiabatic invariant, which refers to the magnetic momentum (μ) remaining constant. Because of the constant μ, the relation $p_\perp^2/B$, where $p_\perp$ is the perpendicular thermal pressure with respect to the magnetic field, remains also constant and the perpendicular heating of plasma resulting from an increase in magnetic field density is betatron acceleration. In shock drift acceleration, a proton population of low velocities parallel to the shock normal first drifts towards the shock by a convective electric field, then along the shock surface due to the magnetic field gradient drift and eventually it ends up in downstream. While drifting along the shock surface, gyromotion around the magnetic field results in protons crossing the shock multiple times. Protons are repeatedly accelerated by the convective electric field in the upstream and decelerated in the downstream. The acceleration, however, exceeds the deceleration because protons spend a longer time in the upstream due to a larger gyroradius. The gained energy is stored in their gyromotion. This appears as increased proton temperature anisotropy $T_\perp/T_\parallel$ in the downstream (Schrijver & Siscoe, 2009), which further provides a source of free energy. This free energy drives the generation of waves and turbulence, which eventually enable the dissipation. The anisotropy in the downstream is greater the more perpendicular the shock is, which is also observed in Paper I in the case of ICME-driven shocks. Shock drift acceleration indeed accelerates particles particularly in quasi-perpendicular interplanetary shocks (Hanson et al., 2020), because a convective electric field parallel to the shock surface accelerating particles is the weaker the more parallel the magnetic field is to the shock normal. In addition, the magnetic field is not compressed in parallel shocks and consequently there is no difference in gyroradius in upstream and downstream.

Successive scattering of protons from solar wind irregularities and waves in both upstream and downstream of a shock results in diffusive shock acceleration. Particles being scattered at both upstream and downstream experience Fermi acceleration, which results from the conservation of the second adiabatic invariant according to which the longitudinal invariant $J = \oint \mathrm{p}_\parallel ds$, where $\mathrm{p}_\parallel$ is the parallel momentum with respect to the magnetic field and the integral is taken over a scattering circuit of a particle, remains constant. The scattering circuit of particles decreases when scattering centres in the upstream approach the shock faster than the centres in the downstream get drawn away from it. Consequently $\mathrm{p}_\parallel$ has to increase for J to remain constant. There is a total increase in the energy of particles because the energy gain in head-on wave-particle interactions, or collisions, in the upstream is

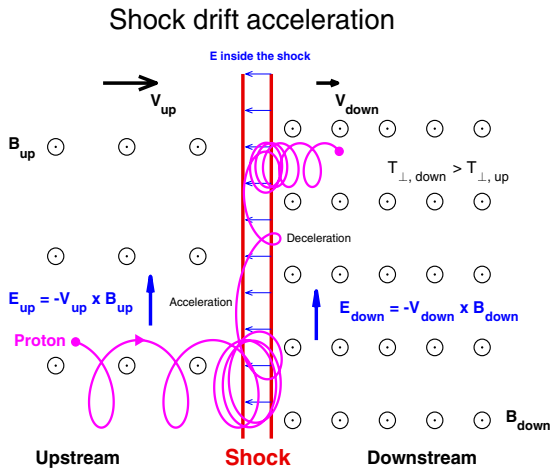

Figure 3.4: Shock drift acceleration. An exemplification of the trajectory of a gyrating proton that experiences shock drift acceleration. Electric field inside a shock resulting from a large difference in the inertia of encountering protons and electrons is illustrated in the figure. Up and down refer to upstream and downstream. The magnitude of the convectional electric field does not change from upstream to downstream because while the flow speed decreases, the magnetic field is compressed across the shock.

larger and than the loss in trailing collisions in the downstream. Diffusive shock acceleration occurs especially when the shock is quasi-parallel because it enables particles crossing a shock relative easily (e.g. Rice et al., 2003; Blanco-Cano, 2010).

Some of the protons encountering a shock get back to the upstream after being accelerated by the shock. These protons are referred to as reflected protons and they can eventually enter the downstream because of being convected back to the shock by the solar wind flow or because of being scattered from irregularities of the turbulent solar wind plasma (Kallenrode, 2004). Protons encountering a shock again are exposed to additional heating. When these reflected protons that participate in the dissipation are present, a shock is called supercritical (Kennel, 1987). Such shocks cover ∼33-50% of ICME shocks (Bavassano-Cattaneo et al., 1986; Zhou & Smith, 2015), and reflected protons occur in the upstream of both quasi-perpendicular (e.g. Sckopke et al., 1990) and quasi-parallel shocks (e.g. Gosling et al., 1982). In the case of a quasi-perpendicular shock, the gyromotion around the magnetic field prevents reflected protons from escaping from the immediate vicinity of the shock and they return to the shock within one gyro-orbit whereas when a shock is quasi-parallel reflected protons can escape further upstream along the magnetic field. Protons

reflected at a quasi-parallel shock form the so-called foreshock region within which they initiate wave growth (e.g. Greenstadt et al., 1995). Foreshock regions of ICME-driven shocks extend to distances of $0.02 - 0.1$ AU upstream from the shock (Kajdič et al., 2012) and have also reported to occur in front of quasi-perpendicular ICME shocks (Blanco-Cano et al., 2016).

Particles that are accelerated to high energies by a shock and emitted permanently far upstream can constitute populations of solar energetic particles (SEPs), which travel along the IMF. Because of their high energies, they are not convected back to the shock. Populations of SEPs accelerated by interplanetary shocks are referred to as gradual SEP events and they can drive space weather disturbances at the Earth (e.g. Kahler, 2001).

3.3 Sheath magnetic fields

Compressed magnetic fields embedded in ICME-driven sheath regions exhibit large directional variations with respect to the field in the preceding solar wind (Fig. 3.1b), the background field being draped around the driving ejecta (Fig. 3.1a). The magnetic field magnitude can also show relatively large variations as is seen in Fig. 3.5a. Furthermore, the level of fluctuations measured by the root-mean-square of the magnetic field (B_{RMS}) in Fig. 3.5b is particularly high immediately downstream of the shock and it remains higher than the corresponding values of the preceding solar wind and trailing ICME ejecta throughout the whole sheath. Because of the decreasing trend of the B_{RMS} shown in Fig. 3.5b, fluctuations in ICME sheaths could be interpreted to manifest the gradual energy dissipation process which ensures an irreversible shock crossing of the solar wind plasma: different electromagnetic waves propagating relative to each other are first generated at the downstream of the shock after which shear between these waves initiates turbulence, which results in dissipation and damping of the waves (see also discussion on the non-linear evolution of Alfvénic waves by Tsurutani et al., 2018). Sheath magnetic fields thus display turbulent nature (see Fig. 3.3), fluctuations being ubiquitous in the sheath.

The above interpretation implies that shocks have an essential role in the generation of magnetic fluctuations in ICME sheaths. Ultra-low frequency (ULF, $\sim 10^{-3} - 10^{0}$ Hz; Greenstadt et al., 1995) waves, which in general refer to waves with frequencies below the natural frequencies of plasma such as plasma frequency and proton gyrofrequency, do occur in the immediate downstream of an ICME shock

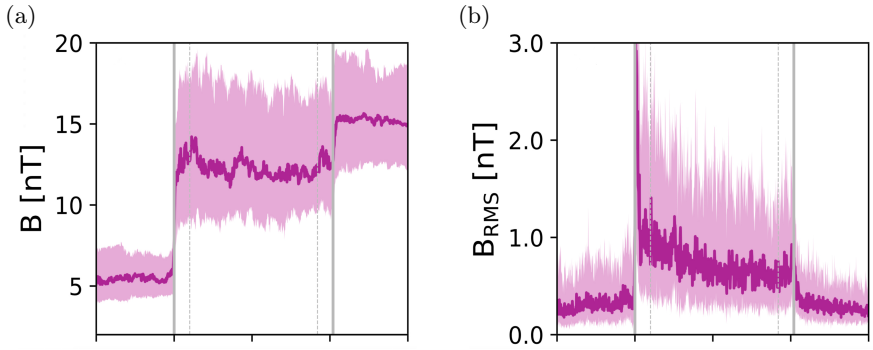

Figure 3.5: ICME sheath magnetic fields. Average variation of (a) magnetic field magnitude and (b) the root-mean-square of magnetic field vector (B_{RMS}) of 89 ICME sheaths observed between 1989-2018. The dark purple curves indicate the medians and shaded regions are bounded by upper and lower quartiles. Shock and ejecta leading edge are marked by grey solid lines. The beginning and ending of sheaths, which are the regions between the solid and dashed grey lines, had higher sampling rate than rest of the data. Adapted from a figure Kilpua et al. (2019a).

(Kajdič et al., 2012; see also Russell et al., 2009). And more precisely, specific waves within the ULF bandwidth such as mirror mode and ion cyclotron waves (e.g. Soucek et al., 2015) have the highest occurrence in the ICME sheath near the shock (Papers I and II). These observations coincide with the power of magnetic field ULF fluctuations being the highest near the shock, in the leading part of the sheath (Kilpua et al., 2013). Moreover, the power of ULF-range fluctuations in the sheath is higher the stronger the shock is and when the shock is quasi-perpendicular (Moissard et al., 2019).

As mentioned in Ch. 1, there are still relatively few studies on fluctuations and waves in ICME-driven sheath regions. However, there is a large amount of literature based on both observations and simulations dedicated to planetary magnetosheaths (for instance see Fairfield, 1976, for the early literature on magnetosheath magnetic fields and discussion of the origin of their fluctuations). Although planetary magnetosheaths are pure propagation sheaths, the results on them can be applied to interpret and discuss discoveries in ICME sheaths. ICME sheaths have many characteristics of propagation sheaths (see Sec. 3.1) and in both cases it is the solar wind plasma and field that is processed by a shock. Simulations of the Earth's magnetosheath with steady-state upstream solar wind (e.g. von Alfthan et al., 2014) for instance imply the shock indeed has an essential role as noted above (see also Winske et al., 1990; Scholer et al., 1997).

The studies of planetary magnetosheaths have demonstrated that there are also other ways to generate fluctuations in the sheath than processes occurring at the shock. For example, fluctuations pre-existing in the upstream solar wind can be convected trough the shock to the downstream in the magnetosheath (Fairfield, 1976). Observations in the vicinity of the Earth (e.g. Rakhmanova et al., 2015) have shown that fluctuations having frequencies low enough ($\lesssim 10^{-2}$ Hz) may be transmitted from the solar wind upstream into the magnetosheath, while higher frequencies are exposed to strong modification by a shock crossing and processes in downstream (see also Yumoto et al., 1984). The transmission of such low-frequency fluctuations is also supported by observations for ICME sheaths where large power of solar wind fluctuations in the ULF range preceding the shock is related to higher power of fluctuations in the sheath (Moissard et al., 2019). Rakhmanova et al. (2015) further noted that fluctuations of larger amplitudes embedded in a solar wind that is dense and has high IMF magnitude penetrate a shock experiencing relatively less modification that is, interestingly, independent from the shock angle. However, the probability of fluctuations in an ICME sheath having a solar wind origin is likely dependent on the location of the shock passage and also on the heliospheric distance (Fig. 6 in Paper III, and Paper IV). A quasi-perpendicular shock namely bends and compresses the IMF more than a quasi-parallel shock, the latter thus being presumably more favourable for pre-existing solar wind fluctuations to pass the shock. The downstream of a quasi-parallel shock is however highly turbulent and fluctuations may actually last longer in the downstream of a quasi-perpendicular shock. The amplification across a quasi-perpendicular shock of southward IMF is in fact argued to explain the geoeffectiveness of ICME sheaths (Tsurutani et al., 1988; Meng et al., 2019).

Sometimes waves pre-existing in the upstream can have a shock-based origin. Namely, ULF waves excited by the reflected ions in the Venusian foreshock are observed to transfer from the upstream to the downstream through the bow shock under quasi-parallel conditions (Shan et al., 2014; see also Blanco-Cano et al., 2006). Corresponding conclusions have not yet been made regarding ICME shocks, but higher-frequency (> 1 Hz) whistler waves occur in both immediate upstream and downstream of an ICME shock (Kajdič et al., 2012, see also Tsurutani et al., 1983).

Magnetic field fluctuations may also be generated within an ICME sheath. For example, the energy stored in temperature anisotropy of protons at the shock might generate magnetic waves later further away from the shock, which manifests the

gradual energy dissipation process. This again emphasises the role the shock has. As was discussed earlier above and in Sec. 2.1, fluctuations also emanate from turbulence, which is ubiquitous in an ICME sheath due to fluctuations already present propagating relative to each other.

Turbulence in an ICME sheath can furthermore be driven by the ICME ejecta. The power of fluctuations in the sheath correlates with the speed of ICME ejecta (Kilpua et al., 2013; Moissard et al., 2019) and thus, as suggested by Moissard et al. (2019), the ejecta driving a shock and sheath in front of it has an imprint in the sheath. This imprint appears as powerful magnetic fluctuations being generated when the kinetic energy of the ejecta is dissipated in turbulent processes in the sheath. Support to this interpretation is provided by the examination of an ICME ejecta observed by the Parker Solar Probe spacecraft at $\sim$0.25 AU. The magnetic field measurements during the event are shown in the upper panel of Fig. 3.6a. The ICME ejecta shown in the figure was not associated with a preceding shock but was preceded by a velocity gradient, which might have eventually steepened to a shock. The lower panel of Fig. 3.6a, however, shows that the ejecta was preceded by a region occupied by magnetic fluctuations. These fluctuations propagated away from the Sun as is implied by Fig. 3.6b, which shows the normalised cross helicity (σ_c; see Tanskanen et al., 2017b) which indicates the balance or imbalance of power in wave packets propagating parallel (negative σ_c) or anti-parallel (positive σ_c) to the background magnetic field (Good et al., 2020). As the background magnetic field was directed towards the Sun, positive σ_c seen in Fig. 3.6b implies that the fluctuations right ahead of the ejecta were indeed propagating away from the Sun and thus away from the ejecta. As stated by Good et al. (2020), the origin of these fluctuations was likely in ejecta–solar wind interaction. Consequently, in an ICME sheath, these wave packets propagating from the ejecta leading edge towards the preceding shock drive turbulence due to their evolution and due to being exposed to shear when moving relatively to wave packets propagating in the opposite direction.

Field line draping and planar magnetic structures

Fluctuations are embedded in the background sheath magnetic field, which is draped around the ejecta. This draping is caused by non-radial flows, which manifest the deflection of the solar wind plasma around the magnetically confined ejecta (Gosling & McComas, 1987; McComas et al., 1988), and it happens qualitatively similar to field line draping in the Earth's magnetosheath (Kaymaz & Siscoe, 2006). Figure 3.7 illustrates the basic principle of magnetic field draping in the equatorial

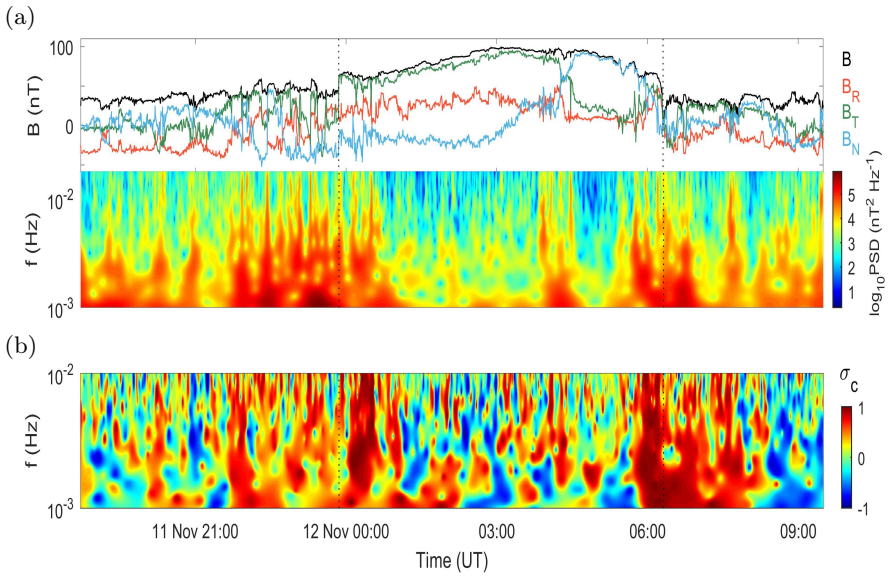

Figure 3.6: Parker Solar Probe observations of an ICME ejecta at ∼0.25 AU. (a) Magnetic field magnitude and components in the spacecraft centred Radial-Tangential-Normal (RTN) coordinates in the upper panel and the wavelet power spectral density of the magnetic field fluctuations on frequencies from 10^{-3} to 10^{-2} Hz in the lower panel. (b) Normalised cross helicity σ_c on frequencies from 10^{-3} to 10^{-2} Hz. Vertical lines indicate the ejecta interval, which is preceded by outwards propagating magnetic field fluctuations of high power. Adapted from a figure in Good et al. (2020).

and solar meridional planes. Figure 3.7a exemplifies how the underlying Parker spiral geometry of IMF affects the draping pattern in the sheath and Fig. 3.7b how the pattern is dependent on the orientation of upstream field and on whether an ejecta is directed north or south of the ecliptic. The field in Fig. 3.7a is bent by the shock and drapes around the ejecta in the west, i.e. at the top of the figure whereas it gradually passes the ejecta at the east.

The draping in the solar meridional plane is a source of out-of-ecliptic fields in ICME sheaths (Fig. 3.7b; Gosling and McComas, 1987; McComas et al., 1989; see also Kilpua et al., 2019). In Fig. 3.7b, the sheath magnetic field at the northern (southern) side with respect to the nose of the ICME is draped introducing a positive (negative) out-of-ecliptic component into sunwards pointing IMF. Moreover, negative out-of-ecliptic fields develop at the northern side of the sheath when the IMF

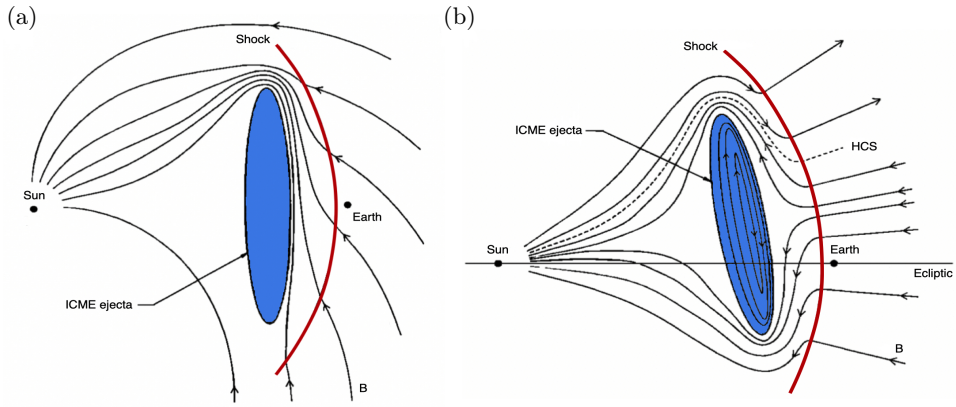

Figure 3.7: Magnetic field line draping around an ICME ejecta. Draping of IMF illustrated in (a) equatorial plane (b) solar meridional plane. Adapted from figures in Gosling and McComas (1987).

changes its direction to anti-sunwards in a HCS crossing. From the perspective of space weather, draping leads to important southward fields in the ecliptic when the ejecta and IMF are directed northwards and sunwards as in Fig. 3.7b, or when they are directed southwards and anti-sunwards, respectively (Gosling & McComas, 1987).

As just discussed, there is an asymmetry in draping due to the Parker spiral orientation, which leads to an enhanced compression of the IMF at the western flank of an ICME sheath (see Fig. 3.7a). This, furthermore, results in out-of-ecliptic field draping of different magnitudes, which causes an asymmetry in geoeffectiveness between the western and eastern flanks (Siscoe et al., 2007). The gradual passing of the magnetic field at the east flank and the draping resulting in out-of-ecliptic fields in an ICME sheath are further illustrated in Fig. 3.8a, which shows a snapshot of a three-dimensional MHD simulation of an ICME ejecta propagating in interplanetary space.

The inhomogeneous solar wind being swept by an ICME ploughing through interplanetary space experiences accretion that further causes the IMF to accumulate into layers in a sheath. Thus deviations from the general draping pattern may occur (Kaymaz & Siscoe, 2006). Due to the draping, sheath fields, however, align tangential to the ejecta leading surface (Jones et al., 2002). This accretion of IMF layers tangential to the ejecta surface can form planar magnetic structures (PMSs), which are periods of magnetic field during which the field direction changes abruptly but remains parallel to a certain single plane (Nakagawa et al., 1989).

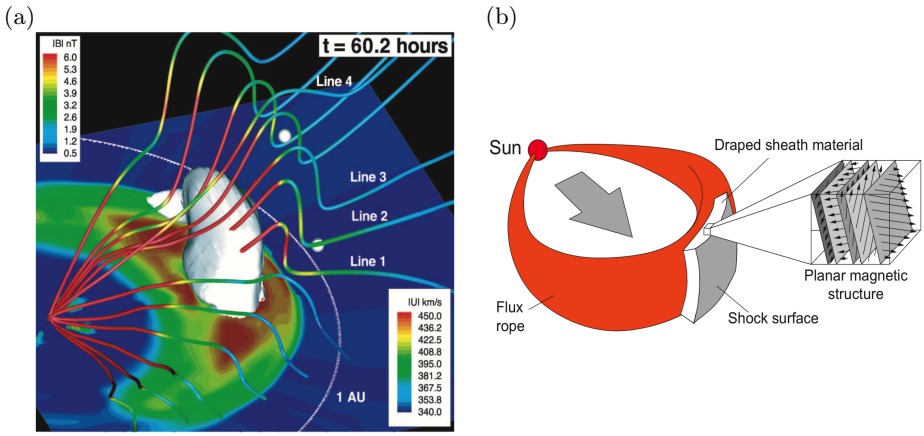

Figure 3.8: Magnetic field line draping and planar magnetic structure. (a) Snapshot at the time of 60.2 hours of a three-dimensional MHD simulation of an ICME showing magnetic field lines draping around the ejecta. The field magnitude is indicated by the colour of a field line and the colour on the equatorial plane shows the solar wind velocity profile. The ejecta is given by a white isosurface and the shock is indicated by an abrupt change of velocity. (b) Planar magnetic structure in an ICME sheath consisting of a period of magnetic field vectors oriented differently but restricted into a single plane that is tangential to the ejecta leading edge. Panel (a) reproduced from a figure in Manchester et al. (2005) and panel (b) reproduced from a figure in Palmerio (2019; originally constructed by Jones et al., 2002).

PMSs are frequently observed in ICME sheaths (Farrugia et al., 1990; Neugebauer et al., 1993), and additionally southward magnetic fields are enhanced during these planar parts (Palmerio et al., 2016). The field line draping and shock passage that aligns solar wind discontinuities are considered as principle processes constructing PMSs in ICME sheaths (Neugebauer et al., 1993; Palmerio et al., 2016), and PMSs particularly occur in the downstream of strong quasi-perpendicular shocks (Kataoka et al., 2005). Thus, draping of the background magnetic field, into which irregular fluctuations discussed above are embedded, modifies global sheath magnetic fields besides the field compression and bending resulting from the shock passage. Consequently, ICME sheaths may display coherent larger-scale magnetic fields (Paper III) whose radial scale extends during the evolution of an ICME as a function of heliospheric distance (Paper IV).

4 Fine structure of ICME sheaths

Although widely studied planetary magnetosheaths provide some applicable knowledge on ICME sheaths, their comprehensive understanding requires the examination of their structure itself. As stated in Ch. 1 and Sec. 3.3, ICME sheaths are relatively little studied, their small-scale structure particularly being inadequately understood. The fine structure of ICME-driven sheath regions is investigated in this thesis in terms of magnetic field fluctuations. Physics related to the research topics and the results reported in Papers I-IV are discussed here. The research of the fine structure is centred on ICME sheaths observed at the distance of 1 AU (Sec. 4.1) but the radial evolution of sheath magnetic fields is also studied (Sec. 4.2).

4.1 Fine structure at 1 AU

An ICME travelling through interplanetary space reaches the orbit of the Earth in a few days, and sheath plasma has had time to accumulate in front of the ejecta leading edge. At a distance of 1 AU, ICME sheaths have characteristic features, which are distinct from the ones of the driving ejecta (Kilpua et al., 2017). Statistical investigations of ICME sheaths, such as the research reported in Papers I-III, are feasible at 1 AU because of nearly continuous spacecraft measurements being available on a long-term basis (e.g. the Advanced Composition Explorer, i.e. ACE, Stone et al., 1998; and Wind, Ogilvie and Desch, 1997). Interplanetary shocks of ICMEs are often quasi-perpendicular at 1 AU (Kilpua et al., 2015) and thus temperature anisotropy exciting instabilities is expected to occur in the sheath (Sec. 3.2). As a consequence, waves appearing in magnetic field data should also occur. Generated waves and other magnetic fluctuations may, however, be localised because of the non-radial extent of 1 AU ICME sheaths have at the orbit of the Earth.

4.1.1 Wave activity – Mirror mode and Alfvén ion cyclotron waves

The occurrence and properties of mirror mode (MM) and Alfvén ion cyclotron (AIC) waves are studied in Papers I and II, respectively, by utilising semi-automated wave identification methods developed in this thesis. These waves are generated by the corresponding instabilities, which regulate plasma by taking place when excess

perpendicular proton temperature ($T_\perp$) relative to the parallel proton temperature ($T_\parallel$) is present in plasma the directions referring to the background magnetic field. Previous research by Liu et al. (2006b) reports plasma in ICME sheaths at 1 AU to have proton temperature anisotropy of $T_\perp/T_\parallel \simeq 1.2 - 1.3$ and thus to be marginally unstable to mirror and ion cyclotron (IC) instabilities (see Sec. 2.1.3 on plasma instabilities). Here the instabilities and results of Papers I and II are discussed.

Mirror instability

The kinetic dispersion relation predicts a non-oscillatory wave mode in the low-frequency limit, which grows when a sufficient temperature anisotropy defined by

$$\frac{T_\perp}{T_\parallel} > 1 + \frac{1}{\beta_\perp} \tag{4.1}$$

is present in a plasma (see also the empirically defined condition Eq. 2.4; Hasegawa, 1975; Southwood & Kivelson, 1993). This wave mode is a MM (Tsurutani et al., 1982; see also Tsurutani et al., 2011c). The generation of MMs originates from compressive displacements of magnetic field that in the low-frequency limit cause an anti-phase response in $p_\perp$ as

$$\frac{\delta p_\perp}{p_\perp} = 2(\,1 - \frac{T_\perp}{T_\parallel}\,)\frac{\delta B}{B}, \tag{4.2}$$

where $\delta p_\perp$ and δB are displacements, or fluctuations, of perpendicular thermal pressure ($p_\perp$) and magnetic field magnitude (B; Hasegawa, 1969; see also Chandrasekhar et al., 1958). This anti-phase response given in Eq. 4.2 causes an imbalance in total perpendicular pressure ($p_\perp + p_B$, where p_B is the magnetic pressure) of plasma along the magnetic field. This is illustrated in Fig. 4.1 where the colour scale shows the change in the total pressure for a given temperature anisotropy as a function of compressive magnetic field fluctuations that locally enhance the field magnitude. Positive values of colour scale indicate that a decrease in $\delta p_\perp/p_\perp$ in Eq. 4.2 is larger than an increase in $\delta p_B/p_B$ given by $\delta B/B$. This causes a deficit in the total pressure. Similarly, a fluctuation weakening the field magnitude causes a surplus in the total pressure.

The generation of MMs changes the distributions of magnetic field and plasma to diminish the inequality in Eq. 4.1 and the pressure imbalance. These changes appear as gradients of magnetic field magnitude, which cause so-called mirror forces

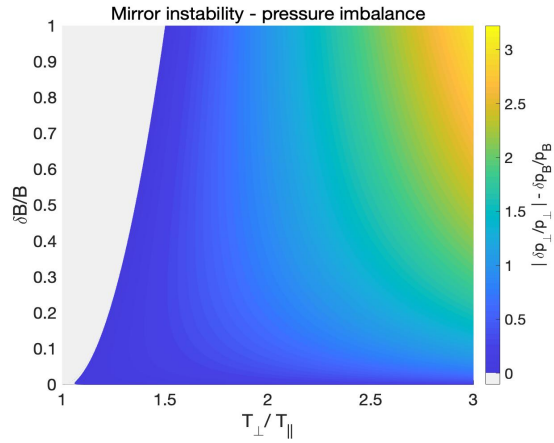

Figure 4.1: Pressure imbalance in mirror instability. The deficit in total pressure, indicated by positive values of the colour scale, resulting from the anti-phase response of $\delta p_\perp/p_\perp$ to $\delta B/B$ as a function of $T_\perp/T_\parallel$ in plasma. There is similarly a surplus in the total pressure when the field magnitude decreases. Note this figure does not take into account mirror instability being dependent on plasma beta (see Eq. 4.1). The figure shows that the imbalance also occurs for the anisotropies observed in ICME sheaths ($T_\perp/T_\parallel \simeq 1.2 - 1.3$; Liu et al., 2006b)

($F = -\mu\nabla B$, where μ is the magnetic moment) applied to particles moving along the field parallel to the gradient, the force being directed to the opposite direction. A strong enough mirror force thus turns particles around at a magnetic mirror point, defined as the point where this turning occurs. Particles can, furthermore, become trapped within a magnetic bottle that consists of two magnetic mirrors facing each other. Consequently, MMs achieving a fully developed state are structures of magnetic bottles that express a magnetic field and plasma configuration that is marginally stable with respect to the instability and along which the total perpendicular pressure remains constant (Kivelson & Southwood, 1996), i.e.

$$\frac{\partial}{\partial s}\left(p_\perp + \frac{B^2}{2\mu_0}\right) = 0, \tag{4.3}$$

where s is a coordinate along the direction of the field.

Plasma particles of different velocities, however, behave differently in the mirror instability, only some of the particles becoming trapped within magnetic bottles, which increases the density in the regions of weakening magnetic field. The gradient of the field magnitude further prevents these trapped particles to penetrate into the

regions of enhanced field where the density correspondingly decreases. The particles of very low $v_{\parallel}$, instead, do not move significantly relatively to the field. These are known as resonant particles.

The response of particle populations of different $v_{\parallel}$ in mirror instability is illustrated in Fig. 4.2a. The untrapped particle population exemplified at the top of the figure has sufficient $v_{\parallel}$ to not become mirror-trapped. In other words, these particles have low pitch angle, which is defined as an angle whose tangent gives the ratio of $v_{\perp}$ to $v_{\parallel}$. The pitch angles of untrapped particles moving along the fluctuating magnetic field vary but the particles conserve their energy. Particles bouncing between regions of enhanced field magnitude at the bottom of the panel are instead trapped and experience acceleration or deceleration according to Fermi acceleration that results from the spatial movement of magnetic mirrors caused by the development of field displacements (see for instance Fig. 2.2 in Ala-Lahti, 2017). This mirror-trapped particle population is defined by those particles whose pitch angle (α) for a given magnetic field magnitude (B) is between the interval

$$\frac{\pi}{2} > |\alpha| > \sin^{-1}\left(\sqrt{\frac{B}{B_{\max}}}\right), \tag{4.4}$$

where $B_{\max}$ is the maximum magnitude of a MM. The resonant particles are illustrated in the figure by blue (red) trajectories and the pitch angle of these particles is close to 90°. Because of not moving relative to the field, they are under the influence of local weakening (strengthening) of the field and they experience betatron acceleration, which cools (heats) the particles.

The cooling of particles and increase in magnetic field magnitude eventually diminish the anti-phase (Eq. 4.2) response and balance the surplus and deficit in the total pressure between the regions of weakening and strengthening magnetic field, respectively. This is summarised in Fig. 4.2b. The cooling balancing the surplus is caused by resonant particles being decelerated by betatron acceleration. In addition, some cooling of plasma is also provided by Fermi deceleration of mirror-trapped particles whose magnetic mirrors move further away during developing field displacements. Although regions of increasing field magnitude heat resonant particles, the decrease in thermal pressure and the deficit is eventually balanced by an increase of magnetic field density. The pressure balance is achieved with a small increase of magnetic field magnitude whereas the field has to weaken relatively much so that sufficient cooling that stabilise the plasma occurs in the regions of weakening field (Kivelson & Southwood, 1996).

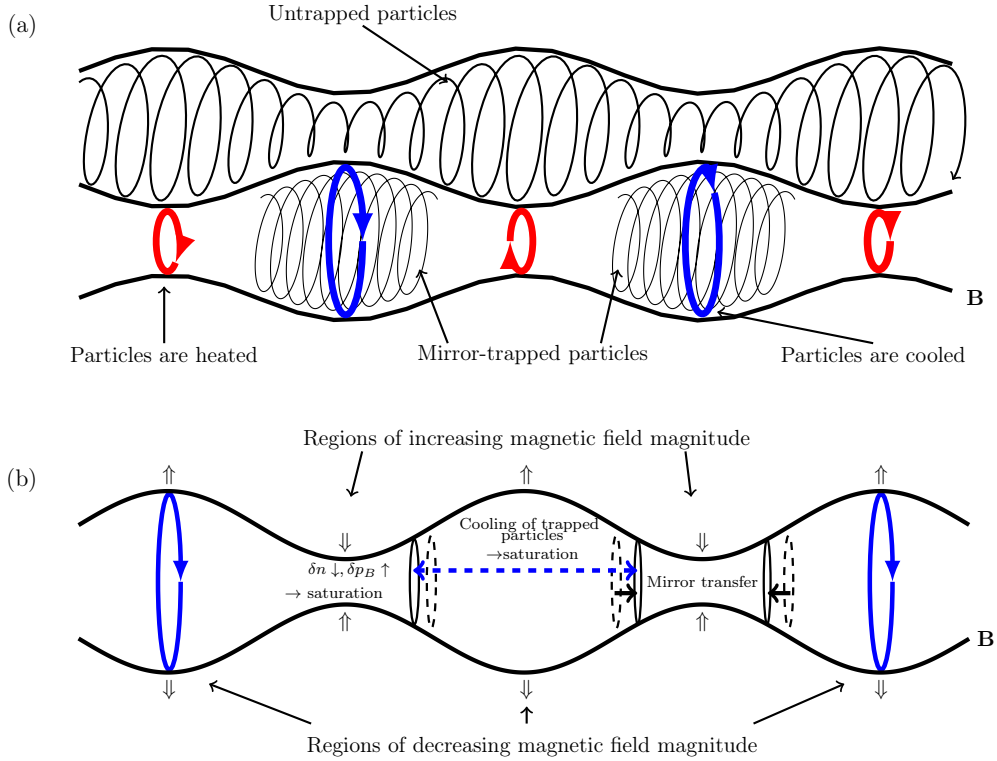

Figure 4.2: Mirror instability. (a) The responses of different particle populations on magnetic fluctuations in mirror-unstable plasma. The black solid trajectory at the top of the panel illustrates the untrapped particle population that has sufficient $v_{\parallel}$ for not being trapped by the magnetic field gradient. The bottom of the panel shows particle populations of very low $v_{\parallel}$, which are either heated (red trajectories) or cooled (blue) depending on whether experiencing an increase or decrease in magnetic field magnitude. Thin black solid trajectory exemplifies mirror-trapped particle population, whose particles are exposed to both acceleration and deceleration. (b) Exemplification of the saturation of MMs. Pressure imbalance appears as a surplus (deficit) in weakening (strengthening) field regions. The surplus is balanced by resonant particles of low pitch angles, which are cooled by betatron acceleration. In addition, Fermi acceleration decelerates mirror-trapped particle population whose magnetic mirrors move further from each other. In the regions of increasing field magnitude, increasing magnetic pressure balances the deficit. Adapted from figures in Ala-Lahti (2017).

Practically all MMs reported in Paper I are dip-like MMs, which means that waves are observed as decreases in magnetic field magnitude. This observation is consistent with the theory discussed above stating a noticeable weakening of field magnitude has to occur when mirror instability is stabilised. Thus, a dip-like MM can form an observable magnetic bottle relatively easily compared to peak-like MMs, which appear as enhancements of field magnitude and for which a minor increase in field magnitude already causes stabilisation.

Alfvén ion cyclotron instability

In the cold plasma limit, which effectively means neglecting thermal effects due to considering plasma waves that propagate faster than the sound, the dispersion equation predicts left- and right-handed (LH and RH, respectively) polarised wave modes, which are referred to as L– and R–modes (e.g. Kilpua & Koskinen, 2017). These wave modes propagate parallel and oscillate transversely with respect to the background magnetic field. The real part of the dispersion equation can be written as

$$\frac{c^2k^2}{\omega^2} = 1 - \frac{\omega_{pe}^2}{\omega(\omega \pm \omega_{ce})} - \frac{\omega_{pi}^2}{\omega(\omega \mp \omega_{ci})}, \tag{4.5}$$

where c is the speed of light, k is the wave vector, ω is the wave angular frequency, ω_{pe} and ω_{pi} are electron and ion plasma frequencies, and ω_{ce} and ω_{ci} are electron and ion cyclotron (IC) frequencies; and for simplicity ions now equals to solely protons. The upper (lower) signs correspond to L–mode (R–mode).

The right-hand side of Eq. 4.5 approaches infinity when the frequency of a wave approaches the cyclotron frequency of a particle. For a L–mode wave this occurs with ions (protons) and for a R–mode wave with electrons, i.e. when ω approaches ω_{ci} and ω_{ce}, respectively. This fundamentally results from ions and electrons gyrating around the background magnetic field in the LH and RH senses. Such particles are said to be in resonance with a wave and efficient energy transfer can occur. Typically, the energy of a wave is absorbed by particles and the wave is damped. However, in the presence of sufficient temperature anisotropy (see Eq. 2.4) the energy transfer is from particles to the wave, causing wave growth. The instabilities driving this growth are electromagnetic cyclotron instabilities. The resonance in which the energy stored in excess temperature anisotropy of ions is transferred to the L–mode is electromagnetic ion cyclotron instability, or Alfvén

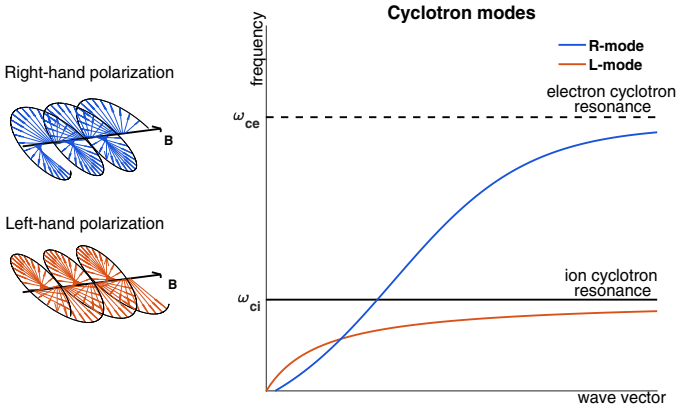

Figure 4.3: Cyclotron waves. Illustration of right-hand (R–mode) and left-hand (L–mode) polarised waves propagating in the direction of background magnetic field and a sketch of the frequencies of these wave modes as a function of the wave vector with respect to electron and ion cyclotron frequencies.

ion cyclotron (AIC) instability (e.g. Kennel & Petschek, 1966; Davidson & Ogden, 1975) and the associated wave is AIC wave.

L– and R–modes propagating in the direction of the background magnetic field, and their frequencies as a function of wave vector are sketched in Fig. 4.3. The figure also exemplifies resonances occurring at ω_{ci} and ω_{ce} and shows the importance of considering the wave frequency when AIC waves are investigated. The frequencies of AIC waves are, namely, theoretically limited to frequencies below the ion cyclotron frequencies, whereas R–mode waves can have higher frequencies. Furthermore, single spacecraft observations that lack electric field measurements have an uncertainty in determining the wave propagation direction and polarisation. This uncertainty results from waves being Doppler-shifted from the plasma frame to spacecraft frame, which can cause a wave being observed with a reversed sense of polarisation compared to the intrinsic one in the plasma frame (e.g. Remya et al., 2014; Li et al., 2019; see also Allen et al., 2015). Studying the wave frequencies in spacecraft and plasma frames can reduce this ambiguity.

AIC wave events observed in Paper II are equally divided into the ones having LH and RH polarisation. Paper II notes that the majority of the identified wave events are exposed to a notable Doppler shift and there is thus an uncertainty in determining the intrinsic sense of polarisation of AIC waves in ICME sheaths. Many

wave events reported in Paper II are observed to have their frequency below the IC frequency in the spacecraft frame (∼72%) and most events show this feature in the solar wind (∼94%) frame. These observations coincide with the recent parallel work by Li et al. (2019, 2020). To extend the discussion in Paper II, polarisation reversal is also possible due to waves propagating through different plasma environments having different ion compositions (Young et al., 1981; Rauch and Roux, 1982; see also Remya et al., 2017b). This results in so-called crossover frequencies above which the L– and and R–modes are not decoupled anymore. The L–mode instead merges with the R–mode, the coupling leading to a polarity reversal (Young et al., 1981; Rauch & Roux, 1982). Additionally, the recent work by Remya et al. (2017b) reported that the ion cyclotron resonance driven by a temperature anisotropy can directly excite waves that have a RH polarisation and a large propagation angle with respect to the background magnetic field. This originates from so-called anomalous resonance in which the ions are overtaking R–mode waves (see Tsurutani & Lakhina, 1997; Remya et al., 2017b) and may be responsible for the observed relatively large number of RH polarised events in Paper II.

MM and AIC waves in ICME sheaths

Both MM and AIC waves are frequently observed in ICME sheaths at 1 AU (in addition to Papers I and II see Liu et al., 2006b; Kajdič et al., 2012; Li et al., 2019, 2020). Figure 4.4 showing the observed events in the space of parallel ion beta ($\beta_{\parallel}$) and ion beta anisotropy ($\beta_{\perp}/\beta_{\parallel}$) summarises the results of Papers I and II. Consistent with previous theoretical suggestions and observations in other plasma environments (e.g. Lacombe & Belmont, 1995; Anderson & Fuselier, 1993; Gary et al., 1993), MM and AIC waves also occupy high and low beta plasmas in ICME sheaths, respectively. Moreover, the figure implies that for a given value of $\beta_{\parallel}$, the instability that requires a lower anisotropy to develop generates waves and thus stabilises the plasma in an ICME sheath. This may be a consequence of relatively weak heating of plasma in ICME sheaths that drives plasma only to a state of marginal instability. Sheath plasma being only marginally unstable with respect to the investigated instabilities is further supported by additional distributions shown in Papers I and II (see for instance Fig. 2 in Paper II). Also, shocks preceding ICMEs are reported to be typically weak ($M_{\mathrm{MS}} \simeq 2.1$; Kilpua et al., 2015), which is why less heating compared to the Earth's magnetosheath ($M_{\mathrm{MS}} \simeq 5.3$; Peredo et al., 1995) can be expected to occur in ICME sheaths.

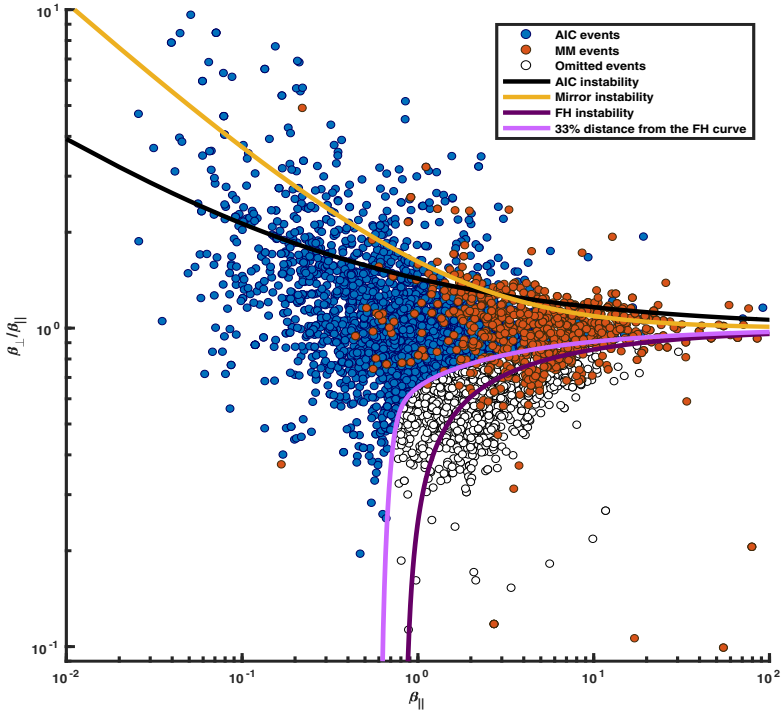

Figure 4.4: Distributions of MMs (orange dots) observed in Paper I and AIC waves (blue dots) observed in Paper II in the ($\beta_\parallel$, $\beta_\perp/\beta_\parallel$)-space. Overplotted curves indicate mirror (yellow) and IC (black) instability threshold curves. The purple curve indicates the threshold curve of parallel firehose (FH) instability, which generates waves that have similar features with those of AIC waves. Events identified close (light purple) to FH instability threshold are omitted (white dots) from AIC wave analysis in Paper II. Plasma beta anisotropy is effectively temperature anisotropy. Reproduced from Paper II.

Temperature anisotropy and the occurrence of both MMs and AIC waves are highest near the shock in ICME sheaths (see Fig. 4 and Fig. 9h in Paper I, and Fig. 5 in Paper II). $T_\perp/T_\parallel$ and AIC waves are most abundant in the immediate downstream of the shock whereas a higher occurrence of MMs extends further away downstream. In addition, $\beta_\perp$, which influences the stability of plasma with respect to the mirror instability (Eq. 4.1), has an increasing trend in the downstream near the shock (see Fig. 9g in Paper I). A possible interpretation of these observations is that heating of plasma in a shock crossing results in a gradual energy dissipation process in which generation of AIC waves happens immediately in the downstream, whereas some of the excess temperature anisotropy is diminished progressively, generating MMs

near the shock especially when the profile of $\beta_\perp$ within the sheath offers the most suitable conditions for the mirror instability to occur.

It is likely that in ICME sheaths the decreasing trend of AIC occurrence from the shock to the ejecta leading edge is, indeed, related to shock-related processes exciting AIC waves. Moreover, as is stated in Paper II, it has been shown in simulations (Shoji et al., 2009) that plasma unstable with respect to the IC instability tends to saturate quickly, and AIC waves are damped relatively fast as they are efficient to lose their energy due to non-linear processes (see also Ronnmark and André, 1991).

Although the possibility of waves being generated in the middle and back of the sheath cannot be excluded, a corresponding scenario to that of AIC waves in the context of MMs is introduced in Paper I. Dip-like MMs can namely be generated near the shock due to the suitable plasma conditions after which they are damped while being convected towards the back of the sheath. Paper I, indeed, reports dip-like MMs along the whole sheath, whose amplitude decreases from the shock towards the leading edge of the trailing ejecta. This scenario is supported by theoretical, numerical and observational studies. Namely in addition to the theoretical prediction that dip-like MMs develop relatively easily compared to peak-like MMs, numerical studies (Califano et al., 2008) as well as observations (Génot et al., 2009) suggest that in weakly mirror unstable plasma, the mirror instability saturates directly in dip-like structures. Furthermore, individual dip-like MMs can trap particles and remain as stable structures, which according to observations in the Earth's magnetosheath are slowly damped (e.g. Soucek et al., 2008; Génot et al., 2011).

This interpretation differs from the observations in the Earth's magnetosheath where the field line draping is also believed to provide free energy for the mirror instability close to the magnetopause where the plasma depletion along the draped field and the intensification of the field due to the consequent pressure deficit result in an enhanced temperature anisotropy and favourable conditions for the mirror instability to occur (Midgley & Davis, 1963; Zwan & Wolf, 1976; Crooker & Siscoe, 1977; Tsurutani et al., 1982). The characteristics of an expansion sheath may diminish the plasma depletion this mechanisms thus being absent in ICME sheaths.

Papers I and II are statistical studies on the occurrence on MM and AIC waves in ICME-driven sheath regions. The origin of waves can also vary between different sheath events. Sometimes additional heating can, for example, be provided by a

shock that is embedded in an ICME sheath (e.g. Lugaz et al., 2016). Moreover, the results may include events having alternative origins to the instabilities. For example, some of the identified events in Paper I may be magnetic decreases which, similar to dip-like MMs, appear as decreases in magnetic field magnitude data (Tsurutani et al., 2011c). Magnetic decreases may originate from turbulent processes in which oppositely travelling Alfvén wave packets interact with each other (Vasquez & Hollweg, 1999; Vasquez et al., 2007b) or in which phase-steepened Alfvénic fluctuations are dissipating (Tsurutani et al., 2002; Dasgupta et al., 2003). As the perpendicular heating is expected to only occur in the downstream of a quasi-perpendicular shock, the events in the immediate downstream of quasi-parallel shocks may be magnetic decreases. The downstream of a quasi-parallel shock is namely strongly turbulent (Fairfield, 1976) the aforementioned processes being presumably more likely than the mirror instability (e.g. Tsurutani et al., 2009; see also Kennel et al., 1984a, 1984b). However, linear magnetic decreases are, similar to MMs, structures across which the magnetic field direction changes only a little and which occur in high-beta plasmas. They can thus be considered as possible remnants of MMs (Winterhalter et al., 1994b). This feature of a small directional change of the magnetic field across a structure was included in the identification algorithm of MMs, and as mentioned above, the MM distribution in Fig. 4.4 indeed occupies the high-beta ICME sheath plasma coinciding with the previous works focusing on the mirror instability.

Future studies can refine the understanding of MM and AIC waves in ICME sheaths achieved by the research in this thesis, for example by further comparing observations in the downstream of quasi-parallel and quasi-perpendicular shocks and examining separately distributions of individual MM events and groups of MMs, so-called MM trains. Also, further research on the polarisation of AIC waves in ICME sheaths and examination of their propagation angle with respect to the background magnetic field would be beneficial.

4.1.2 Longitudinal coherence

ICMEs sheaths have considerable radial and non-radial sizes when they reach the orbit of the Earth. On average sheaths at these distances have radial width of 0.13 AU (Kilpua et al., 2017) and can extend to several tens of degrees in longitude (de Lucas et al., 2011). This raises the question as to whether magnetic fluctuations are local in ICME sheaths. For example, the geometry of an ICME-driven shock front is expected to vary, the generation of MM and AIC waves possibly occurring only in

the downstream of the quasi-perpendicular parts (see for instance IMF passing the shock in Fig. 3.7). The coherence of magnetic field fluctuations in ICME sheaths in the longitudinal, that is non-radial, direction is studied in Paper III by examining the correlation of sheath magnetic field measurements from two spacecraft at $\sim$1 AU.

Figure 4.5 shows the averaged Pearson correlation coefficient (σ_{P}) of ICME sheath magnetic fields as a function of low- and high-pass filtered cutoff frequency. Magnetic field components and magnitude in the GSE coordinates are considered separately and together. σ_{tot} namely indicates the total or overall Pearson correlation computed by applying the averaging estimator of correlation coefficients proposed by Olkin and Pratt (1958) for the σ_{P} values of the magnitude ($|B|$) and components. The figure also shows the correlations for the level of fluctuations (B_{RMS}), which is enhanced in geoeffective sheaths (Kilpua et al., 2019a). Low-pass-filtered curves imply that coherent global magnetic fields are embedded in ICME sheaths. Paper III discusses the main processes that could result in these coherent fields and concludes them to be the bending of the field by the shock at the front of the sheath and the field draping around the driving magnetically confined ejecta at the back of the sheath. These two processes are associated with the generation of PMSs in the sheath (Sec. 3.3; Palmerio et al., 2016).

Despite the global sheath magnetic field, even relatively small non-radial spacecraft separations ($\lesssim 0.01$ AU) can result in low correlation coefficients between unfiltered sheath magnetic field measurements (see Fig. 3 in Paper III). High-pass-filtered magnetic field data in Fig. 4.5, furthermore, display in general very low correlations and together with decreasing B_{RMS} suggest that fluctuations highly limited in spatial extent are present. These observations are interesting especially from the perspective of ICME sheaths' capability to drive space weather effects due to out-of-ecliptic fields within the sheaths (see Sec. 2.2). In addition to the asymmetry of out-of-ecliptic component between the western and eastern flanks mentioned earlier (Sec. 3.3), localised magnetic fluctuations in ICME sheaths can cause considerable spatial variation in geoeffectiveness (see also for instance Osmane et al., 2015). High-pass-filtered data in Fig. 4.5 namely show very low and even zero correlations for frequencies below 10^{-2} Hz, and this feature also applies to the B_z component, which represents the out-of-ecliptic field component. The frequency boundary of 10^{-2} Hz is significant because the fluctuations below that are able to transmit to the Earth's magnetosheath (Rakhmanova et al., 2015).

The longitudinal extent, or scale, of magnetic fields in ICME sheaths is illustrated in

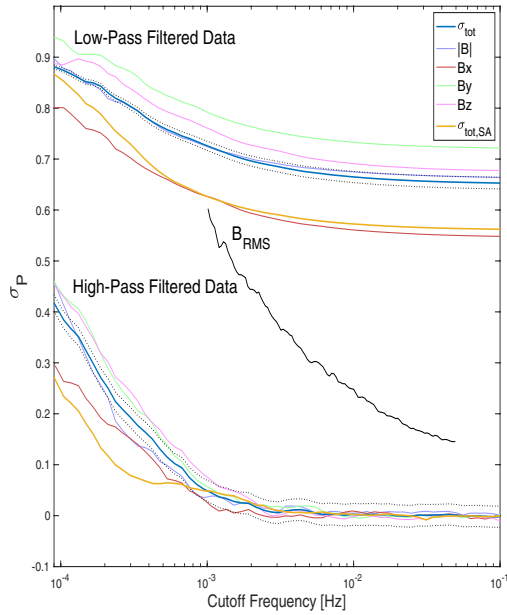

Figure 4.5: Pearson correlation coefficient (σ_{P}) of magnetic field measurements as a function of frequency filtered magnetic field data. Correlation is given for both low- and high-pass-filtered data, and for the level of fluctuations (B_{RMS}) as a function of cutoff frequency. The total Pearson correlation (σ_{tot}; blue curve) is plotted with the lower and upper bounds for a 95% confidence interval (black dots). The magnetic field components are expressed in the Geocentric Solar Ecliptic (GSE) coordinate system. $|B|$ is the magnetic field magnitude. The subscript SA refers to events being aligned according to the preceding shock instead of finding highest possible correlation for an event. Reproduced from Paper III.

Fig. 4.6, which sketches an ICME in Earth-centred interplanetary space. For ICME sheaths these scales of different magnetic field components and magnitude have the values of 0.024, 0.149, 0.035 and 0.030 AU for B_x, B_y, B_z and $|B|$, respectively. The figure also shows the corresponding scales of the solar wind and ICME ejecta with the values of 0.014, 0.016, 0.014 and 0.023 AU for the solar wind and 0.065, 0.094, 0.061, 0.260 AU for the ICME ejecta. In addition, the scale of σ_{tot} (0.035 AU) for the ICME sheath is shown. The scale indicates the non-radial distance at which no correlation is anymore expected to occur in magnetic field. This scale is referred to as the so-called scale length. The scale lengths of the ICME sheath are directly examined in Paper III whereas the comparable ones of the solar wind and ICME ejecta are given by Richardson and Paularena (2001) and Lugaz et al. (2018), respectively. Similar to Paper III, these scale lengths of the solar wind and ejecta

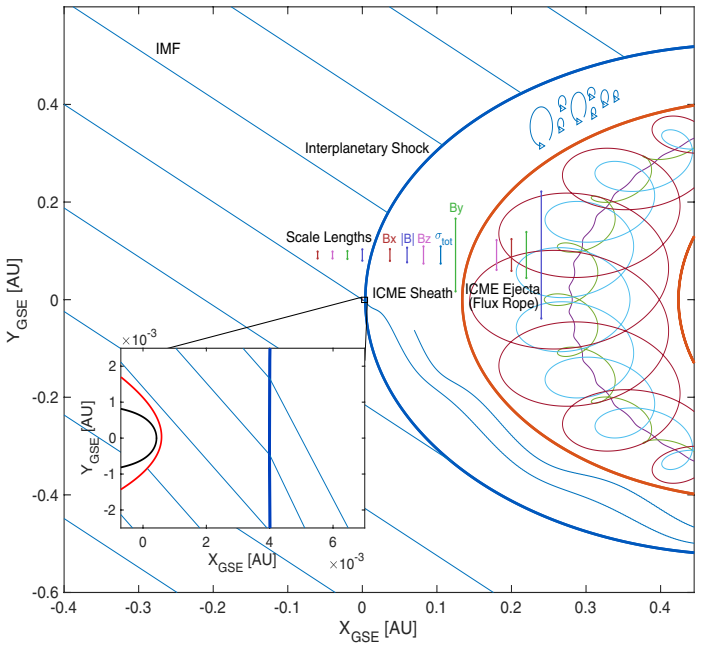

Figure 4.6: Sketch of an ICME in Earth-centred interplanetary space in the ecliptic plane of the GSE coordinates. The ICME sheath is preceded by an interplanetary shock (dark blue curve) and driven by ICME ejecta, bounded by orange curves, within which there is a flux rope illustrated with an exaggerated twist. Blue lines show the interplanetary magnetic field (IMF), which has 45° Parker spiral angle at the Earth's distance from the Sun. The sheath is occupied by magnetic fluctuations and field lines drape around the ICME ejecta. Also, turbulent progress of fluctuations is exemplified by the eddies within the sheath. Scale lengths of the solar wind (Richardson & Paularena, 2001), ICME sheath (Paper III), and ICME ejecta (Lugaz et al., 2018) are illustrated in the y-direction, all lengths being constructed from magnetic field measurements in the GSE coordinates. Near-Earth space is shown in the inset where red and black curves indicate the bow shock and magnetopause boundaries during nominal solar wind conditions. Reproduced from Paper III.

in Fig. 4.6 are constructed by extrapolating the linear fittings of the magnetic field correlation coefficients as a function of the non-radial distance until no correlation occurs in the field (see Fig. 3 in Paper III). These scale lengths of the solar wind are comparable to the ones given by linear approximations of the exponential fittings of the solar wind spatial coherence reported by Matthaeus et al. (2005) and Wicks et al. (2009).

In Fig. 4.6, the spatial extent of B_y component in the ICME sheath is large compared to that of B_x and to any other magnetic field parameter. The difference in the scale lengths between the x- and y-components, 0.024 and 0.149 AU respectively, likely emanates from the aforementioned physical processes that change the background field direction increasing the component in the y-direction. Consequently, measurements of B_y are dominated by the large-scale structure, rather than small fluctuations. Therefore, a high correlation is observed. Any local fluctuations of B_x are instead significant deviations from the mean field because of the reduced large-scale x-component. This leads to a low correlation of B_x. Quite similarly to B_x in the sheath, the scale lengths of the solar wind estimated from correlation coefficients are expected to remain small despite the large-scale structure the IMF has in the heliosphere: any spatial irregularities, such as turbulent fluctuations, in the average field cause low correlation between field measurements when examining the IMF over a few day's time scales at a given heliospheric distance when transitions such as the HCS are absent. The magnetically confined ejecta instead typically has a structure exhibiting a smooth field rotation, which is distinguishable in measurements. This results in relatively high correlation coefficients (see Fig. 3.1). All scale lengths of the sheath are moreover larger than those of the solar wind but generally smaller than the ones of the ejecta. Thus, Paper III shows the magnetic fields in the sheath are more coherently structured and well correlated in comparison to the solar wind despite the highly fluctuating magnetic fields embedded in sheaths.

4.2 Radial evolution of sheath magnetic fields

Studying the radial evolution of ICME sheaths is essential to construct a comprehensive picture that involves the understanding of possible features observed at 1 AU. In addition to the role ICME sheaths have in the context of fundamental plasma physics, research on their radial evolution can be highly beneficial from the space weather prediction point of view when attempts to explain the origin of southward magnetic fields embedded in ICME sheaths are made. The radial evolution of ICME sheaths has been under increasing interest recently (Janvier et al., 2019; Kay et al., 2020; Lugaz et al., 2020; Salman et al., 2020; see also Tsurutani et al., 2020), and Paper IV belongs to this forefront research having the focus on the evolution of magnetic fluctuations within an ICME sheath.

The radial evolution of AIC waves and especially MMs in ICME sheaths is sketched in the level of discussion in Papers I and II, in which waves observed at the back of

the sheath are suggested to be waves generated in the vicinity of the shock that are then convected towards the leading edge of the ejecta. Paper IV, however, reports direct observations of the same ICME-driven sheath region observed at distances of 0.47 and 1.08 AU associated with a small angular separation of spacecraft. In addition, in Paper IV the observations from the sheath are discussed with respect to the ones from the preceding solar wind.

The magnetic field measurements of the studied ICME event in Paper IV are shown in Fig. 4.7a. Measurements are given at 0.47 AU by MESSENGER (Solomon et al., 2007) and at 1.08 AU by the STEREO-B (Kaiser et al., 2008) spacecraft, which were close to a radial alignment during the event. The longitudinal separation between the spacecraft is 1° in heliographic longitude and 7° in heliographic latitude around the time of the event. The data illustrate that the profiles of magnetic field components and magnitude within this ICME sheath differ notably between two radial distances. For example, the tangential component is negative during almost the entire sheath at 0.47 AU whereas it has a significant period of positive values at 1.08 AU. The duration of the sheath also increases from ∼5 hours to ∼8.5 hours from 0.47 to 1.08 AU, implying that upstream plasma is swept downstream of the shock and added to the sheath material.

Figure 4.7b shows probability distributions of normalised magnetic fluctuations in the sheath and solar wind at the two radial distances. Fluctuations are determined as $\delta B(t, \Delta t) = |\mathbf{B}(t) - \mathbf{B}(t + \Delta t)|$ over a range of time intervals Δt and normalised to the mean field magnitude (B) between the times t and $t + \Delta t$. The sheath distributions at 0.47 and 1.08 AU show a relatively high level of similarity between each other. Largest-scale sheath distributions are evenly spaced along the $\delta B/B$ axis and the distributions of the smallest timescales peak sharply at low $\delta B/B$. Some of the minor differences probably originate from the shock geometry changing from quasi-parallel to quasi-perpendicular. Comparison of the sheath and solar wind distributions, however, displays some differences. Closer to the Sun, distributions in the sheath have developed tails ($\delta B/B > 2$) absent in the preceding solar wind. These tails indicate at least partly compressive fluctuations since purely rotational fluctuations are limited below the value of two (e.g. Matteini et al., 2018). Despite of the fact that ICME sheaths are interaction regions in which local sources may significantly produce new fluctuations that have formed close to the observation point and that are thus "young" in age, the observation of this shift in the distributions towards higher $\delta B/B$ values seen with the solar wind–sheath transition at 0.47 AU suggests that the solar wind entering the sheath experiences qualitatively similar

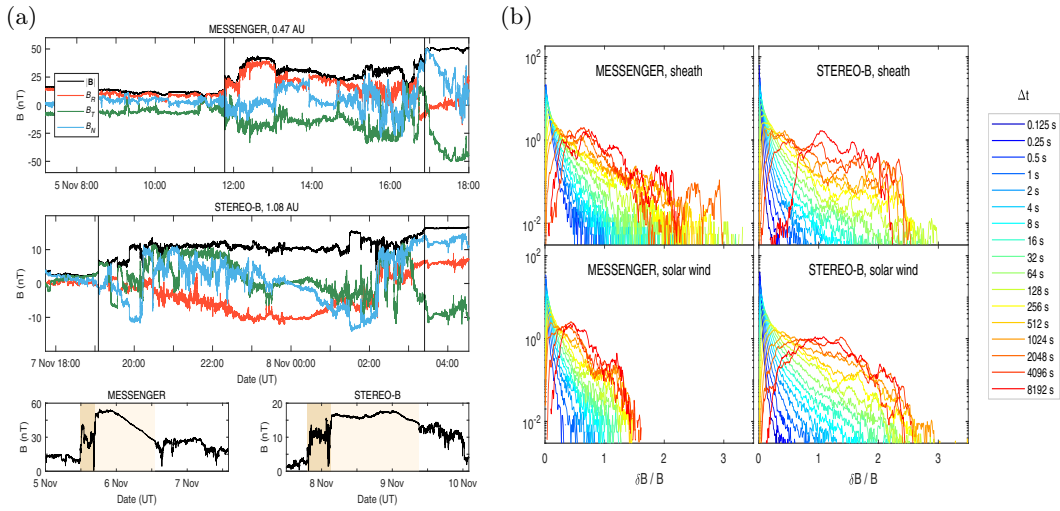

Figure 4.7: Magnetic field fluctuations in the ICME sheath studied in Paper IV. (a) The upper panels show the magnetic field measurements in the RTN coordinates given by the MESSENGER and STEREO-B spacecraft. The bottom panels show the whole ICME on a bigger scale and the sheath and ejecta are indicated by darker and lighter shades of beige, respectively. (b) Probability distributions of $\delta B/B$ across a range of timescales Δt for the preceding solar wind and the studied sheath itself at the distances of 0.47 and 1.08 AU. Reproduced from Paper IV.

"aging effect" as the solar wind propagating further away from the Sun. Namely, at a greater distance from the Sun, the solar wind distributions have a larger level of similarity with the sheath distributions. Further investigation of magnetic field fluctuations in terms of spectral slopes in Paper IV implies that turbulence in the solar wind magnetic field may not be fully developed yet at 0.47 AU whereas the sheath displays features of developed Kolmogorov-like turbulence. Alternatively, turbulence has to be described by different models in the solar wind and in the sheath (see Tsurutani et al., 2018), and the deeper spectral slope of the sheath might imply a growth in intermittency relative to the solar wind at 0.47 AU. Paper IV also notes that steepened slopes with heliospheric distance may likewise result from turbulences in both the solar wind and sheath developing intermittency.

Further investigation of sheath fluctuations can be obtained by exploring whether they consist of coherent structures or stochastic fluctuations. The permutation entropy and statistical complexity (Bandt & Pompe, 2002; Rosso et al., 2007) are utilised in Paper IV for this purpose. The permutation entropy quantifies the prob-

ability distribution of fluctuation patterns in a time series by indicating the randomness inherent in a process, as stated by Weck et al. (2015). Repetition of just a few fluctuation patterns implies a greater degree of predictability and lower permutation entropy. The permutation entropy is normalised with a uniform probability distribution, which maximises the entropy by considering all possible fluctuation patterns being equally likely thus representing the highest possible unpredictability of a system. The distribution of fluctuations patterns, i.e. different amplitude orderings or permutations, is constructed from sets of evenly spaced data points in a time series. The number of data points in a set is determined by the so-called embedded dimension (d) and the spacing of the points is given by the embedded delay (τ), which effectively defines the time resolution. A set of evenly spaced data points for a given d and τ is thus $s = (x_t, x_{t+\tau}, ..., x_{t+\tau(d-1)})$ and its permutation is the index set $\{1, 2, ..., d\}$ arranged according to the ranking of the amplitudes x_i in the set s in ascending order (see Weck et al., 2015). The probabilities of different permutations in a time series further define the permutation entropy. Paper IV uses the normalised Shannon entropy (H), which for a given d is

$$H(d) = \frac{-1}{\log_2 d!} \sum_{i=1}^{d!} p_i \log_2 p_i, \tag{4.6}$$

where the denominator is the entropy of a uniform probability distribution and p_i is a probability of a permutation occurring in a time series.

The statistical complexity measures whether, for given permutation entropy, some fluctuation patterns are privileged among those accessible to the system, as stated by Weck et al. (2015), and thus it indicates possible physical structure embedded in the probability distribution of amplitude orderings. In practice, the statistical complexity measures how non-zero probabilities in Eq. 4.6 are distributed and attains its maximum for a given H when several fluctuation patterns are privileged and the rest of the patterns have negligible probabilities. Minimum complexity on the other hand corresponds to a situation in which the value of H is constituted of only one privileged fluctuation pattern, all other patterns being equally likely. Paper IV uses the Jensen–Shannon complexity (C) defined as

$$C(P) = Q(P, P_e)H(P), \tag{4.7}$$

where P is the probability distribution of fluctuation patterns constituted of the aforementioned probabilities p_i and the quantity Q indicates the disequilibrium P has from the uniform distribution P_e. Together, the permutation entropy and

statistical complexity inform how random fluctuations are and whether correlational structure occurs in these fluctuations, i.e. whether deterministic and chaotic or alternatively stochastic fluctuations occur in a system. Low (high) complexity associated with high (intermediate) permutation entropy suggests fluctuations are stochastic (chaotic) in nature. Since the analysis is only strictly valid for stationary time series, a form of stationarity has been imposed by taking the difference of successive data points in the analysed time series, as is stated in Paper IV. For additional discussion see Weck et al. (2015) and Osmane et al. (2019).

Figure 4.8 shows H and C in the sheath and preceding solar wind as a function of τ and indicates that high H and low C are generally observed for all τ in both the sheath and solar wind, consistent with the presence of highly stochastic fluctuations. ICME sheath measurements, however, display power-law falls (rises) in H (C) at large values of τ and a minor increase (decrease) of general values from 0.47 to 1.08 AU. The former feature is much weaker for the upstream solar wind, H (C) remaining at higher (lower) values than in the sheath. As stated in Paper IV, a greater large-scale complexity in the sheath compared to the solar wind agrees with the general understanding of sheath plasma, i.e. the sheath plasma contains a variable mix of coherent, ordered structures and random, disordered fluctuations. As the large-scale structure of sheath magnetic fields becomes less prevalent with reducing scale, complexity decreases towards values found in the relatively unstructured solar wind. This large-scale structure, however, occurs rather in the field components than in compressive fluctuations with respect to the background field: the lower complexity values of the compressive field magnitude fluctuations suggest that they are comparatively less structured and more stochastic than the Alfvénic sheath fluctuations. This interpretation of large-scale structure in the sheath is consistent with Paper III and does not contradict Papers I and II. Although instabilities may frequently regulate plasma in the sheath generating magnetic wave packets, the occurrence of a certain wave mode most often constitutes only a minor proportion of a sheath as is reported in Papers I and II. Thus, a structure possibly emanating from certain wave modes is overtaken by unstructured fluctuations. This is comparable to ubiquitous small-scale fluctuations having origins so alternating that no coherent structure is formed in the field.

Furthermore, two intervals of PMSs are embedded in the ICME sheath studied in Paper IV, both of which grow significantly as a fraction of the total sheath interval with radial distance. At both spacecraft, the intervals are located in the immediate downstream of the shock and right in front of the driving ejecta. The fractional

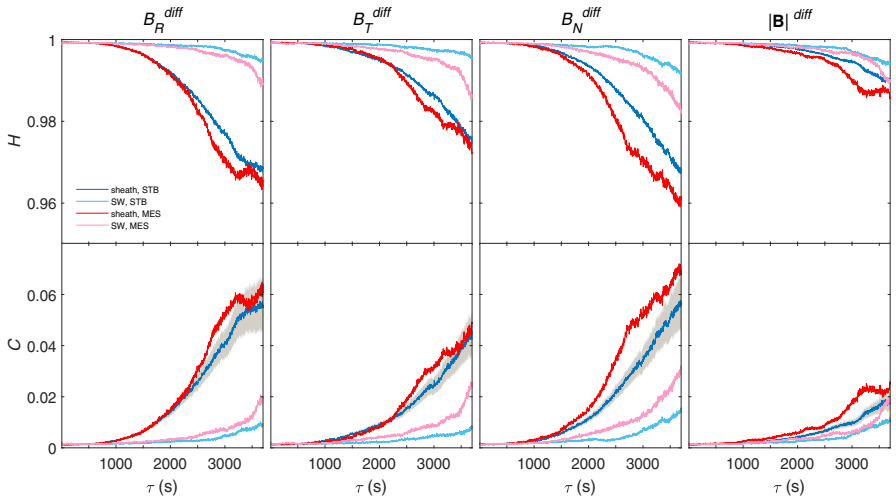

Figure 4.8: Permutation entropy (H) and Jensen-Shannon complexity (C) in ICME sheath and solar wind as a function of embedded delay (τ). The values in the sheath (solar wind) observed at 0.47 and 1.08 AU are illustrated by red (pink) and dark (pale) blue lines. Permutations are computed for an embedded dimension of $d = 5$, the embedded delay varying from $\tau = 2$ s to $\tau = 3700$ s in steps of 1 s. The uncertainty range in C for the sheath at STEREO-B is shown by the grey shading. A form of stationarity is imposed to the magnetic field data by taking the difference (*diff*) of successive points in the time series because of the analysis being only strictly valid for stationary time series. H and C are computed from this stationary data. Reproduced from Paper IV.

growth of the PMSs may result from the steady accumulation of the solar wind in the sheath with a distance which, more precisely, may be caused by systematic field bending by the shock and accumulation of the field draping at the back of the sheath. Although a higher value of complexity may be explained by the presence of planar sheath magnetic fields, an ambiguity still remains because simultaneously to the fractional growth of PMSs there is, as noted above, a minor decrease in the general value of the complexity from 0.47 to 1.08 AU in the sheath. This decrease in the complexity can result from an active intermittent turbulent energy cascade that with distance extends to larger scales where the structure embedded in the sheath fields is more prevalent. Consequently, the fractional growth of planar fields is overtaken by the development of turbulence and the structure in the sheath fields becomes less prevalent also at larger scales at greater heliospheric distances.

5 Concluding remarks

The research conducted in this thesis has aimed at increasing the understanding of ICME-driven sheath regions by investigating their fine structure and its radial evolution. To achieve this purpose, a collection of in-situ studies on the magnetic field configuration of ICME sheaths observed in the inner heliosphere has been constructed by utilising mainly statistical methods. The included studies significantly contribute to the current state-of-the-art not only due to the aforementioned discoveries made but also because of the methods the studies have developed and used to analyse data. The contribution of this thesis is detailed below and is followed by a discussion on future prospects and challenges.

5.1 Impact of conducted research

Papers I and II are the first comprehensive studies on ICME-driven sheath regions that investigate the occurrence of specific plasma wave modes (MM and AIC waves). Previous statistical works on this topic (Liu et al., 2006b; Kilpua et al., 2013) have only reported a general description of how favourable plasma conditions in ICME sheaths are for plasma instabilities, such as mirror and ion cyclotron instabilities, to occur or how fluctuations in a certain frequency range are distributed within the sheath. Thus, Papers I and II represent a significant proceeding to a more detailed level of research on ICME sheaths by identifying specific wave events (Paper II) or individual waves (Paper I) within sheaths. Previously, only the very immediate downstream of ICME shock has been investigated at this level of detail (Kajdič et al., 2012). The very recent work of Li et al. (2019, 2020) has continued the proceeding set in this thesis by exploring in detail electromagnetic waves near the proton cyclotron frequency in ICME sheaths with consistent results with Papers I and II as discussed previously.

The impact of Papers I and II is twofold. First of all, the discoveries of Papers I and II have contributed to fundamental space plasma physics due to their novel way of examining wave occurrence in ICME sheaths. These studies report that MM and AIC waves frequently occur in ICME sheaths at 1 AU and particularly in the vicinity of the shock. This suggests that shock heating is the most likely mechanism that provides sufficient free energy, or equivalently heating, for the

instabilities to occur in ICME sheaths. The investigated wave modes and also the plasma in general in ICME sheaths are, however, observed to follow the marginal instability thresholds reasonably well, which suggests mirror and IC instabilities efficiently regulate the sheath plasma. Consequently, the instability that requires weaker temperature anisotropy for given $\beta_{\parallel}$ occurs and regulates plasma generating magnetic field waves. This differs from the situation in planetary magnetosheaths where plasma is typically more unstable exceeding both instability thresholds for a given $\beta_{\parallel}$ (e.g. Soucek et al., 2015). The role of wave damping and convection are interesting topics for the future research on ICME sheaths. For example, the understanding given by Papers I and II may be refined by investigating the variation of wave occurrence in ICME sheaths in studies that use radially aligned spacecraft and high-resolution data of the latest missions.

Secondly, an important outcome of Papers I and II is the development of the wave identification algorithms that can be applied in future studies of MM and AIC waves, not only in ICME sheaths at varying heliospheric distances, but in other space plasma environments as well. It is, however, noted that the algorithms were designed for statistical studies and additional confirmation of waves are recommended in case studies. This note emanates from the features of the wave distributions shown in Fig. 4.4: there is likely a non-zero probability of observations including some false-positive events. This probability can be reduced by further refining the algorithms. An example of such refinement is omitting events in the vicinity of the parallel firehose instability threshold in Paper II. The figure, nevertheless, does manifest suitability of the algorithms in statistical studies. Despite the identification of MM and AIC waves being solely based on investigation of magnetic field data, the wave distributions in ($\beta_{\parallel}$, $\beta_{\perp}/\beta_{\parallel}$)-space are consistent with previous works (e.g. Gary et al., 1993).

Papers III and IV show that both longitudinal and radial separations between spacecraft observing the same ICME sheath result in differences in magnetic field measurements, the latter indicating radial evolution during sheath propagation. The earlier work on longitudinal coherence of large-scale heliospheric structures contains investigations of interplanetary shocks (Koval & Szabo, 2010) and ICME ejecta (Lugaz et al., 2018). Thus, Paper III completes efforts to understand ICMEs comprehensively. The same applies to Paper IV and the radial evolution of ICMEs (e.g. Good et al., 2018). In addition, Paper IV belongs to those few studies so far that utilise the permutation entropy and statistical complexity (e.g. Osmane et al., 2019), thus adapting the method in the context of space plasmas. One of

the key novel results of Papers III and IV is the discovery of ICME sheaths being more coherently structured and well correlated compared to the ambient solar wind despite sheaths generally being turbulent plasma environments. The results of Paper III are, however, statistical: the simultaneity of low-frequency coherent fields and spatially localised high-frequency fluctuations may result in highly varying magnetic field in an ICME sheath, which show little correlation even for small longitudinal spacecraft separations (Fig. 3 in Paper III). In Paper IV, although some observations are almost certainly due to radial evolution, spatial inhomogeneities cannot be ruled out, which indicates a demand for future studies.

Papers III and IV together with the earlier work (e.g. Palmerio et al., 2016; Lugaz et al., 2020) suggest that physical processes, such as the shock crossing and field draping, are essential physical processes that result in the formation of large-scale structured sheath fields, such as PMSs, in the inner heliosphere. Despite varying solar wind conditions an ICME encounters, such as Parker spiral which changes the shock angle with heliospheric distance, these structures can remain and even grow in the sheath during its propagation in interplanetary space. Consequently, at the orbit of the Earth, magnetic fields embedded in ICME sheaths exhibit coherent large-scale structure that is likely associated with the presence of a geoeffective out-of-ecliptic field component. As discussed above, sheath magnetic fields may additionally be occupied by fluctuations that have strong spatial inhomogeneity in the longitudinal direction due to their origin and generation being surprisingly local. An important space weather implication of this thesis is that such localised fluctuations that have an out-of-ecliptic field component can cause longitudinal variance on the geoeffectiveness of the sheath.

5.2 Future proceeding

Results of the research conducted in this thesis highlight the complex nature of ICME-driven sheaths and imply that only further investigations can lead to an understanding of ICME-driven sheath regions that enables including them in models that make accurate predictions on space weather during an ICME passage. A highly beneficial improvement would be an increasing number of studies utilising radially and longitudinally aligned spacecraft that observe the same sheath.

In addition to the ACE and Wind spacecraft located at the first Lagrangian point (L1) in the solar wind, the Deep Space Climate Observatory (DSCOVR) spacecraft was recently launched to L1 and provides new high-quality data, which can be utilised in further studies. These spacecraft at L1 may together offer an extensive set of data for investigations focusing on localised fluctuations embedded in sheath magnetic fields. The occurrence of such fluctuations that also have a significant out-of-ecliptic component ought to be studied profoundly, especially from the space weather point of view. A transfer of these fluctuations from the solar wind into the Earth's magnetosheath is also a necessary future research topic.

The ACE and Wind spacecraft have, however, been offering continuous measurements effectively over 20 years and an uncertainty gradually increases concerning the continuity of those missions. Moreover, during this 20 year life span, their longitudinal separation has barely exceeded the value of 0.01 AU, which is a small distance from the perspective of an ICME. As the non-radial width of an ICME sheath can be 1 AU at the orbit of the Earth, much larger longitudinal spacecraft separations are needed to examine more extensively the variation of sheath magnetic fields. This emphasises a demand for a multi-spacecraft mission at so-called mesoscale separations ($\sim$0.01 – 0.2 AU; Lugaz et al., 2018), which would also be highly beneficial to investigating other large-scale heliospheric structures and the solar wind in general. The benefits of a multi-spacecraft mission at varying spacecraft separations are already exemplified by the discoveries of the current multi-spacecraft missions passing the Earth's magnetosheath (e.g. the Cluster mission; Escoubet et al., 2001; Dimmock et al., 2019).

An alternative to multi-spacecraft observations is to construct a statistical understanding of longitudinal field variations in ICME sheaths by estimating the location of a spacecraft path relative to an ICME sheath from single spacecraft observations, i.e. whether a spacecraft enters the sheath at its nose or flank (see for instance Fig. 4 in Kilpua et al., 2017). Several works have estimated the spacecraft path for example by taking the angle between a shock normal and radial direction as an approximation of a spacecraft crossing distance from an ICME nose (e.g. Savani et al., 2015) and by estimating the angle between the normal of a PMS at the back of a sheath and the axis of a flux rope-like ICME ejecta (Jones et al., 2002). These methods are, however, exposed to complicating factors, such as the shape of the shock (see Fig. 3.2) and ejecta geometry, which results in relatively large uncertainties. Additionally, the latter approach is less useful when the trajectory of a spacecraft and PMS are close to parallel, presumably occurring near the flanks

of an ICME (Jones et al., 2002). A successful estimation of a spacecraft crossing distance from the nose of an ICME ejecta and shock would be useful information also in multi-spacecraft studies.

Very high-resolution and high-quality measurements are provided by recently launched Parker Solar Probe and Solar Orbiter (Müller et al., 2013). New extensive high-resolution measurements could be used to solve difficulties regarding plasma wave studies such as the ones reported in Paper II. Parker Solar Probe and Solar Orbiter are furthermore an addition to a number of spacecraft missions offering measurements at different heliospheric distances, and occasions when an ICME is observed by radially aligned spacecraft are expected to occur. Such events enable further studies on the radial evolution of ICME sheaths in a similar way as is done in Paper IV (see also Kilpua et al., 2019b; Lugaz et al., 2020; Salman et al., 2020). Research using radially aligned multi-spacecraft measurements to investigate how structures such as the HCS and SIRs or rotational and tangential discontinuities in the solar wind (e.g. Tsurutani & Smith, 1979; Lepping & Behannon, 1986) become swept by an ICME and consequently how these structures appear in an ICME sheath would give important results concerning the modelling of ICME sheaths. In addition, efforts to understand field draping at different distances from the Sun in detail would be valuable.

Finally, a lot can be achieved by single spacecraft missions and so far current missions do offer possibilities to continue the research on the radial evolution of ICMEs. However, based on the work in this thesis and on following current multi-spacecraft missions, a scientifically desirable action in the future would be a multi-spacecraft mission at $\sim$1 AU dedicated to non-radial scales relevant to ICMEs.

6 Summary of papers and the author's contribution

A summary of the four articles included in this thesis is given here, followed by a description of the author's contribution for each of them.

6.1 Paper I

Ala-Lahti, M., Kilpua, E. K. J., Dimmock, A. P., Osmane, A., Pulkkinen, T. I., and Souček, J.: Statistical analysis of mirror mode waves in sheath regions driven by interplanetary coronal mass ejection, *Annales Geophysicae*, 36, 793-808, 2018.

Summary: A statistical analysis of mirror mode (MM) waves that investigates the occurrence and features of MMs in ICME-driven sheath regions is constructed. MMs are compressive and linearly polarised waves, which appear as increases (peaks) and decreases (dips) in magnetic field magnitude. Based on these characteristics, a semi-automated algorithm that identifies MMs from solely in-situ magnetic field data is first developed. The algorithm is then used to analyse 91 ICME sheath regions from January 1997 to April 2015. The results imply MMs are common structures in ICME sheaths and occur almost exclusively as dip-like structures in mirror stable plasma. MMs have largest amplitude and occurrence near the shock, and the shock heating and compression is concluded as the dominant source of free energy that is manifested by a presence of proton temperature anisotropy in plasma. MMs are observed throughout the sheath, and the ones at the back of the sheath are suggested to be remnants of MMs generated near the shock.

The author's contribution: Developed and coded the MM identification algorithm, constructed the analysis from the output of the algorithm, in charge of interpretation of the results, wrote the manuscript.

6.2 Paper II

Ala-Lahti, M., Kilpua, E. K. J., Souček, J., Pulkkinen, T. I., and Dimmock, A. P.: Alfvén ion cyclotron waves in sheath regions driven by interplanetary coronal mass ejections, *Journal of Geophysical Research: Space Physics*, 124, 3893-3909, 2019.

Summary: A statistical analysis of Alfvén ion cyclotron (AIC) waves that investigates the occurrence and properties of AICs in ICME-driven sheath regions is constructed. An automated method identifying AIC waves from solely in-situ magnetic field data is developed. The identification applies the theoretical characteristics of AIC waves that have been confirmed from observations in the Earth's magnetosheath. These features are the transverse left-hand polarisation and quasi-parallel propagation direction with respect to the background magnetic field. The algorithm is then used to analyse 91 ICME sheath regions from January 1997 to April 2015. AIC waves are observed frequently in ICME sheaths their occurrence being the highest in the vicinity of the shock. The results reinforce the discovery made in Paper I that the shock heating and compression have a crucial role in generating wave activity in ICME sheaths. The majority of observed AIC waves have their frequency below the ion cyclotron frequency and occur in low $\beta_{\parallel}$ plasma.

The author's contribution: Developed and coded the AIC wave identification algorithm, constructed the analysis from the output of the algorithm, in charge of interpretation of the results, wrote the manuscript.

6.3 Paper III

Ala-Lahti, M., Ruohotie, J., Good, S. W., Kilpua E. K. J., and Lugaz, N.: Spatial coherence of interplanetary coronal mass ejection sheaths at 1 AU, *Journal of Geophysical Research: Space Physics*, 125, e2020JA028002, 2020.

Summary: A statistical analysis of the longitudinal spatial coherence of ICME-driven sheath regions near 1 AU is constructed. 29 ICME sheaths, from which the majority were observed during 2000–2002 when the Wind spacecraft performed prograde orbits, are analysed by comparing the in-situ measurements of the ACE and Wind spacecraft. Pearson correlation coefficients are computed for the magnetic field magnitude and components, and for low- and high-pass filtered data. The magnetic field coherence is further estimated in the longitudinal direction by extrapolating the correlation to the distance of zero correlation. The results imply that sheath magnetic fields are more coherently structured and well correlated compared to the solar wind. The largest coherence is observed in the GSE y-direction. The study suggests the field draping and shock passage cause the observed results.

The author's contribution: Designed the project, contributed to constructing the results and analysis, in charge of interpretation of the results, wrote the manuscript.

6.4 Paper IV

Good, S. W., **Ala-Lahti, M.**, Palmerio, E., Kilpua E. K. J., and Osmane, A.: Radial evolution of magnetic field fluctuations in an interplanetary coronal mass ejection sheath, *The Astrophysical Journal*, 893, 110, 2020.

Summary: A case study of the radial evolution of an ICME-driven sheath region is constructed. The analysis consists in studying the magnetic field configuration of an ICME sheath observed by MESSENGER at 0.47 AU and STEREO-B at 1.08 AU while the spacecraft were close to a radial alignment in November 2010. Radial changes in magnetic field fluctuations are investigated by constructing statistical distributions and average spectral properties, and by utilising the permutation entropy and statistical complexity that together constitute a novel way to study space plasmas. The radial development of magnetic planarity is also studied. At 0.47 AU, the solar wind entering the sheath is reported to experience the similar "aging effect" that the wind has when propagating in interplanetary space. Consistent with Paper III, a large-scale structure occurs in the sheath. This structure is absent in the solar wind at 0.47 and 1.08 AU. The study reports planar magnetic structures (PMSs) to occur in the sheath behind the shock and in front of the ejecta leading edge. These PMSs grow significantly with radial distance and the growth is suggested to originate from the solar wind plasma experiencing steady state accumulation in the sheath, which results from the shock crossing and reduced non-radial deflection.

The author's contribution: Contributed to designing the project, performed the analysis of the permutation entropy and statistical complexity and produced Fig. 4, wrote partially Sec. 4 in the manuscript, participated in analysing the results.

References

Ala-Lahti, M. (2017). *Mirror mode waves in coronal mass ejection-driven sheath regions* (Master's thesis, University of Helsinki). Retrieved from http://urn.fi/urn:nbn:fi-fe2017112251961

Alfvén, H. (1942). Existence of electromagnetic-hydrodynamic waves. *Nature*, *150*(3805), 405-406. doi: 10.1038/150405d0

Alfvén, H. (1943). On the existence of electromagnetic-hydrodynamic Waves. *Arkiv for Matematik, Astronomi och Fysik*, *29B*, 1-7.

Allen, R. C., Zhang, J. C., Kistler, L. M., Spence, H. E., Lin, R. L., Klecker, B., ... Jordanova, V. K. (2015). A statistical study of EMIC waves observed by Cluster: 1. Wave properties. *Journal of Geophysical Research (Space Physics)*, *120*(7), 5574-5592. doi: 10.1002/2015JA021333

Anderson, B. J., & Fuselier, S. A. (1993). Magnetic pulsations from 0.1 to 4.0 Hz and associated plasma properties in the Earth's subsolar magnetosheath and plasma depletion layer. *Journal of Geophysical Research*, *98*(A2), 1461-1480. doi: 10.1029/92JA02197

André, M., Li, W., Toledo-Redondo, S., Khotyaintsev, Y. V., Vaivads, A., Graham, D. B., ... Saito, Y. (2016). Magnetic reconnection and modification of the Hall physics due to cold ions at the magnetopause. *Geophysical Research Letters*, *43*(13), 6705-6712. doi: 10.1002/2016GL069665

Axford, W. I., & Hines, C. O. (1961). A unifying theory of high-latitude geophysical phenomena and geomagnetic storms. *Canadian Journal of Physics*, *39*, 1433. doi: 10.1139/p61-172

Bale, S. D., Badman, S. T., Bonnell, J. W., Bowen, T. A., Burgess, D., Case, A. W., ... Wygant, J. R. (2019). Highly structured slow solar wind emerging from an equatorial coronal hole. *Nature*, *576*(7786), 237-242. doi: 10.1038/s41586-019-1818-7

Balogh, A., Bothmer, V., Crooker, N. U., Forsyth, R. J., Gloeckler, G., Hewish, A., ... Mikić, Z. (1999). The solar origin of corotating interaction regions and their formation in the inner heliosphere. *Space Science Reviews*, *89*, 141-178. doi: 10.1023/A:1005245306874

Bame, S. J., Asbridge, J. R., Feldman, W. C., & Kearney, P. D. (1974). The quiet corona: Temperature and temperature gradient. *Solar Physics*, *35*(1), 137-152. doi: 10.1007/BF00156963

Bame, S. J., Hundhausen, A. J., Asbridge, J. R., & Strong, I. B. (1968). Solar

wind ion composition. *Physical Review Letters*, *20*, 393–395. doi: 10.1103/PhysRevLett.20.393

Bandt, C., & Pompe, B. (2002). Permutation entropy: A natural complexity measure for time series. *Physical Review Letters*, *88*, 174102. Retrieved from https://link.aps.org/doi/10.1103/PhysRevLett.88.174102 doi: 10.1103/PhysRevLett.88.174102

Bartels, J., Heck, N. H., & Johnston, H. F. (1939). The three-hour-range index measuring geomagnetic activity. *Terrestrial Magnetism and Atmospheric Electricity (Journal of Geophysical Research)*, *44*(4), 411. doi: 10.1029/TE044i004p00411

Bavassano-Cattaneo, M. B., Tsurutani, B. T., Smith, E. J., & Lin, R. P. (1986). Subcritical and supercritical interplanetary shocks: magnetic field and energetic particle observations. *Journal of Geophysical Research*, *91*(A11), 11929-11935. doi: 10.1029/JA091iA11p11929

Belcher, J. W., & Davis, J., Leverett. (1971). Large-amplitude Alfvén waves in the interplanetary medium, 2. *Journal of Geophysical Research*, *76*(16), 3534. doi: 10.1029/JA076i016p03534

Birkeland, K. (1908). *The Norwegian aurora polaris expedition 1902–1903* (Vol. 1). Aschehoug.

Blanco-Cano, X. (2010). Bow shocks in the solar wind: Lessons towards understanding interplanetary shocks. In *Twelfth international solar wind conference* (Vol. 1216, p. 459-465). doi: 10.1063/1.3395903

Blanco-Cano, X., Kajdič, P., Aguilar-Rodríguez, E., Russell, C. T., Jian, L. K., & Luhmann, J. G. (2016). Interplanetary shocks and foreshocks observed by STEREO during 2007-2010. *Journal of Geophysical Research (Space Physics)*, *121*(2), 992-1008. doi: 10.1002/2015JA021645

Blanco-Cano, X., Omidi, N., & Russell, C. T. (2006). Macrostructure of collisionless bow shocks: 2. ULF waves in the foreshock and magnetosheath. *Journal of Geophysical Research (Space Physics)*, *111*(A10), A10205. doi: 10.1029/2005JA011421

Boteler, D. H., Pirjola, R. J., & Nevanlinna, H. (1998). The effects of geomagnetic disturbances on electrical systems at the Earth's surface. *Advances in Space Research*, *22*(1), 17-27. doi: 10.1016/S0273-1177(97)01096-X

Bothmer, V., & Schwenn, R. (1998). The structure and origin of magnetic clouds in the solar wind. *Annales Geophysicae*, *16*(1), 1-24. doi: 10.1007/s00585-997-0001-x

Brekke, A. (2012). *Physics of the upper polar atmosphere*. Springer-Verlag Berlin Heidelberg. doi: 10.1007/978-3-642-27401-5

Bruno, R., & Carbone, V. (2013). The solar wind as a turbulence laboratory. *Living*

Reviews in Solar Physics, *10*(1), 2. doi: 10.12942/lrsp-2013-2

Bruno, R., Carbone, V., Vörös, Z., D'Amicis, R., Bavassano, B., Cattaneo, M. B., ... Kovács, P. (2009). Coordinated study on solar wind turbulence during the Venus-Express, ACE and Ulysses alignment of August 2007. *Earth Moon and Planets*, *104*(1-4), 101-104. doi: 10.1007/s11038-008-9272-9

Burlaga, L. F. (1983). Corotating pressure waves without fast streams in the solar wind. *Journal of Geophysical Research*, *88*(A8), 6085-6094. doi: 10.1029/JA088iA08p06085

Burlaga, L. F. (1988). Magnetic clouds and force-free fields with constant alpha. *Journal of Geophysical Research*, *93*(A7), 7217-7224. doi: 10.1029/JA093iA07p07217

Burlaga, L. F., Klein, L., Sheeley, J., N. R., Michels, D. J., Howard, R. A., Koomen, M. J., ... Rosenbauer, H. (1982). A magnetic cloud and a coronal mass ejection. *Geophysical Research Letters*, *9*(12), 1317-1320. doi: 10.1029/GL009i012p01317

Burlaga, L. F., Sittler, E., Mariani, F., & Schwenn, R. (1981). Magnetic loop behind an interplanetary shock: Voyager, Helios, and IMP 8 observations. *Journal of Geophysical Research*, *86*(A8), 6673-6684. doi: 10.1029/JA086iA08p06673

Cahill, L. J., & Amazeen, P. G. (1963). The boundary of the geomagnetic field. *Journal of Geophysical Research*, *68*(7), 1835-1843. doi: 10.1029/JZ068i007p01835

Califano, F., Hellinger, P., Kuznetsov, E., Passot, T., Sulem, P. L., & TráVníČEk, P. M. (2008). Nonlinear mirror mode dynamics: Simulations and modeling. *Journal of Geophysical Research (Space Physics)*, *113*(A8), A08219. doi: 10.1029/2007JA012898

Chandrasekhar, S., Kaufman, A. N., & Watson, K. M. (1958). The stability of the pinch. *Proceedings of the Royal Society of London Series A*, *245*(1243), 435-455. doi: 10.1098/rspa.1958.0094

Chapman, S., & Ferraro, V. C. A. (1931). A new theory of magnetic storms. *Terrestrial Magnetism and Atmospheric Electricity (Journal of Geophysical Research)*, *36*(2), 77. doi: 10.1029/TE036i002p00077

Chen, C. H. K., Klein, K. G., & Howes, G. G. (2019). Evidence for electron Landau damping in space plasma turbulence. *Nature Communications*, *10*, 740. doi: 10.1038/s41467-019-08435-3

Chi, Y., Shen, C., Luo, B., Wang, Y., & Xu, M. (2018). Geoeffectiveness of stream interaction regions from 1995 to 2016. *Space Weather*, *16*(12), 1960-1971. doi: 10.1029/2018SW001894

Coles, W. A., & Maagoe, S. (1972). Solar-wind velocity from ips observations. *Journal of Geophysical Research (1896-1977)*, *77*(28), 5622-5624. doi: 10.1029/

JA077i028p05622

Crooker, N. U., & Siscoe, G. L. (1977). A mechanism for pressure anisotropy and mirror instability in the dayside magnetosheath. *Journal of Geophysical Research*, *82*(1), 185. doi: 10.1029/JA082i001p00185

Dasgupta, B., Tsurutani, B. T., & Janaki, M. S. (2003). A kinetic approach to the ponderomotive force. *Geophysical Research Letters*, *30*(21), 2128. doi: 10.1029/2003GL017385

Davidson, R. C., & Ogden, J. M. (1975). Electromagnetic ion cyclotron instability driven by ion energy anisotropy in high-beta plasmas. *Physics of Fluids*, *18*(8), 1045-1050. doi: 10.1063/1.861253

de Lucas, A., Schwenn, R., dal Lago, A., Marsch, E., & Clúa de Gonzalez, A. L. (2011). Interplanetary shock wave extent in the inner heliosphere as observed by multiple spacecraft. *Journal of Atmospheric and Solar-Terrestrial Physics*, *73*(10), 1281-1292. doi: 10.1016/j.jastp.2010.12.011

Dimmock, A. P., Russell, C. T., Sagdeev, R. Z., Krasnoselskikh, V., Walker, S. N., Carr, C., ... Balikhin, M. A. (2019). Direct evidence of nonstationary collisionless shocks in space plasmas. *Science Advances*, *5*(2), eaau9926. doi: 10.1126/sciadv.aau9926

Dungey, J. W. (1961). Interplanetary magnetic field and the auroral zones. *Physical Review Letters*, *6*(2), 47-48. doi: 10.1103/PhysRevLett.6.47

Ebert, R. W., McComas, D. J., Elliott, H. A., Forsyth, R. J., & Gosling, J. T. (2009). Bulk properties of the slow and fast solar wind and interplanetary coronal mass ejections measured by Ulysses: Three polar orbits of observations. *Journal of Geophysical Research (Space Physics)*, *114*(A1), A01109. doi: 10.1029/2008JA013631

Echim, M. M., Lemaire, J., & Lie-Svendsen, Ø. (2011). A review on solar wind modeling: Kinetic and fluid aspects. *Surveys in Geophysics*, *32*(1), 1-70. doi: 10.1007/s10712-010-9106-y

Escoubet, C. P., Fehringer, M., & Goldstein, M. (2001). *Introduction* The Cluster mission. *Annales Geophysicae*, *19*, 1197-1200. doi: 10.5194/angeo-19-1197-2001

Eyni, M., & Steinitz, R. (1978). The cooling of solar wind protons from Mariner 2 data. *Journal of Geophysical Research*, *83*(A1), 215-216. doi: 10.1029/JA083iA01p00215

Fairfield, D. H. (1971). Average and unusual locations of the Earth's magnetopause and bow shock. *Journal of Geophysical Research*, *76*(28), 6700. doi: 10.1029/JA076i028p06700

Fairfield, D. H. (1976). Magnetic fields of the magnetosheath. *Reviews of Geophysics*

and Space Physics, *14*, 117-134. doi: 10.1029/RG014i001p00117

Farris, M. H., & Russell, C. T. (1994). Determining the standoff distance of the bow shock: Mach number dependence and use of models. *Journal of Geophysical Research*, *99*(A9), 17681-17690. doi: 10.1029/94JA01020

Farrugia, C. J., Dunlop, M. W., Geurts, F., Balogh, A., Southwood, D. J., Bryant, D. A., ... Etemadi, A. (1990). An interplanetary planar magnetic structure oriented at a large ($\sim$ 80 deg) angle to the Parker spiral. *Geophysical Research Letters*, *17*(8), 1025-1028. doi: 10.1029/GL017i008p01025

Fenrich, F. R., & Luhmann, J. G. (1998). Geomagnetic response to magnetic clouds of different polarity. *Geophysical Research Letters*, *25*(15), 2999-3002. doi: 10.1029/98GL51180

Fox, N. J., Velli, M. C., Bale, S. D., Decker, R., Driesman, A., Howard, R. A., ... Szabo, A. (2016). The Solar Probe Plus mission: Humanity's first visit to our star. *Space Science Reviews*, *204*(1-4), 7-48. doi: 10.1007/s11214-015-0211-6

Gary, G. A. (2001). Plasma beta above a solar active region: Rethinking the paradigm. *Solar Physics*, *203*(1), 71-86. doi: 10.1023/A:1012722021820

Gary, S. P. (1992). The mirror and ion cyclotron anisotropy instabilities. *Journal of Geophysical Research*, *97*(A6), 8519-8529. doi: 10.1029/92JA00299

Gary, S. P., Fuselier, S. A., & Anderson, B. J. (1993). Ion anisotropy instabilities in the magnetosheath. *Journal of Geophysical Research*, *98*(A2), 1481-1488. doi: 10.1029/92JA01844

Génot, V., Broussillou, L., Budnik, E., Hellinger, P., Trávníček, P. M., Lucek, E., & Dandouras, I. (2011). Timing mirror structures observed by Cluster with a magnetosheath flow model. *Annales Geophysicae*, *29*(10), 1849-1860. doi: 10.5194/angeo-29-1849-2011

Génot, V., Budnik, E., Hellinger, P., Passot, T., Belmont, G., Trávníček, P. M., ... Dandouras, I. (2009). Mirror structures above and below the linear instability threshold: Cluster observations, fluid model and hybrid simulations. *Annales Geophysicae*, *27*(2), 601-615. doi: 10.5194/angeo-27-601-2009

Gloeckler, G., Geiss, J., Balsiger, H., Bedini, P., Cain, J. C., Fischer, J., ... Wilken, B. (1992). The Solar Wind Ion Composition Spectrometer. *Astronomy and Astrophysics Supplement Series*, *92*(2), 267-289.

Gold, T. (1955). *Gas dynamics of cosmic clouds*. North Holland Publishing Co., Amsterdam, *103*.

Gonzalez, W. D., Joselyn, J. A., Kamide, Y., Kroehl, H. W., Rostoker, G., Tsurutani, B. T., & Vasyliunas, V. M. (1994). What is a geomagnetic storm? *Journal of Geophysical Research*, *99*(A4), 5771-5792. doi: 10.1029/93JA02867

Good, S. W. (2016). *The structure and evolution of interplanetary coronal mass*

ejections observed by MESSENGER and Venus Express (Doctoral dissertation, Imperial College London). doi: 10.25560/50710

Good, S. W., Forsyth, R. J., Eastwood, J. P., & Möstl, C. (2018). Correlation of ICME magnetic fields at radially aligned spacecraft. *Solar Physics*, *293*(3), 52. doi: 10.1007/s11207-018-1264-y

Good, S. W., Kilpua, E. K. J., Ala-Lahti, M., Osmane, A., Bale, S. D., & Zhao, L. L. (2020). Cross Helicity of the 2018 November Magnetic Cloud Observed by the Parker Solar Probe. *The Astrophysical Journal Letters*, *900*(2), L32. doi: 10.3847/2041-8213/abb021

Gopalswamy, N., Lara, A., Kaiser, M. L., & Bougeret, J. L. (2001). Near-Sun and near-Earth manifestations of solar eruptions. *Journal of Geophysical Research*, *106*(A11), 25261-25278. doi: 10.1029/2000JA004025

Gosling, J. T., Asbridge, J. R., Bame, S. J., & Feldman, W. C. (1976). Solar wind speed variations: 1962-1974. *Journal of Geophysical Research*, *81*(A28), 5061-5070. doi: 10.1029/JA081i028p05061

Gosling, J. T., Bame, S. J., McComas, D. J., Phillips, J. L., Pizzo, V. J., Goldstein, B. E., & Neugebauer, M. (1993). Latitudinal variation of solar wind corotating stream interaction regions: Ulysses. *Geophysical Research Letters*, *20*(24), 2789-2792. doi: 10.1029/93GL03116

Gosling, J. T., & McComas, D. J. (1987). Field line draping about fast coronal mass ejecta: A source of strong out-of-the-ecliptic interplanetary magnetic fields. *Geophysical Research Letters*, *14*(4), 355-358. doi: 10.1029/GL014i004p00355

Gosling, J. T., McComas, D. J., Phillips, J. L., & Bame, S. J. (1991). Geomagnetic activity associated with Earth passage of interplanetary shock disturbances and coronal mass ejections. *Journal of Geophysical Research*, *96*(A5), 7831-7839. doi: 10.1029/91JA00316

Gosling, J. T., Riley, P., McComas, D. J., & Pizzo, V. J. (1998). Overexpanding coronal mass ejections at high heliographic latitudes: Observations and simulations. *Journal of Geophysical Research*, *103*(A2), 1941-1954. doi: 10.1029/97JA01304

Gosling, J. T., Thomsen, M. F., Bame, S. J., Feldman, W. C., Paschmann, G., & Sckopke, N. (1982). Evidence for specularly reflected ions upstream from the quasi-parallel bow shock. *Geophysical Research Letters*, *9*(12), 1333-1336. doi: 10.1029/GL009i012p01333

Grandin, M. (2017). *Multi-instrument and modelling studies of the ionospheres at Earth and Mars* (Doctoral dissertation, University of Oulu). Retrieved from http://urn.fi/urn:isbn:9789526216157

Grandin, M., Aikio, A. T., & Kozlovsky, A. (2019). Properties and geoeffectiveness

of solar wind high-speed streams and stream interaction regions during solar cycles 23 and 24. *Journal of Geophysical Research (Space Physics)*, *124*(6), 3871-3892. doi: 10.1029/2018JA026396

Greenstadt, E. W., Le, G., & Strangeway, R. J. (1995). ULF waves in the foreshock. *Advances in Space Research*, *15*(8-9), 71-84. doi: 10.1016/0273-1177(94)00087-H

Gringauz, K. I., Bezrokikh, V. V., Ozerov, V. D., & Rybchinskii, R. E. (1960). A study of the interplanetary ionized gas, high-energy electrons and corpuscular radiation from the Sun by means of the three-electrode trap for charged particles on the second Soviet cosmic rocket. *Soviet Physics Doklady*, *5*, 361.

Gurnett, D. A., Marsch, E., Pilipp, W., Schwenn, R., & Rosenbauer, H. (1979). Ion acoustic waves and related plasma observations in the solar wind. *Journal of Geophysical Research*, *84*(A5), 2029-2038. doi: 10.1029/JA084iA05p02029

Hanslmeier, A. (2007). *The Sun and space weather* (Vol. 347). doi: 10.1007/978-1-4020-5604-8

Hanson, E. L. M., Agapitov, O. V., Vasko, I. Y., Mozer, F. S., Krasnoselskikh, V., Bale, S. D., ... Giles, B. (2020). Shock drift acceleration of ions in an interplanetary shock observed by MMS. *The Astrophysical Journal Letters*, *891*(1), L26. doi: 10.3847/2041-8213/ab7761

Hartle, R. E., & Sturrock, P. A. (1968). Two-fluid model of the solar wind. *Astrophysical Journal*, *151*, 1155. doi: 10.1086/149513

Hasegawa, A. (1969). Drift mirror instability of the magnetosphere. *Physics of Fluids*, *12*, 2642-2650. doi: 10.1063/1.1692407

Hasegawa, A. (1975). Plasma instabilities and nonlinear effects. *Springer Verlag Springer Series on Physics Chemistry Space*, *8*.

Hellinger, P., Trávníček, P., Kasper, J. C., & Lazarus, A. J. (2006). Solar wind proton temperature anisotropy: Linear theory and *WIND*/SWE observations. *Geophysical Research Letters*, *33*(9), L09101. doi: 10.1029/2006GL025925

Hoeksema, J. T., Wilcox, J. M., & Scherrer, P. H. (1982). Structure of the heliospheric current sheet in the early portion of sunspot cycle 21. *Journal of Geophysical Research*, *87*(A12), 10331-10338. doi: 10.1029/JA087iA12p10331

Hoeksema, J. T., Wilcox, J. M., & Scherrer, P. H. (1983). The structure of the heliospheric current sheet: 1978-1982. *Journal of Geophysical Research*, *88*(A12), 9910-9918. doi: 10.1029/JA088iA12p09910

Horbury, T. S., Forman, M. A., & Oughton, S. (2005). Spacecraft observations of solar wind turbulence: an overview. *Plasma Physics and Controlled Fusion*, *47*(12B), B703-B717. doi: 10.1088/0741-3335/47/12B/S52

Hundhausen, A. J., Bame, S. J., & Ness, N. F. (1967). Solar wind thermal

anisotropies: Vela 3 and IMP 3. *Journal of Geophysical Research*, *72*, 5265. doi: 10.1029/JZ072i021p05265

Huttunen, E. K. J., & Koskinen, H. E. J. (2004). Importance of post-shock streams and sheath region as drivers of intense magnetospheric storms and high-latitude activity. *Annales Geophysicae*, *22*(5), 1729-1738. doi: 10.5194/angeo-22-1729-2004

Huttunen, E. K. J., Koskinen, H. E. J., & Schwenn, R. (2002). Variability of magnetospheric storms driven by different solar wind perturbations. *Journal of Geophysical Research (Space Physics)*, *107*(A7), 1121. doi: 10.1029/2001JA900171

Iroshnikov, P. S. (1964). Turbulence of a conducting fluid in a strong magnetic field. *Soviet Astronomy*, *7*, 566.

Janvier, M., Winslow, R. M., Good, S., Bonhomme, E., Démoulin, P., Dasso, S., ... Boakes, P. D. (2019). Generic magnetic field intensity profiles of interplanetary coronal mass ejections at Mercury, Venus, and Earth from superposed epoch analyses. *Journal of Geophysical Research (Space Physics)*, *124*(2), 812-836. doi: 10.1029/2018JA025949

Ji, S., Oh, S. P., Ruszkowski, M., & Markevitch, M. (2016). The efficiency of magnetic field amplification at shocks by turbulence. *Monthly Notices of the Royal Astronomical Society*, *463*(4), 3989-4003. doi: 10.1093/mnras/stw2320

Jian, L., Russell, C. T., Luhmann, J. G., & Skoug, R. M. (2006). Properties of stream interactions at one AU during 1995 – 2004. *Solar Physics*, *239*(1-2), 337-392. doi: 10.1007/s11207-006-0132-3

Jones, G. H., Balogh, A., & Smith, E. J. (2003). Solar magnetic field reversal as seen at Ulysses. *Geophysical Research Letters*, *30*(19), 8028. doi: 10.1029/2003GL017204

Jones, G. H., Rees, A., Balogh, A., & Forsyth, R. J. (2002). The draping of heliospheric magnetic fields upstream of coronal mass ejecta. *Geophysical Research Letters*, *29*(11), 1520. doi: 10.1029/2001GL014110

Kahler, S. W. (2001). The correlation between solar energetic particle peak intensities and speeds of coronal mass ejections: Effects of ambient particle intensities and energy spectra. *Journal of Geophysical Research*, *106*(A10), 20947-20956. doi: 10.1029/2000JA002231

Kaiser, M. L., Kucera, T. A., Davila, J. M., St. Cyr, O. C., Guhathakurta, M., & Christian, E. (2008). The STEREO mission: An introduction. *Space Science Reviews*, *136*(1-4), 5-16. doi: 10.1007/s11214-007-9277-0

Kajdič, P., Blanco-Cano, X., Aguilar-Rodriguez, E., Russell, C. T., Jian, L. K., & Luhmann, J. G. (2012). Waves upstream and downstream of interplane-

tary shocks driven by coronal mass ejections. *Journal of Geophysical Research (Space Physics)*, *117*(A6), A06103. doi: 10.1029/2011JA017381

Kallenrode, M.-B. (2004). *Space physics: An introduction to plasmas and particles in the heliosphere and magnetospheres.* Springer-Verlag. doi: 10.1007/978-3-662-09959-9

Kasper, J. C., & Klein, K. G. (2019). Strong preferential ion heating is limited to within the solar Alfvén surface. *The Astrophysical Journal Letters*, *877*(2), L35. doi: 10.3847/2041-8213/ab1de5

Kataoka, R., Watari, S., Shimada, N., Shimazu, H., & Marubashi, K. (2005). Downstream structures of interplanetary fast shocks associated with coronal mass ejections. *Geophysical Research Letters*, *32*(12), L12103. doi: 10.1029/2005GL022777

Kay, C., Nieves-Chinchilla, T., & Jian, L. K. (2020). FIDO-SIT: The first forward model for the in situ magnetic field of CME-driven sheaths. *Journal of Geophysical Research (Space Physics)*, *125*(2), e27423. doi: 10.1029/2019JA027423

Kaymaz, Z., & Siscoe, G. (2006). Field-line draping around ICMEs. *Solar Physics*, *239*(1-2), 437-448. doi: 10.1007/s11207-006-0308-x

Kennel, C. F. (1987). Critical Mach numbers in classical magnetohydrodynamics. *Journal of Geophysical Research*, *92*(A12), 13427-13437. doi: 10.1029/JA092iA12p13427

Kennel, C. F., Edmiston, J. P., & Hada, T. (1985). A quarter century of collisionless shock research. *Washington DC American Geophysical Union Geophysical Monograph Series*, *34*, 1-36. doi: 10.1029/GM034p0001

Kennel, C. F., Edmiston, J. P., Scarf, F. L., Coroniti, F. V., Russell, C. T., Smith, E. J., ... Temerin, M. (1984b). Structure of the November 12, 1978, quasi-parallel interplanetary shock. *Journal of Geophysical Research*, *89*(A7), 5436-5452. doi: 10.1029/JA089iA07p05436

Kennel, C. F., & Petschek, H. E. (1966). Limit on stably trapped particle fluxes. *Journal of Geophysical Research*, *71*, 1. doi: 10.1029/JZ071i001p00001

Kennel, C. F., Scarf, F. L., Coroniti, F. V., Russell, C. T., Wenzel, K. P., Sanderson, T. R., ... Scholer, M. (1984a). Plasma and energetic particle structure upstream of a quasi-parallel interplanetary shock. *Journal of Geophysical Research*, *89*(A7), 5419-5435. doi: 10.1029/JA089iA07p05419

Kilpua, E., & Koskinen, H. (2017). *Introduction to plasma physics* (1st ed.). Finland: LIMES.

Kilpua, E. K. J., Fontaine, D., Moissard, C., Ala-Lahti, M., Palmerio, E., Yordanova, E., ... Turc, L. (2019a). Solar wind properties and geospace impact of coronal mass ejection-driven sheath regions: Variation and driver dependence. *Space*

Weather, *17*(8), 1257-1280. doi: 10.1029/2019SW002217

Kilpua, E. K. J., Good, S. W., Palmerio, E., Asvestari, E., Lumme, E., Ala-Lahti, M., ... Futaana, Y. (2019b). Multipoint observations of the June 2012 interacting interplanetary flux ropes. *Frontiers in Astronomy and Space Sciences*, *6*, 50. doi: 10.3389/fspas.2019.00050

Kilpua, E. K. J., Hietala, H., Koskinen, H. E. J., Fontaine, D., & Turc, L. (2013). Magnetic field and dynamic pressure ULF fluctuations in coronal-mass-ejection-driven sheath regions. *Annales Geophysicae*, *31*(9), 1559-1567. doi: 10.5194/angeo-31-1559-2013

Kilpua, E. K. J., Koskinen, H. E. J., & Pulkkinen, T. I. (2017). Coronal mass ejections and their sheath regions in interplanetary space. *Living Reviews in Solar Physics*, *14*(1), 5. doi: 10.1007/s41116-017-0009-6

Kilpua, E. K. J., Lumme, E., Andreeova, K., Isavnin, A., & Koskinen, H. E. J. (2015). Properties and drivers of fast interplanetary shocks near the orbit of the Earth (1995-2013). *Journal of Geophysical Research (Space Physics)*, *120*(6), 4112-4125. doi: 10.1002/2015JA021138

Kivelson, M. G., & Russell, C. T. (1995). *Introduction to space physics*. Cambridge University Press. doi: 10.1017/9781139878296

Kivelson, M. G., & Southwood, D. J. (1996). Mirror instability II: The mechanism of nonlinear saturation. *Journal of Geophysical Research*, *101*(A8), 17365-17372. doi: 10.1029/96JA01407

Kiyani, K. H., Osman, K. T., & Chapman, S. C. (2015). Dissipation and heating in solar wind turbulence: from the macro to the micro and back again. *Philosophical Transactions of the Royal Society of London Series A*, *373*(2041), 20140155-20140155. doi: 10.1098/rsta.2014.0155

Klein, L. W., & Burlaga, L. F. (1982). Interplanetary magnetic clouds at 1 AU. *Journal of Geophysical Research*, *87*(A2), 613-624. doi: 10.1029/JA087iA02p00613

Kolmogorov, A. N. (1962). A refinement of previous hypotheses concerning the local structure of turbulence in a viscous incompressible fluid at high reynolds number. *Journal of Fluid Mechanics*, *13*(1), 82–85. doi: 10.1017/S0022112062000518

Koskinen, H. (2011). *Physics of space storms: From the solar surface to the earth*. Springer-Verlag. doi: 10.1007/978-3-642-00319-6

Koval, A., & Szabo, A. (2010). Multispacecraft observations of interplanetary shock shapes on the scales of the Earth's magnetosphere. *Journal of Geophysical Research (Space Physics)*, *115*(A12), A12105. doi: 10.1029/2010JA015373

Kraichnan, R. H. (1965). Inertial-range spectrum of hydromagnetic turbulence. *The Physics of Fluids*, *8*(7), 1385–1387.

Lacombe, C., & Belmont, G. (1995). Waves in the Earth's magnetosheath: observations and interpretations. *Advances in Space Research*, *15*(8-9), 329-340. doi: 10.1016/0273-1177(94)00113-F

Lakhina, G. S., & Buti, B. (1976). Stability of solar wind double ion streams. *Journal of Geophysical Research*, *81*(13), 2135. doi: 10.1029/JA081i013p02135

Lepping, R. P., & Behannon, K. W. (1986). Magnetic field directional discontinuities: Characteristics between 0.46 and 1.0 AU. *Journal of Geophysical Research*, *91*(A8), 8725-8741. doi: 10.1029/JA091iA08p08725

Lepping, R. P., Wu, C. C., Berdichevsky, D. B., & Szabo, A. (2015). *Wind* magnetic clouds for 2010 - 2012: Model parameter fittings, associated shock waves, and comparisons to earlier periods. *Solar Physics*, *290*(8), 2265-2290. doi: 10.1007/s11207-015-0755-3

Li, Q. H., Yang, L., Wu, D. J., & Wang, T. Y. (2019). Electromagnetic waves around the proton cyclotron frequency in the sheath regions of interplanetary magnetic clouds: STEREO observations. *The Astrophysical Journal*, *874*(1), 55. doi: 10.3847/1538-4357/ab06f7

Li, Q. H., Yang, L., Xiang, L., & Wu, D. J. (2020). Spatial distribution of electromagnetic waves near the proton cyclotron frequency in ICME sheath regions associated with quasi-perpendicular shocks: *Wind* observations. *The Astrophysical Journal*, *892*(2), 98. doi: 10.3847/1538-4357/ab7cde

Lindsay, G. M., Russell, C. T., & Luhmann, J. G. (1995). Coronal mass ejection and stream interaction region characteristics and their potential geomagnetic effectiveness. *Journal of Geophysical Research*, *100*(A9), 16999-17014. doi: 10.1029/95JA00525

Liu, Y., Richardson, J. D., Belcher, J. W., Kasper, J. C., & Skoug, R. M. (2006b). Plasma depletion and mirror waves ahead of interplanetary coronal mass ejections. *Journal of Geophysical Research (Space Physics)*, *111*(A9), A09108. doi: 10.1029/2006JA011723

Liu, Y., Richardson, J. D., Belcher, J. W., Wang, C., Hu, Q., & Kasper, J. C. (2006a). Constraints on the global structure of magnetic clouds: Transverse size and curvature. *Journal of Geophysical Research (Space Physics)*, *111*(A12), A12S03. doi: 10.1029/2006JA011890

Lugaz, N., Farrugia, C. J., Winslow, R. M., Al-Haddad, N., Galvin, A. B., Nieves-Chinchilla, T., ... Janvier, M. (2018). On the spatial coherence of magnetic ejecta: Measurements of coronal mass ejections by multiple spacecraft longitudinally separated by 0.01 AU. *The Astrophysical Journal Letters*, *864*(1), L7. doi: 10.3847/2041-8213/aad9f4

Lugaz, N., Farrugia, C. J., Winslow, R. M., Al-Haddad, N., Kilpua, E. K. J., & Riley,

P. (2016). Factors affecting the geoeffectiveness of shocks and sheaths at 1 AU. *Journal of Geophysical Research (Space Physics)*, *121*(11), 10,861-10,879. doi: 10.1002/2016JA023100

Lugaz, N., Winslow, R. M., & Farrugia, C. J. (2020). Evolution of a long-duration coronal mass ejection and its sheath region between Mercury and Earth on 9-14 July 2013. *Journal of Geophysical Research (Space Physics)*, *125*(1), e27213. doi: 10.1029/2019JA027213

MacBride, B. T., Smith, C. W., & Vasquez, B. J. (2010). Inertial-range anisotropies in the solar wind from 0.3 to 1 AU: Helios 1 observations. *Journal of Geophysical Research (Space Physics)*, *115*(A7), A07105. doi: 10.1029/2009JA014939

Manchester, I., W. B., Gombosi, T. I., De Zeeuw, D. L., Sokolov, I. V., Roussev, I. I., Powell, K. G., ... Zurbuchen, T. H. (2005). Coronal mass ejection shock and sheath structures relevant to particle acceleration. *The Astrophysical Journal*, *622*(2), 1225-1239. doi: 10.1086/427768

Marsch, E., Pilipp, W. G., Thieme, K. M., & Rosenbauer, H. (1989). Cooling of solar wind electrons inside 0.3 AU. *Journal of Geophysical Research*, *94*(A6), 6893-6898. doi: 10.1029/JA094iA06p06893

Marsch, E., & Tu, C. Y. (1997). Intermittency, non-Gaussian statistics and fractal scaling of MHD fluctuations in the solar wind. *Nonlinear Processes in Geophysics*, *4*(2), 101-124. doi: 10.5194/npg-4-101-1997

Marubashi, K. (1986). Structure of the interplanetary magnetic clouds and their solar origins. *Advances in Space Research*, *6*(6), 335-338. doi: 10.1016/0273-1177(86)90172-9

Matteini, L., Landi, S., Hellinger, P., Pantellini, F., Maksimovic, M., Velli, M., ... Marsch, E. (2007). Evolution of the solar wind proton temperature anisotropy from 0.3 to 2.5 AU. *Geophysical Research Letters*, *34*(20), L20105. doi: 10.1029/2007GL030920

Matteini, L., Stansby, D., Horbury, T. S., & Chen, C. H. K. (2018). On the 1/f spectrum in the solar wind and its connection with magnetic compressibility. *The Astrophysical Journal Letters*, *869*(2), L32. doi: 10.3847/2041-8213/aaf573

Matthaeus, W. H., Dasso, S., Weygand, J. M., Milano, L. J., Smith, C. W., & Kivelson, M. G. (2005). Spatial correlation of solar-wind turbulence from two-point measurements. *Physical Review Letters*, *95*(23), 231101. doi: 10.1103/PhysRevLett.95.231101

Matthaeus, W. H., & Velli, M. (2011). Who needs turbulence? A review of turbulence effects in the heliosphere and on the fundamental process of reconnection. *Space Science Reviews*, *160*(1-4), 145-168. doi: 10.1007/s11214-011-9793-9

McComas, D. J., Bame, S. J., Barraclough, B. L., Feldman, W. C., Funsten, H. O.,

Gosling, J. T., ... Neugebauer, M. (1998). Ulysses' return to the slow solar wind. *Geophysical Research Letters*, *25*(1), 1-4. doi: 10.1029/97GL03444

McComas, D. J., Ebert, R. W., Elliott, H. A., Goldstein, B. E., Gosling, J. T., Schwadron, N. A., & Skoug, R. M. (2008). Weaker solar wind from the polar coronal holes and the whole Sun. *Geophysical Research Letters*, *35*(18), L18103. doi: 10.1029/2008GL034896

McComas, D. J., Gosling, J. T., Bame, S. J., Smith, E. J., & Cane, H. V. (1989). A test of magnetic field draping induced B_z perturbations ahead of fast coronal mass ejecta. *Journal of Geophysical Research*, *94*(A2), 1465-1471. doi: 10.1029/JA094iA02p01465

McComas, D. J., Gosling, J. T., Winterhalter, D., & Smith, E. J. (1988). Interplanetary magnetic field draping about fast coronal mass ejecta in the outer heliosphere. *Journal of Geophysical Research*, *93*(A4), 2519-2526. doi: 10.1029/JA093iA04p02519

Meng, X., Tsurutani, B. T., & Mannucci, A. J. (2019). The solar and interplanetary causes of superstorms (minimum Dst $\leq$ -250 nT) during the space age. *Journal of Geophysical Research (Space Physics)*, *124*(6), 3926-3948. doi: 10.1029/2018JA026425

Midgley, J. E., & Davis, J., L. (1963). Calculation by a moment technique of the perturbation of the geomagnetic field by the solar wind. *Journal of Geophysical Research*, *68*, 5111. doi: 10.1029/JZ068i018p05111

Miyake, W., & Mukai, T. (1987). Proton temperature properties in the solar wind. *Planetary and Space Science*, *35*(2), 185-189. doi: 10.1016/0032-0633(87)90087-0

Miyoshi, Y., & Kataoka, R. (2005). Ring current ions and radiation belt electrons during geomagnetic storms driven by coronal mass ejections and corotating interaction regions. *Geophysical Research Letters*, *32*(21), L21105. doi: 10.1029/2005GL024590

Moissard, C., Fontaine, D., & Savoini, P. (2019). A study of fluctuations in magnetic cloud-driven sheaths. *Journal of Geophysical Research (Space Physics)*, *124*(11), 8208-8226. doi: 10.1029/2019JA026952

Montagud-Camps, V., Grappin, R., & Verdini, A. (2018). Turbulent heating between 0.2 and 1 AU: A numerical study. *The Astrophysical Journal*, *853*(2), 153. doi: 10.3847/1538-4357/aaa1ea

Moore, R. L., Sterling, A. C., & Suess, S. T. (2007). The width of a solar coronal mass ejection and the source of the driving magnetic explosion: A test of the standard scenario for CME production. *The Astrophysical Journal*, *668*(2), 1221-1231. doi: 10.1086/521215

Müller, D., Marsden, R. G., St. Cyr, O. C., & Gilbert, H. R. (2013). *Solar Orbiter* Exploring the Sun-heliosphere connection. *Solar Physics*, *285*(1-2), 25-70. doi: 10.1007/s11207-012-0085-7

Mursula, K., & Hiltula, T. (2003). Bashful ballerina: Southward shifted heliospheric current sheet. *Geophysical Research Letters*, *30*(22), 2135. doi: 10.1029/2003GL018201

Nakagawa, T., Nishida, A., & Saito, T. (1989). Planar magnetic structures in the solar wind. *Journal of Geophysical Research*, *94*(A9), 11761-11775. doi: 10.1029/JA094iA09p11761

Ness, N. F., Scearce, C. S., & Seek, J. B. (1964). Initial results of the Imp 1 magnetic field experiment. *Journal of Geophysical Research*, *69*(17), 3531-3569. doi: 10.1029/JZ069i017p03531

Neugebauer, M., Clay, D. R., & Gosling, J. T. (1993). The origins of planar magnetic structures in the solar wind. *Journal of Geophysical Research*, *98*(A6), 9383-9390. doi: 10.1029/93JA00216

Neugebauer, M., & Snyder, C. W. (1966). Mariner 2 observations of the solar wind 1. Average properties. *Journal of Geophysical Research*, *71*, 4469. doi: 10.1029/JZ071i019p04469

Nieves-Chinchilla, T., Vourlidas, A., Raymond, J. C., Linton, M. G., Al-haddad, N., Savani, N. P., ... Hidalgo, M. A. (2018). Understanding the internal magnetic field configurations of ICMEs using more than 20 years of *Wind* observations. *Solar Physics*, *293*(2), 25. doi: 10.1007/s11207-018-1247-z

Norqvist, P., André, M., Eliasson, L., Eriksson, A. I., Blomberg, L., Lühr, H., & Clemmons, J. H. (1996). Ion cyclotron heating in the dayside magnetosphere. *Journal of Geophysical Research*, *101*(A6), 13179-13194. doi: 10.1029/95JA03596

Odstrčil, D., Dryer, M., & Smith, Z. (1996). Propagation of an interplanetary shock along the heliospheric plasma sheet. *Journal of Geophysical Research*, *101*(A9), 19973-19986. doi: 10.1029/96JA00479

Ogilvie, K. W., & Desch, M. D. (1997). The *Wind* spacecraft and its early scientific results. *Advances in Space Research*, *20*(4-5), 559-568. doi: 10.1016/S0273-1177(97)00439-0

Olkin, I., & Pratt, J. W. (1958). Unbiased estimation of certain correlation coefficients. *The Annals of Mathematical Statistics*, *29*(1), 201–211. doi: 10.1214/aoms/1177706717

Ontiveros, V., & Vourlidas, A. (2009). Quantitative measurements of coronal mass ejection-driven shocks from LASCO observations. *The Astrophysical Journal*, *693*(1), 267-275. doi: 10.1088/0004-637X/693/1/267

Osmane, A., Dimmock, A. P., Naderpour, R., Pulkkinen, T. I., & Nykyri, K. (2015). The impact of solar wind ULF B_z fluctuations on geomagnetic activity for viscous timescales during strongly northward and southward IMF. *Journal of Geophysical Research (Space Physics)*, *120*(11), 9307-9322. doi: 10.1002/2015JA021505

Osmane, A., Dimmock, A. P., & Pulkkinen, T. I. (2019). Jensen-Shannon complexity and permutation entropy analysis of geomagnetic auroral currents. *Journal of Geophysical Research (Space Physics)*, *124*(4), 2541-2551. doi: 10.1029/2018JA026248

Oughton, S., Dmitruk, P., & Matthaeus, W. H. (2004). Reduced magnetohydrodynamics and parallel spectral transfer. *Physics of Plasmas*, *11*(5), 2214-2225. doi: 10.1063/1.1705652

Oughton, S., & Matthaeus, W. H. (2005). Parallel and perpendicular cascades in solar wind turbulence. *Nonlinear Processes in Geophysics*, *12*(2), 299-310. doi: 10.5194/npg-12-299-2005

Oughton, S., Matthaeus, W. H., Wan, M., & Osman, K. T. (2015). Anisotropy in solar wind plasma turbulence. *Philosophical Transactions of the Royal Society of London Series A*, *373*(2041), 20140152-20140152. doi: 10.1098/rsta.2014.0152

Owens, M. J., & Cargill, P. (2004). Non-radial solar wind flows induced by the motion of interplanetary coronal mass ejections. *Annales Geophysicae*, *22*(12), 4397-4406. doi: 10.5194/angeo-22-4397-2004

Owens, M. J., & Forsyth, R. J. (2013). The heliospheric magnetic field. *Living Reviews in Solar Physics*, *10*(1), 5. doi: 10.12942/lrsp-2013-5

Palmerio, E. (2019). *Magnetic structure and geoeffectiveness of coronal mass ejections* (Doctoral dissertation, University of Helsinki). Retrieved from http://urn.fi/urn:isbn:978-951-51-2804-1

Palmerio, E., Kilpua, E. K. J., & Savani, N. P. (2016). Planar magnetic structures in coronal mass ejection-driven sheath regions. *Annales Geophysicae*, *34*(2), 313-322. doi: 10.5194/angeo-34-313-2016

Parker, E. N. (1958). Dynamics of the interplanetary gas and magnetic fields. *Astrophysical Journal*, *128*, 664. doi: 10.1086/146579

Peredo, M., Slavin, J. A., Mazur, E., & Curtis, S. A. (1995). Three-dimensional position and shape of the bow shock and their variation with Alfvénic, sonic, and magnetosonic Mach numbers and interplanetary magnetic field orientation. *Journal of Geophysical Research*, *100*(A5), 7907-7916. doi: 10.1029/94JA02545

Pesses, M. E., van Allen, J. A., Tsurutani, B. T., & Smith, E. J. (1984). High

time resolution observations of co-rotating interaction region proton events by Pioneer II. *Journal of Geophysical Research*, *89*(A1), 37-46. doi: 10.1029/JA089iA01p00037

Pitňa, A., Šafránková, J., Němeček, Z., & Franci, L. (2017). Decay of solar wind turbulence behind interplanetary shocks. *The Astrophysical Journal*, *844*(1), 51. doi: 10.3847/1538-4357/aa7bef

Pizzo, V. J. (1991). The evolution of corotating stream fronts near the ecliptic plane in the inner solar system. 2. Three-dimensional tilted-dipole fronts. *Journal of Geophysical Research*, *96*(A4), 5405-5420. doi: 10.1029/91JA00155

Pomoell, J., & Poedts, S. (2018). EUHFORIA: European heliospheric forecasting information asset. *Journal of Space Weather and Space Climate*, *8*, A35. doi: 10.1051/swsc/2018020

Price, C. P., Swift, D. W., & Lee, L. C. (1986). Numerical simulation of nonoscillatory mirror waves at the Earth's magnetosheath. *Journal of Geophysical Research*, *91*(A1), 101-112. doi: 10.1029/JA091iA01p00101

Rakhmanova, L., Riazantseva, M., Zastenker, G., & Šafránková, J. (2015). Modification of small- and middle-scale solar wind structures by the bow shock and magnetosheath: Correlation analysis. *Planetary and Space Science*, *115*, 12-18. doi: 10.1016/j.pss.2015.03.003

Rauch, J. L., & Roux, A. (1982). Ray tracing of ULF waves in a multicomponent magnetospheric plasma: Consequences for the generation mechanism of ion cyclotron waves. *Journal of Geophysical Research*, *87*(A10), 8191-8198. doi: 10.1029/JA087iA10p08191

Remya, B., Lee, K. H., Lee, L. C., & Tsurutani, B. T. (2017b). Coherency and ellipticity of electromagnetic ion cyclotron waves: Satellite observations and simulations. *Journal of Geophysical Research (Space Physics)*, *122*(3), 3374-3396. doi: 10.1002/2016JA023588

Remya, B., Reddy, R. V., Tsurutani, B. T., & Lakhina, G. S. (2017a). Comment on "Effects of electron temperature anisotropy on proton mirror instability evolution" by Ahmadi et al. (2016). *Journal of Geophysical Research (Space Physics)*, *122*(1), 745-747. doi: 10.1002/2016JA023148

Remya, B., Reddy, R. V., Tsurutani, B. T., Lakhina, G. S., & Echer, E. (2013). Ion temperature anisotropy instabilities in planetary magnetosheaths. *Journal of Geophysical Research (Space Physics)*, *118*(2), 785-793. doi: 10.1002/jgra.50091

Remya, B., Tsurutani, B. T., Reddy, R. V., Lakhina, G. S., Falkowski, B. J., Echer, E., & Glassmeier, K. H. (2014). Large-amplitude, circularly polarized, compressive, obliquely propagating electromagnetic proton cyclotron waves throughout

the Earth's magnetosheath: Low plasma β conditions. *The Astrophysical Journal*, *793*(1), 6. doi: 10.1088/0004-637X/793/1/6

Rice, W. K. M., Zank, G. P., & Li, G. (2003). Particle acceleration and coronal mass ejection driven shocks: Shocks of arbitrary strength. *Journal of Geophysical Research (Space Physics)*, *108*(A10), 1369. doi: 10.1029/2002JA009756

Richardson, I. G., & Cane, H. V. (2012). Solar wind drivers of geomagnetic storms during more than four solar cycles. *Journal of Space Weather and Space Climate*, *2*, A01. doi: 10.1051/swsc/2012001

Richardson, J. D., & Paularena, K. I. (2001). Plasma and magnetic field correlations in the solar wind. *Journal of Geophysical Research*, *106*(A1), 239-252. doi: 10.1029/2000JA000071

Richardson, J. D., & Smith, C. W. (2003). The radial temperature profile of the solar wind. *Geophysical Research Letters*, *30*(5), 1206. doi: 10.1029/2002GL016551

Riley, P., & Crooker, N. U. (2004). Kinematic treatment of coronal mass ejection evolution in the solar wind. *The Astrophysical Journal*, *600*(2), 1035-1042. doi: 10.1086/379974

Riley, P., Linker, J. A., Mikić, Z., Odstrcil, D., Zurbuchen, T. H., Lario, D., & Lepping, R. P. (2003). Using an MHD simulation to interpret the global context of a coronal mass ejection observed by two spacecraft. *Journal of Geophysical Research (Space Physics)*, *108*(A7), 1272. doi: 10.1029/2002JA009760

Ripoll, J. F., Claudepierre, S. G., Ukhorskiy, A. Y., Colpitts, C., Li, X., Fennell, J. F., & Crabtree, C. (2020). Particle dynamics in the Earth's radiation belts: Review of current research and open questions. *Journal of Geophysical Research (Space Physics)*, *125*(5), e26735. doi: 10.1029/2019JA026735

Roberts, O. W., Narita, Y., & Escoubet, C. P. (2017). Direct measurement of anisotropic and asymmetric wave vector spectrum in ion-scale solar wind turbulence. *The Astrophysical Journal Letters*, *851*(1), L11. doi: 10.3847/2041-8213/aa9bf3

Ronnmark, K., & André, M. (1991). Convection of ion cyclotron waves to ion-heating regions. *Journal of Geophysical Research*, *96*(A10), 17573-17579. doi: 10.1029/91JA01793

Rosso, O. A., Larrondo, H. A., Martin, M. T., Plastino, A., & Fuentes, M. A. (2007). Distinguishing noise from chaos. *Physical Review Letters*, *99*, 154102. Retrieved from https://link.aps.org/doi/10.1103/PhysRevLett.99.154102 doi: 10.1103/PhysRevLett.99.154102

Russell, C. T. (2000). The polar cusp. *Advances in Space Research*, *25*(7-8), 1413-1424. doi: 10.1016/S0273-1177(99)00653-5

Russell, C. T., Jian, L. K., Blanco-Cano, X., & Luhmann, J. G. (2009). STEREO

observations of upstream and downstream waves at low Mach number shocks. *Geophysical Research Letters*, *36*(3), L03106. doi: 10.1029/2008GL036991

Russell, C. T., & Mulligan, T. (2002). On the magnetosheath thicknesses of interplanetary coronal mass ejections. *Planetary and Space Science*, *50*(5-6), 527-534. doi: 10.1016/S0032-0633(02)00031-4

Salman, T. M., Winslow, R. M., & Lugaz, N. (2020). Radial evolution of coronal mass ejections between MESSENGER, Venus Express, STEREO, and L1: Catalog and analysis. *Journal of Geophysical Research (Space Physics)*, *125*(1), e27084. doi: 10.1029/2019JA027084

Sari, J. W., & Valley, G. C. (1976). Interplanetary magnetic field power spectra: Mean field radial or perpendicular to radial. *Journal of Geophysical Research*, *81*(A31), 5489-5500. doi: 10.1029/JA081i031p05489

Savani, N. P., Vourlidas, A., Szabo, A., Mays, M. L., Richardson, I. G., Thompson, B. J., ... Nieves-Chinchilla, T. (2015). Predicting the magnetic vectors within coronal mass ejections arriving at Earth: 1. Initial architecture. *Space Weather*, *13*(6), 374-385. doi: 10.1002/2015SW001171

Scholer, M., Kucharek, H., & Jayanti, V. (1997). Waves and turbulence in high Mach number nearly parallel collisionless shocks. *Journal of Geophysical Research*, *102*(A5), 9821-9834. doi: 10.1029/97JA00345

Schrijver, C. K., & Siscoe, G. L. (2009). *Heliophysics: Plasma physics of the local cosmos*. Cambridge University Press. doi: 10.1017/CBO9781107340657

Schwenn, R. (1990). Large-scale structure of the interplanetary medium. In R. Schwenn & E. Marsch (Eds.), *Physics of the inner heliosphere i: Large-scale phenomena* (pp. 99–181). Springer Berlin Heidelberg. doi: 10.1007/978-3-642-75361-9_3

Schwenn, R., dal Lago, A., Huttunen, E., & Gonzalez, W. D. (2005). The association of coronal mass ejections with their effects near the Earth. *Annales Geophysicae*, *23*(3), 1033-1059. doi: 10.5194/angeo-23-1033-2005

Sckopke, N., Paschmann, G., Brinca, A. L., Carlson, C. W., & Luehr, H. (1990). Ion thermalization in quasi-perpendicular shocks involving reflected ions. *Journal of Geophysical Research*, *95*(A5), 6337-6352. doi: 10.1029/JA095iA05p06337

Shan, L., Lu, Q., Wu, M., Gao, X., Huang, C., Zhang, T., & Wang, S. (2014). Transmission of large-amplitude ULF waves through a quasi-parallel shock at Venus. *Journal of Geophysical Research (Space Physics)*, *119*(1), 237-245. doi: 10.1002/2013JA019396

Shoji, M., Omura, Y., Tsurutani, B. T., Verkhoglyadova, O. P., & Lembege, B. (2009). Mirror instability and L-mode electromagnetic ion cyclotron instability: Competition in the Earth's magnetosheath. *Journal of Geophysical Research*

(Space Physics), *114*(A10), A10203. doi: 10.1029/2008JA014038

Siscoe, G., MacNeice, P. J., & Odstrcil, D. (2007). East-west asymmetry in coronal mass ejection geoeffectiveness. *Space Weather*, *5*(4), S04002. doi: 10.1029/2006SW000286

Siscoe, G., & Odstrcil, D. (2008). Ways in which ICME sheaths differ from magnetosheaths. *Journal of Geophysical Research (Space Physics)*, *113*(A9), A00B07. doi: 10.1029/2008JA013142

Slavin, J. A., Tsurutani, B. T., Smith, E. J., Jones, D. E., & Sibeck, D. G. (1983). Average configuration of the distant (<220 R_e) magnetotail: Initial ISEE-3 magnetic field results. *Geophysical Research Letters*, *10*(10), 973-976. doi: 10.1029/GL010i010p00973

Smith, E. J. (2001). The heliospheric current sheet. *Journal of Geophysical Research*, *106*(A8), 15819-15832. doi: 10.1029/2000JA000120

Smith, E. J., Tsurutani, B. T., & Rosenberg, R. L. (1978). Observations of the interplanetary sector structure up to heliographic latitudes of 16°: Pioneer 11. *Journal of Geophysical Research*, *83*(A2), 717-724. doi: 10.1029/JA083iA02p00717

Smith, E. J., & Wolfe, J. H. (1976). Observations of interaction regions and corotating shocks between one and five AU: Pioneers 10 and 11. *Geophysical Research Letters*, *3*(3), 137-140. doi: 10.1029/GL003i003p00137

Snyder, C. W., Neugebauer, M., & Rao, U. R. (1963). The solar wind velocity and its correlation with cosmic-ray variations and with solar and geomagnetic activity. *Journal of Geophysical Research*, *68*, 6361. doi: 10.1029/JZ068i024p06361

Solomon, S. C., McNutt, R. L., Gold, R. E., & Domingue, D. L. (2007). MESSENGER mission overview. *Space Science Reviews*, *131*(1-4), 3-39. doi: 10.1007/s11214-007-9247-6

Sonett, C. P., & Abrams, I. J. (1963). The Distant geomagnetic field 3. Disorder and shocks in the magnetopause. *Journal of Geophysical Research*, *68*(5), 1233-1263. doi: 10.1029/JZ068i005p01233

Soucek, J., Escoubet, C. P., & Grison, B. (2015). Magnetosheath plasma stability and ULF wave occurrence as a function of location in the magnetosheath and upstream bow shock parameters. *Journal of Geophysical Research (Space Physics)*, *120*(4), 2838-2850. doi: 10.1002/2015JA021087

Soucek, J., Lucek, E., & Dandouras, I. (2008). Properties of magnetosheath mirror modes observed by Cluster and their response to changes in plasma parameters. *Journal of Geophysical Research (Space Physics)*, *113*(A4), A04203. doi: 10.1029/2007JA012649

Southwood, D. J., & Kivelson, M. G. (1993). Mirror instability. I - Physical mechanism of linear instability. *Journal of Geophysical Research*, *98*(A6), 9181-9187.

doi: 10.1029/92JA02837

Stone, E. C., Cummings, A. C., Heikkila, B. C., & Lal, N. (2019). Cosmic ray measurements from Voyager 2 as it crossed into interstellar space. *Nature Astronomy*, *3*, 1013-1018. doi: 10.1038/s41550-019-0928-3

Stone, E. C., Cummings, A. C., McDonald, F. B., Heikkila, B. C., Lal, N., & Webber, W. R. (2013). Voyager 1 observes low-energy galactic cosmic rays in a region depleted of heliospheric ions. *Science*, *341*(6142), 150-153. doi: 10.1126/science.1236408

Stone, E. C., Frandsen, A. M., Mewaldt, R. A., Christian, E. R., Margolies, D., Ormes, J. F., & Snow, F. (1998). The Advanced Composition Explorer. *Space Science Reviews*, *86*, 1-22. doi: 10.1023/A:1005082526237

Sugiura, M., & Kamei, T. (1991). Equatorial Dst index 1957–1986. *ISGI Publications Office*.

Tanskanen, E. I., Hynönen, R., & Mursula, K. (2017a). Seasonal variation of high-latitude geomagnetic activity in individual years. *Journal of Geophysical Research (Space Physics)*, *122*(10), 10,058-10,071. doi: 10.1002/2017JA024276

Tanskanen, E. I., Slavin, J. A., Fairfield, D. H., Sibeck, D. G., Gjerloev, J., Mukai, T., ... Nagai, T. (2005a). Magnetotail response to prolonged southward IMF B_z intervals: Loading, unloading, and continuous magnetospheric dissipation. *Journal of Geophysical Research (Space Physics)*, *110*(A3), A03216. doi: 10.1029/2004JA010561

Tanskanen, E. I., Slavin, J. A., Tanskanen, A. J., Viljanen, A., Pulkkinen, T. I., Koskinen, H. E. J., ... Eastwood, J. (2005b). Magnetospheric substorms are strongly modulated by interplanetary high-speed streams. *Geophysical Research Letters*, *32*(16), L16104. doi: 10.1029/2005GL023318

Tanskanen, E. I., Snekvik, K., Slavin, J. A., Pérez-Suárez, D., Viljanen, A., Goldstein, M. L., ... Mursula, K. (2017b). Solar cycle occurrence of Alfvénic fluctuations and related geoefficiency. *Journal of Geophysical Research (Space Physics)*, *122*(10), 9848-9857. doi: 10.1002/2017JA024385

Thompson, M. J., Christensen-Dalsgaard, J., Miesch, M. S., & Toomre, J. (2003). The internal rotation of the sun. *Annual Review of Astronomy and Astrophysics*, *41*(1), 599-643. doi: 10.1146/annurev.astro.41.011802.094848

Tsurutani, B. T., Dasgupta, B., Galvan, C., Neugebauer, M., Lakhina, G. S., Arballo, J. K., ... Buti, B. (2002). Phase-steepened Alfvén waves, proton perpendicular energization and the creation of magnetic holes and magnetic decreases: The ponderomotive force. *Geophysical Research Letters*, *29*(24), 2233. doi: 10.1029/2002GL015652

Tsurutani, B. T., Echer, E., & Gonzalez, W. D. (2011a). The solar and interplanetary

causes of the recent minimum in geomagnetic activity (MGA23): a combination of midlatitude small coronal holes, low IMF B_Z variances, low solar wind speeds and low solar magnetic fields. *Annales Geophysicae*, *29*(5), 839-849. doi: 10.5194/angeo-29-839-2011

Tsurutani, B. T., Gonzalez, W. D., Gonzalez, A. L. C., Guarnieri, F. L., Gopalswamy, N., Grande, M., ... Vasyliunas, V. (2006). Corotating solar wind streams and recurrent geomagnetic activity: A review. *Journal of Geophysical Research (Space Physics)*, *111*(A7), A07S01. doi: 10.1029/2005JA011273

Tsurutani, B. T., Gonzalez, W. D., Tang, F., Akasofu, S. I., & Smith, E. J. (1988). Origin of interplanetary southward magnetic fields responsible for major magnetic storms near solar maximum (1978-1979). *Journal of Geophysical Research*, *93*(A8), 8519-8531. doi: 10.1029/JA093iA08p08519

Tsurutani, B. T., Guarnieri, F. L., Echer, E., Lakhina, G. S., & Verkhoglyadova, O. P. (2009). Magnetic decrease formation from <1 AU to ∼5 AU: Corotating interaction region reverse shocks. *Journal of Geophysical Research (Space Physics)*, *114*(A8), A08105. doi: 10.1029/2008JA013927

Tsurutani, B. T., Jones, D. E., & Sibeck, D. G. (1984b). The two-lobe structure of the distant ($X \geq 200$ R_e) magnetotail. *Geophysical Research Letters*, *11*(10), 1066-1069. doi: 10.1029/GL011i010p01066

Tsurutani, B. T., & Lakhina, G. S. (1997). Some basic concepts of wave-particle interactions in collisionless plasmas. *Reviews of Geophysics*, *35*(4), 491-501. doi: 10.1029/97RG02200

Tsurutani, B. T., Lakhina, G. S., & Hajra, R. (2020). The physics of space weather/solar-terrestrial physics (STP): What we know now and what the current and future challenges are. *Nonlinear Processes in Geophysics*, *27*(1), 75-119. doi: 10.5194/npg-27-75-2020

Tsurutani, B. T., Lakhina, G. S., Sen, A., Hellinger, P., Glassmeier, K.-H., & Mannucci, A. J. (2018). A review of Alfvénic turbulence in high-speed solar wind streams: Hints from cometary plasma turbulence. *Journal of Geophysical Research (Space Physics)*, *123*(4), 2458-2492. doi: 10.1002/2017JA024203

Tsurutani, B. T., Lakhina, G. S., Verkhoglyadova, O. P., Echer, E., Guarnieri, F. o. L., Narita, Y., & Constantinescu, D. O. (2011c). Magnetosheath and heliosheath mirror mode structures, interplanetary magnetic decreases, and linear magnetic decreases: Differences and distinguishing features. *Journal of Geophysical Research (Space Physics)*, *116*(A2), A02103. doi: 10.1029/2010JA015913

Tsurutani, B. T., Lakhina, G. S., Verkhoglyadova, O. P., Gonzalez, W. D., Echer, E., & Guarnieri, F. L. (2011b). A review of interplanetary discontinuities

and their geomagnetic effects. *Journal of Atmospheric and Solar-Terrestrial Physics*, *73*(1), 5-19. doi: 10.1016/j.jastp.2010.04.001

Tsurutani, B. T., Slavin, J. A., Smith, E. J., Okida, R., & Jones, D. E. (1984a). Magnetic structure of the distant geotail from -60 to -220 R_e: ISEE-3. *Geophysical Research Letters*, *11*(1), 1-4. doi: 10.1029/GL011i001p00001

Tsurutani, B. T., & Smith, E. J. (1979). Interplanetary discontinuities: Temporal variations and the radial gradient from 1 to 8.5 AU. *Journal of Geophysical Research*, *84*(A6), 2773-2787. doi: 10.1029/JA084iA06p02773

Tsurutani, B. T., Smith, E. J., Anderson, R. R., Ogilvie, K. W., Scudder, J. D., Baker, D. N., & Bame, S. J. (1982). Lion roars and nonoscillatory drift mirror waves in the magnetosheath. *Journal of Geophysical Research*, *87*(A8), 6060-6072. doi: 10.1029/JA087iA08p06060

Tsurutani, B. T., Smith, E. J., & Jones, D. E. (1983). Waves observed upstream of interplanetary shocks. *Journal of Geophysical Research*, *88*(A7), 5645-5656. doi: 10.1029/JA088iA07p05645

Tsurutani, B. T., Wu, S. T., Zhang, T. X., & Dryer, M. (2003). Coronal mass ejection (CME)-induced shock formation, propagation and some temporally and spatially developing shock parameters relevant to particle energization. *Astronomy and Astrophysics*, *412*, 293-304. doi: 10.1051/0004-6361:20031413

van Allen, J. A., & Frank, L. A. (1959). Radiation around the Earth to a radial distance of 107,400 km. *Nature*, *183*(4659), 430-434. doi: 10.1038/183430a0

Vasquez, B. J., Abramenko, V. I., Haggerty, D. K., & Smith, C. W. (2007b). Numerous small magnetic field discontinuities of Bartels rotation 2286 and the potential role of Alfvénic turbulence. *Journal of Geophysical Research (Space Physics)*, *112*(A11), A11102. doi: 10.1029/2007JA012504

Vasquez, B. J., & Hollweg, J. V. (1999). Formation of pressure-balanced structures and fast waves from nonlinear Alfvén waves. *Journal of Geophysical Research*, *104*(A3), 4681-4696. doi: 10.1029/1998JA900090

Vasquez, B. J., Smith, C. W., Hamilton, K., MacBride, B. T., & Leamon, R. J. (2007a). Evaluation of the turbulent energy cascade rates from the upper inertial range in the solar wind at 1 AU. *Journal of Geophysical Research (Space Physics)*, *112*(A7), A07101. doi: 10.1029/2007JA012305

Velli, M., Grappin, R., & Mangeney, A. (1989). Turbulent cascade of incompressible unidirectional Alfvén waves in the interplanetary medium. *Physical Review Letters*, *63*(17), 1807-1810. doi: 10.1103/PhysRevLett.63.1807

von Alfthan, S., Pokhotelov, D., Kempf, Y., Hoilijoki, S., Honkonen, I., Sandroos, A., & Palmroth, M. (2014). Vlasiator: First global hybrid-Vlasov simulations of Earth's foreshock and magnetosheath. *Journal of Atmospheric and Solar-*

Terrestrial Physics, *120*, 24-35. doi: 10.1016/j.jastp.2014.08.012

von Steiger, R., Schwadron, N. A., Fisk, L. A., Geiss, J., Gloeckler, G., Hefti, S., ... Zurbuchen, T. H. (2000). Composition of quasi-stationary solar wind flows from Ulysses/Solar Wind Ion Composition Spectrometer. *Journal of Geophysical Research*, *105*(A12), 27217-27238. doi: 10.1029/1999JA000358

Wang, Y. M., Sheeley, J., N. R., Walters, J. H., Brueckner, G. E., Howard, R. A., Michels, D. J., ... Simnett, G. M. (1998). Origin of streamer material in the outer corona. *The Astrophysical Journal*, *498*(2), L165-L168. doi: 10.1086/311321

Webb, D. F., & Howard, T. A. (2012). Coronal mass ejections: Observations. *Living Reviews in Solar Physics*, *9*(1), 3. doi: 10.12942/lrsp-2012-3

Weck, P. J., Schaffner, D. A., Brown, M. R., & Wicks, R. T. (2015). Permutation entropy and statistical complexity analysis of turbulence in laboratory plasmas and the solar wind. *Physical Review E*, *91*(2), 023101. doi: 10.1103/PhysRevE.91.023101

Wei, F., Feng, X., Yang, F., & Zhong, D. (2006). A new non-pressure-balanced structure in interplanetary space: Boundary layers of magnetic clouds. *Journal of Geophysical Research (Space Physics)*, *111*(A3), A03102. doi: 10.1029/2005JA011272

Wicks, R. T., Chapman, S. C., & Dendy, R. O. (2009). Spatial correlation of solar wind fluctuations and their solar cycle dependence. *The Astrophysical Journal*, *690*(1), 734-742. doi: 10.1088/0004-637X/690/1/734

Wilson, I., Lynn B., Stevens, M. L., Kasper, J. C., Klein, K. G., Maruca, B. A., Bale, S. D., ... Salem, C. S. (2018). The statistical properties of solar wind temperature parameters near 1 AU. *The Astrophysical Journal Supplement Series*, *236*(2), 41. doi: 10.3847/1538-4365/aab71c

Winske, D., Omidi, N., Quest, K. B., & Thomas, V. A. (1990). Re-forming supercritical quasi-parallel shocks 2. Mechanism for wave generation and front re-formation. *Journal of Geophysical Research*, *95*(A11), 18821-18832. doi: 10.1029/JA095iA11p18821

Winterhalter, D., Neugebauer, M., Goldstein, B. E., Smith, E. J., Bame, S. J., & Balogh, A. (1994b). Ulysses field and plasma observations of magnetic holes in the solar wind and their relation to mirror-mode structures. *Journal of Geophysical Research*, *99*(A12), 23371-23382. doi: 10.1029/94JA01977

Winterhalter, D., Smith, E. J., Burton, M. E., Murphy, N., & McComas, D. J. (1994a). The heliospheric plasma sheet. *Journal of Geophysical Research*, *99*(A4), 6667-6680. doi: 10.1029/93JA03481

Yashiro, S., Gopalswamy, N., Michalek, G., St. Cyr, O. C., Plunkett, S. P., Rich,

N. B., & Howard, R. A. (2004). A catalog of white light coronal mass ejections observed by the SOHO spacecraft. *Journal of Geophysical Research (Space Physics)*, *109*(A7), A07105. doi: 10.1029/2003JA010282

Yoon, P. H. (2017). Kinetic instabilities in the solar wind driven by temperature anisotropies. *Reviews of Modern Plasma Physics*, *1*(1), 4. doi: 10.1007/s41614-017-0006-1

Yordanova, E., Balogh, A., Noullez, A., & von Steiger, R. (2009). Turbulence and intermittency in the heliospheric magnetic field in fast and slow solar wind. *Journal of Geophysical Research (Space Physics)*, *114*(A8), A08101. doi: 10.1029/2009JA014067

Yordanova, E., Vaivads, A., André, M., Buchert, S. C., & Vörös, Z. (2008). Magnetosheath plasma turbulence and its spatiotemporal evolution as observed by the Cluster Spacecraft. *Physical Review Letters*, *100*(20), 205003. doi: 10.1103/PhysRevLett.100.205003

Young, D. T., Perraut, S., Roux, A., de Villedary, C., Gendrin, R., Korth, A., ... Jones, D. (1981). Wave-particle interactions near Ω_{He+} observed in GEOS 1 and 2 1. Propagation of ion cyclotron waves in He^+ -rich plasma. *Journal of Geophysical Research*, *86*(A8), 6755-6772. doi: 10.1029/JA086iA08p06755

Yumoto, K., Saito, T., Tsurutani, B. T., Smith, E. J., & Akasofu, S. I. (1984). Relationship between the IMF magnitude and Pc 3 magnetic pulsations in the magnetosphere. *Journal of Geophysical Research*, *89*(A11), 9731-9740. doi: 10.1029/JA089iA11p09731

Zhou, X., & Smith, E. J. (2015). Supercriticality of ICME and CIR shocks. *Journal of Geophysical Research (Space Physics)*, *120*(3), 1526-1536. doi: 10.1002/2014JA020700

Zwan, B. J., & Wolf, R. A. (1976). Depletion of solar wind plasma near a planetary boundary. *Journal of Geophysical Research*, *81*(10), 1636. doi: 10.1029/JA081i010p01636